DEUTSCHES ELEKTRONEN-SYNCHROTRON DESY

DESY 69/21
July 1969

Electromagnetic Interactions

Review talk given at the Lund International Conference on Elementary Particles, 1969

by

E. Lohrmann

Deutsches Elektronen-Synchrotron DESY, Hamburg

2 HAMBURG 52 · NOTKESTIEG 1

Electromagnetic Interactions

E. Lohrmann

Deutsches Elektronen-Synchrotron DESY, Hamburg

(Review talk given at the Lund International Conference on Elementary Particles, June 25 - July 1, 1969)

1. Introductory Remarks

In this paper the following three subjects will be covered: (i) Status of quantum electrodynamics and electron-muon universality, (ii) photoproduction, and (iii) elastic and inelastic electron-nucleon scattering. The last two subjects are very relevant to the question of strong interactions since the amplitudes for photo- and electroproduction processes are directly related to the matrix element of the electromagnetic current between hadron states. They provide supplementary information to most aspects of strong interaction physics, and share with them the unsatisfactory state of their theoretical understanding.

In the selection of material I have been led by simplicity as a guiding line, and I apologize to the many authors of important contributions, which could not be included. A number of excellent and much more detailled review papers are available in the literature (1 - 3).

2. Test of Quantum Electrodynamics and Electron-Muon Universality

2.1 Fine Structure Constant

Conflicting measurements of the fine structure constant α have provided somewhat of a stumbling block in recent years. However, a number of recent accurate experiments seem to converge to a value around $1/\alpha = 137.036$ which will be used throughout this paper in the numerical predictions of the theory. Table 1 gives a survey of the results of the most accurate experiments.

Comments: The classical, very accurate value of Lamb and collaborators (4) is now the only one which disagrees with the bulk of the other accurate data. It was obtained by combining the fine structure interval $2\,S_{1/2} - 2\,P_{3/2}$ in deuterium with the Lamb shift, (deuterium is favoured because of its smaller line width compared to hydrogen) to get the $2\,S_{1/2} - 2\,P_{1/2}$ interval. If the result of a recent measurement of the Lamb shift in deuterium is used (Cosens (5)), instead of Lamb's old value, one gets $1/\alpha = 137.0373\ (6)$, which is much closer to the other measurements of α. However, considering the difficulty and past history of these measurements, it seems wise to wait for a remeasurement of the fine structure interval in deuterium.

Two new measurements of the fine structure interval in hydrogen (6,7) give values compatible with the very accurate measurements of α from the Josephson effect (8).

The Josephson effect is based on observing voltage steps (height V) generated in a Josephson junction, when it is irradiated by a microwave frequency ν. The basic relation $2eV = h\nu$ can be used to calculate α from a measurement of V and ν. This relation seems to be completely insensitive to the nature of the materials involved (9), and therefore the value of α given by the Josephson experiment may be considered reliable until further notice.

The very accurate value for the hydrogen hyperfine structure interval (10) does unfortunately not lead to a clear cut value for α because one has to consider corrections coming from the structure and finite size of the proton. Both the size and the error of these corrections cannot be evaluated with sufficient precision because they involve strong interactions (11). The error given on $1/\alpha$ comes entirely from these theoretical uncertainties and is a guess only.

Measurements on muonium instead of hydrogen avoid these difficulties of the strong interaction physics of the proton. A recent measurement on muonium (12) falls in with the present best value of $1/\alpha = 137.036O$, however, it is less accurate than the other measurements. The authors claim, that the main uncertainty comes from the experimental error on the muon magnetic moment.

2.2 Lamb Shift

Measurement of the $2\,S_{1/2} - 2\,P_{1/2}$ interval in hydrogen affords an accurate test of higher order corrections in the theory of the hydrogen atom. The two lowest order corrections which enter into the calculations are shown below.

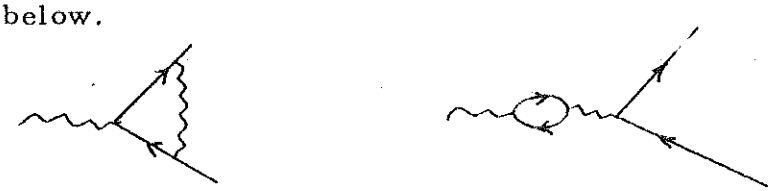

They concern radiative corrections at the electron vertex and corrections due to vacuum polarization. The most accurate theoretical prediction (13) includes of course also higher order corrections.

Table 2 shows experimental and theoretical results. The two experiments disagree by O.O9 MHz, which is somewhat more than the quoted errors. Therefore the quoted experimental average and its error is a guess only. It is O.24 MHz away from the theoretical value. The combined error (experiment plus theory) for this difference could be O.1O MHz or even bigger. Before the errors are better understood, it is probably premature to worry too much about the discrepancy.

2.3 Anomalous Magnetic Moment of Electron and Muon:

The g - factor of the electron or muon is modified by higher order corrections in Q.E.D. Measurement of $\frac{g-2}{2}$, which gives the deviation

from the Dirac value, is a test for these corrections. It is more sensitive for the muon than for the electron, since larger invariant momentum transfers contribute to the corrections in the case of the muon.

There is a recent very beautiful result obtained with the CERN muon storage ring (16). (See Table 3).

The results for μ^+ and μ^- agree within the errors:

$\frac{g-2}{2}(\mu^- - \mu^+) = (50 \pm 75) \times 10^{-8}$. This is required under CPT invariance. Table 3 shows also the result of a somewhat older experiment for the electron. The results for $\frac{g-2}{2}$ for both the muon and the electron disagree with the best theoretical calculations by about twice the quoted errors. Similar as for the Lamb shift, it seems premature to attach too great a significance to the discrepancy, in view of the difficulty of these highly precise experiments.

This completes the survey of high precision experiments on Q.E.D. On all three subjects - fine structure constant, Lamb shift and anomalous magnetic moments - there remain small discrepancies of at most two to three times the quoted errors. This is not evidence enough to cast doubt at the validity of Q.E.D. at the present time. However, one feels somewhat ill at ease and new experimental and theoretical results will be of great interest.

2.4 High Energy Experiments

The idea here is to test Q.E.D. in a situation where the magnitude of a four-vector characteristic of the experiment is as large as possible. As a rule this four-vector will be associated with a virtual electron or photon.

Calling q^2 the square of this four momentum transfer, a possible deviation of a measured cross section from the predictions of Q.E.D. might be parametrized as follows:

$$\sigma_{exp} = \sigma_{QED} \quad (1 + q^2/\Lambda^2) \quad (2.1) \quad \text{or (See Ref. 18)}$$

$$\text{or: } \sigma_{exp} = \sigma_{QED} \quad (1 + q^4/\Lambda^{*4}) \quad (2.2)$$

Both Λ^2 and Λ^{*4} can be positive or negative. In our metric $q^2 = E^2 - p^2 = m^2 > o$, and q^2 is called time-like if $q^2 > o$ and space-like if $q^2 < o$. There is no intuitively simple interpretation of equations (2.1) and (2.2) in terms of modifications of Q.E.D., therefore they can serve at best as a help to compare the sensitivity of different experiments (18).

2.5 Large Angle Electron-Positron Pair-Production:

The two Bethe-Heither graphs and the Compton graph for this process are shown below:

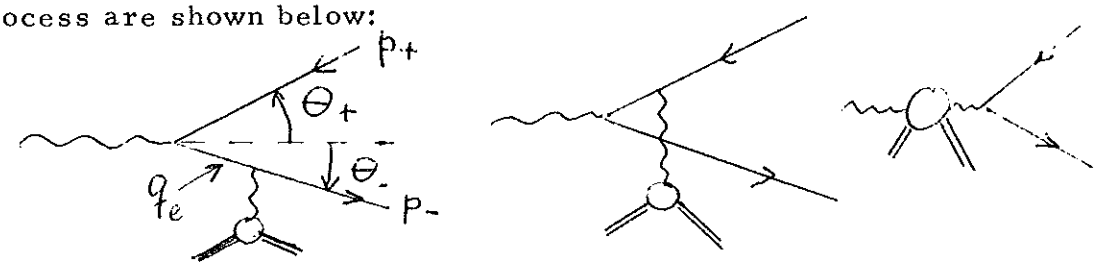

In an experiment symmetric with respect to e^+ and e^- the influence of the Compton term can be kept small. At large angles and energies the electron propagator assumes large space-like values. In a symmetrical arrangement ($\theta_+ = \theta_-$, $|\vec{p}_+| = |\vec{p}_-|$) one has

$$q_e^2 \approx -4 \cdot |\vec{p}_t|^2 \cdot (1 - \cos\theta_\pm)$$

For small angles q_e^2 can be expressed in terms of the invariant mass of the $e^+ - e^-$-system:

$$M^2(e^+e^-) \approx -2\, q_e^2$$

Figure 1 shows the results of an experiment carried out at DESY (19). There is no deviation from theory. Parametrizing the result according to

$$\sigma_{exp} / \sigma_{theory} = A (1 + M^{4}_{e^+e^-} / \Lambda'^{4}) \quad (3)$$

the authors obtain a cut-off parameter $|\Lambda'| > 1.6$ GeV with 95 % confidence. Experiments carried out at Cornell (20) and CEA (21) also gave agreement with theory.

2.6 Large Angle $\mu^+ \mu^-$ Pair Production:

Experiments for large momentum transfers were carried out at CEA and Cornell (22). Both experiments are consistent with QED. Parametrizing the result according to $\sigma_{exp} / \sigma_{th} = (1 + M^2_{\mu\mu} / \Lambda^2)$ the authors obtain $|\Lambda| > 0.95$ GeV (95 % confidence, CEA) and $\Lambda^{-2} = -0.10 \pm 0.05$ GeV^2 ($|\Lambda| > 2.2$ GeV, 95 % confidence) from Cornell. Fig. 2 shows the most recent Cornell results.

2.7 Bremsstrahlung of Electrons and Muons at large Angles:

The lowest order diagrams describing the process are shown below.

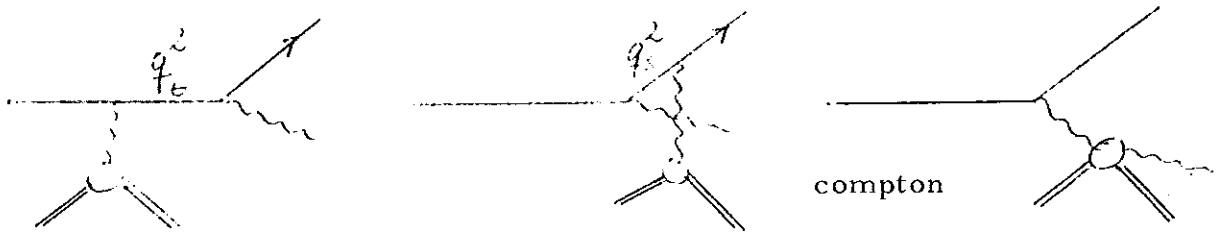

Both time-like (q_t^2) and space-like (q_s^2) values of the electron (muon) propagator contribute. This experiment gives therefore evidence supplementary to the wide angle pair experiments. Figure 3 gives a summary of results obtained for large angle electron (23) and muon (24) Bremsstrahlung.

There is no deviation from theory. Parametrizing the electron-bremsstrahlung result according to

$$\sigma_{exp} / \sigma_{th} = (1 + M_{e\gamma}^2 / \Lambda^2),$$

a cut-off parameter of $|\Lambda| > 1.6$ GeV with 95 % confidence is obtained.

2.8 Electron-Electron Scattering:

The two lowest order diagrams are shown below.

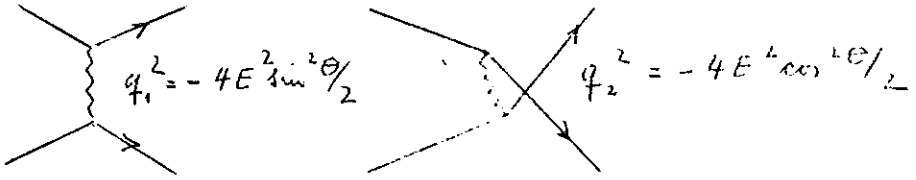

The four-momentum of the exchanged photon is space-like. The most accurate experimental information for this process comes from a storage ring experiment at Stanford at 2 E = 2 x 550 MeV. No deviation from Q.E.D. was observed. In order to quote an accuracy for the experiment, each of the two amplitudes was multiplied by a form factor

$$G(q^2) = (1 - q^2/\Lambda^2)^{-1}$$

The data, when fitted to this form, gave $\Lambda^{-2} = -(0.06 \pm 0.06)$ GeV^{-2}, consistent with Q.E.D. (25)

2.9 Unusual Couplings:

If the electron, muon or photon would have additional unusual interactions not foreseen in the frame-work of Q.E.D., this could lead to apparent discrepancies between experiment and Q.E.D. Low (26) has discussed possibilities for such couplings and suggested an experimental

search. Suppose e.g. there were a heavy electron e^* which could decay electromagnetically via $e^* \rightarrow e + \gamma$

Unsuccessful searches for this particle in the reaction

$$e + p \rightarrow e^* + p \rightarrow e + \gamma + p$$

have been carried out (27, 28, 29). The mass range in which the search was sensitive extended from 100 MeV to 1300 MeV.

In this connection it is interesting to remember the extremely low upper limit for the decay branching ratio (30, 31)

$$\Gamma(\mu \rightarrow e\gamma) / \Gamma(\mu \rightarrow e\nu\bar{\nu}) < 0.6 \times 10^{-8}$$

showing that electron (muon) number is conserved to very high accuracy. If this conservation law would be multiplicative, the reaction

$$e^- e^- \rightarrow \mu^- \mu^-$$

would be possible.

Absence of this reaction was demonstrated in an experiment at the Stanford storage ring (32). At 2 x 525 MeV an upper limit for the cross section is

$$\sigma < 0.67 \times 10^{-32} cm^2 \quad (95\ \%\ \text{confidence})$$

This limit is not sensitive enough(by roughly a factor of 10^5) to come into the region of weak interaction cross-sections.

2.10 Electron-Muon Universality:

Wide angle pair experiments and bremsstrahlung experiments with both electrons and muons have yielded consistent results in agreement with Q.E.D. This means, that muon and electron behave alike, even if they have large space-like or time-like four-momenta. There are slight

discrepancies for the anomalous magnetic moments of both muons and electrons, but they should at present not be taken seriously.

Elastic ep - and μp scattering tests the e- μ equality for coupling to large space-like photon four-momenta. Fig. 4 shows the comparison of ep and μp scattering (33). Again electrons and muons seem to give consistent results.

Electron-muon universality for coupling to time-like photons can be checked by comparing the branching ratio of vector meson decay into e^+e^- versus $\mu^+\mu^-$. For the ρ meson the branching ratios are

$$\Gamma(\rho \to \mu^+\mu^-)/\Gamma_{all} = (6.3 \pm 1.0) \times 10^{-5}$$
$$\Gamma(\rho \to e^+e^-)/\Gamma_{all} = (6.2 \pm 0.6) \times 10^{-5}$$

Again these two values agree with each other.
(A correction of the ratio due to the e -μ mass difference is negligible compared to the experimental errors).

3. Photoproduction

3.1 Vector Meson Dominance

The hadronic electromagnetic current can be connected with the fields of the vector mesons, which have the same quantum number as the photon:

$$j_\mu(x) = -\left[\frac{m_\rho^2}{2\gamma_\rho}\rho_\mu(x) + \frac{m_\omega^2}{2\gamma_\omega}\omega_\mu(x) + \frac{m_\phi^2}{2\gamma_\phi}\phi_\mu(x)\right] \quad (3.1)$$

$\gamma_\rho, \gamma_\omega, \gamma_\phi$, generally γ_V , are the vector meson-photon coupling constants.

The history of this equation can be traced back to papers by Sakurai, Gell-Mann, Zachariasen, Nambu, Sharp and Wagner (34). Work by Kroll, Lee and Zumino (35), by Zimmermann (36), by H. Joos (37) and Haag and Nishijima (38) has put this relation on a firmer theoretical basis.

Equ. (3.1) refers to vector meson fields with mass $m_V = 0$. Practical application demands an extrapolation of the amplitude to the real vector meson mass. Assuming that the amplitude changes very little for this extrapolation and disregarding other questions as to the uniqueness of the extrapolation, one obtains from Equ. (3.1):

$$\sigma(\gamma p \to X) = \sum_{V=\rho,\omega,\phi} \frac{\pi\alpha}{\gamma_V^2} \sigma_{TR}(V p \to X) +$$

+ interference terms (3.2)

σ_{TR} refers to the cross section for a transversely polarized vector meson.

Equ. (3.2) connects photoproduction processes with reactions produced by vector mesons.

In order to use it for real physical applications, i.e. to obtain a connection between photoproduction and reactions of real vector mesons, one must assume, that the amplitudes change only little if one extrapolates from $m_V = 0$ to the real mass of the vector mesons. It is this assumption which is actually tested if one checks equ. (3.2) experimentally.

The extrapolation from $\underline{k}^2 = 0$ to $\underline{k}^2 = m_V^2$ may not be unique. For example, there is an infinity of equivalent polarization vectors for the photon due to gauge invariance:

$$e'_\mu = e_\mu + \beta k_\mu$$

(β = arbitrary number)

They are equivalent in the sense that they give the same photoproduction cross section. The photon state is therefore not unique. It can be reached by the extrapolation from a real vector meson state to mass zero by a continuum of non-equivalent vector meson states (39).

3.2 Measurement of the Coupling Constants :

(i) Leptonic decays of vector mesons: Example: $\rho \rightarrow e^+e^-$.

The branching ratio is:

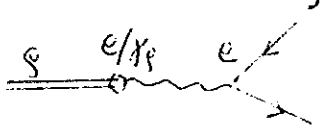

$$\mathcal{B} = \Gamma(\rho \rightarrow e^+e^-)/\Gamma_{tot}(\rho) = \frac{\alpha^2}{12}\left(\frac{4\pi}{\gamma_\rho^2}\right)\frac{m_\rho}{\Gamma_{tot}(\rho)}\left(1 - \frac{4m_e^2}{m_\rho^2}\right)^{1/2}\left(1 + 2\frac{m_e^2}{m_\rho^2}\right) \qquad (3.3)$$

Second method : (ii) Storage ring experiments of the type

$$e^+e^- \rightarrow \rho \rightarrow \pi^+\pi^-$$
$$\rightarrow \omega \rightarrow \pi^+\pi^-\pi^o$$
$$\rightarrow \phi \rightarrow k\bar{k} \text{ or } \pi^+\pi^-\pi^o$$

Example:

$$\sigma(e^+e^- \rightarrow \pi^+\pi^-) = \frac{\pi a^2}{12} \cdot \beta_\pi^3 \cdot \frac{1}{E^2} \cdot |F_\pi(2E)|^2 \qquad (3.4)$$

β_π = pion velocity

E = storage ring energy

$F_\pi(K)$ = pion form factor

Near the ρ resonance F_π has a Breit-Wigner shape:

$$F_\pi(2E) = \frac{m_\rho^2 \left(g_{\gamma\pi\pi} / 2\gamma_\rho \right)}{m_\rho^2 - 4E^2 - i\, m_\rho \Gamma_\rho} \qquad (3.5)$$

$g_{\gamma\pi\pi}$ is the ρ - 2π coupling constant, related to the ρ width as follows:

$$\Gamma(\rho \to \pi\pi) = \frac{g_{\gamma\pi\pi}^2}{4\pi} \cdot \frac{m_\rho}{12} \cdot \left[1 - \frac{4 m_\pi^2}{m_\rho^2} \right]^{3/2} \qquad (3.6)$$

In order to interpret the experiments one starts from the directly measured cross section at resonance:

$$\sigma(E_R) = \pi \lambda^2 (2J+1) \frac{\Gamma(\rho \to e^+e^-)\, \Gamma(\rho \to \pi\pi)}{\Gamma_{tot}^2(\rho)} \qquad (3.7)$$

Noting that

$$\Gamma(\rho \to \pi\pi) \approx \Gamma_{tot}(\rho), \quad \lambda = \frac{2}{m_\rho}, \quad J = 1$$

we have at resonance

$$\sigma(E_R) = \frac{12\pi}{m_\rho^2} \cdot \frac{\Gamma(\rho \to e^+e^-)}{\Gamma_{tot}(\rho)} = \frac{12\pi}{m_\rho^2} \cdot B \qquad (3.8)$$

Both methods, leptonic decay of vector mesons and storage ring experiments, can therefore be said to give the branching ratio B as the directly measured quantity. The coupling constant γ_ρ can then be obtained with the help of Equ. (3.3), which requires the knowledge

of $\Gamma(\rho)$. This introduces an additional uncertainty, since one obtains different values of $\Gamma(\rho)$ depending on the type of experiment and on the shape of the resonance assumed for fitting the data. For example, Gounaris and Sakurai (40) give, instead of Equ. (3.5), the following expression for the form factor near resonances which should account for the finite ρ width:

$$F_\pi(E) = \frac{m_\rho^2 (1 + d \cdot \Gamma_\rho / m_\rho)}{m_\rho^2 - 4E^2 - i m_\rho \Gamma_\rho (k/k_\rho)^3 \cdot m_\rho / 2E} \qquad (3.9)$$

d = O.48 for m_ρ = 775 MeV, it is a moderately complicated function of m_ρ.

The storage ring experiment at Orsay gave (41)

$$m_\rho = 760 \pm 5.5 \text{ MeV} \qquad \Gamma_\rho = 112 \pm 11.5 \text{ MeV}$$

from a fit to the form factor Equ. (3.5), and

$$m_\rho = 770 \pm 4 \text{ MeV} \qquad \Gamma_\rho = 111 \pm 6 \text{ MeV}$$

from a fit to Equ. (3.9)

A summary of recent experimental results on the branching ratios for leptonic decays of vector mesons and on the coupling constants γ_V is given in Table 4.* There are still difficulties with the values of γ_V^2 for all three vector mesons:

ρ meson: The measurements of the leptonic decays have a possible contribution from $\omega \to e^+e^-$, in addition there is some doubt on the width of the ρ. Moreover the measurement of Ref. (46) is not in good agreement with the rest of the measurements.

ω meson: The measurements from CERN and Orsay disagree by not quite two standard deviations.

ϕ meson: The calculation of the leptonic branching ratio from the

* For a complete listing of all references see Ref. 52.

storage ring experiments requires knowledge of the decay branching ratios of the ϕ into $K^o_L K^o_S$, $K^+ K^-$ and $\pi^+\pi^-\pi^o$ about which there is still some controversy, since the storage ring values for the branching ratios are not in good accord with the 'world data' (52).

In this situation the calculation of a 'best' value for the branching ratios and of their errors from these measurements requires some optimism and guesswork - the result of this is also shown in Table 4.

Values for the coupling constants following from these values and from Equ. (3.3) are given in Table 5. They are compared with various theoretical predictions.

The simplest prediction from SU_3 plus a mixing angle of $\cos\Theta = \sqrt{2/3}$ from SU_6 gives $1/\gamma_\varsigma : 1/\gamma_\omega : 1/\gamma_\phi = 3 : 1 : -\sqrt{2}$.

Various models of mass breaking in SU_3 lead to modifications from these numbers. They are listed in Table 5. Because of the statistical and systematic errors of the data, none of these schemes can be firmly excluded at present, although Sakurai's predictions seem to disagree most with the data. A quark model calculation (55) reproduces the data fairly well, the slight discrepancies are presumably not to be taken seriously due to the limited accuracy of the measurements and of the model.

One can derive a relation between the coupling constants from Weinberg's first sum rule (56).

$$m_\varsigma \Gamma(\varsigma \to e^+e^-)/3 = m_\omega \Gamma(\omega \to e^+e^-) + m_\phi \Gamma(\phi \to e^+e^-)$$

Fig. 5 shows a test of this relation in graphical form.
It is satisfied within the errors.

3.3 Photoproduction of Vector Mesons on Hydrogen

Reactions: $\gamma p \to p\rho^0$
$p\omega$
$p\phi$

A summary of total cross sections as a function of photon energy for the three vector mesons is given in Fig. 6. The ρ^0 and ϕ cross sections are fairly independent of photon energy above about 2 GeV. This is taken as evidence for the diffractive nature of these reactions. For the ω cross section there seems to be a substantial non-diffractive part at lower energy. Therefore the magnitude of the diffractive part of the ω cross section can only be roughly guessed at present. One obtains (57)

$$\sigma_{diff}(\gamma p \to p\omega) \approx (1.9 \pm 0.9)\,\mu b$$

In the spirit of a diffraction model one fits the differential cross sections for ρ^0 and ϕ production to the relation

$$d\sigma/dt = d\sigma/dt\ (0) \cdot \exp\left[-B \cdot |t| \right]$$

Figures 7 and 8 show a summary of results of measurements made at various energies.

Independent evidence for the diffractive nature of ρ^0 production on hydrogen comes from a measurement with linearly polarized photons (68); for diffractive production the polarization vectors of photon and ρ^0 meson are parallel. In the ρ^0 meson CMS system, its decay angular distribution into $\pi^+\pi^-$ is proportional to $(\vec{\varepsilon} \cdot \vec{p}_\pi)^2$. If one measures the yield of decay pions in a direction parallel ($\sigma_{\parallel}$) and perpendicular ($\sigma_{\perp}$) to the polarization of the photon, the diffraction model predicts $\sigma_{\perp} \gtrsim 0$ and

$$\Sigma = \frac{\sigma_{\parallel} - \sigma_{\perp}}{\sigma_{\parallel} + \sigma_{\perp}} = 1$$

Figure 9 shows the result for a photon energy of 2.0 - 2.8 GeV. It is consistent with pure diffraction production.

Another check can be made by comparing ρ^0 photo production on the proton and the deuteron. Measurements made at Cornell (63) indicate that the ρ^0 production has a small but noticeable non-diffractive part. However, the effect is not very big and the uncertainties in treating the nuclear physics of the deuteron are such that it appears difficult to make a quantitative estimate of the effect. Measurements made with the deuterium bubble chamber at DESY (70) indicate, that ρ^0 production on the proton and the neutron is equal and consistent with pure diffraction production, with an accuracy of about 20 % (from measurements of the reactions $\gamma d \to d\rho^0$ and $\gamma d \to p n \rho^0$). Additional evidence for the diffractive nature of ρ^0 production comes from the fact, that the deuterium bubble chamber results show a very small cross section for $\gamma d \to pp\rho^-$, which cannot proceed by diffraction, as opposed to $\gamma d \to$ [illegible].

3.4 ρ^0 Photo-Production on Heavy Nuclei

The complications introduced by nuclear physics are very evident for the interpretation of ρ^0-photoproduction on heavy nuclei. The cross section as a function of the mass number A of the nucleus can be fitted to a diffractive optical model of ρ^0 production inside a heavy nucleus. The A dependence of the forward cross section depends - among other things - on the absorption coefficient of ρ^0 mesons inside nuclear matter. In principle these experiments allow one to get the total ρ^0-nucleon cross section $\sigma(\rho N)$ In practice it turns out that the result depends appreciably on the details of the nuclear model used.

Table 6 summarizes the results of three experiments (made at Cornell (71), DESY (73) and SLAC (74). It is very difficult to compare directly the experimental data of the groups, since they were obtained at different energies. Therefore, it is not clear, how much of the discrepancies between the values of $\sigma(\rho N)$ should be attributed to differences in the treatment of the data and how much to discrepancies between the data. For examble, Bulos et al. (74) mention, that they get a value $\sigma(\rho N) = 30$ mb if they treat the data of Mc. Clellan et al. (71) by their method of analysis, whereas Mc. Clellan et al. themselves quote $\sigma(\rho N) = 38 \pm 3$ mb as their best value.

From the evidence of table 6 we may therefore only conclude, that the total ρ- N cross section is somewhere between 30 mb and 38 mb. It is interesting to note, that the quark model predicts:

$$\sigma(\rho N) = 1/2\ (\sigma(\pi^+ N) + \sigma(\pi^- N)\ ) \approx 28 \text{ mb at } 4 \text{ GeV}.$$

3.5 Comparison of Vector Meson Production with the Vector Meson Dominance Model:

Application of Equ. (3.2) to ρ production gives:

$$\left.\frac{d\sigma}{dt}\right|_{t=0} (\gamma p \to \rho p) = \frac{\alpha\pi}{\gamma_\rho^2} \cdot \left.\frac{d\sigma}{dt}\right|_{t=0} (\rho p \to \rho p) \qquad (3.10)$$

Assuming that the forward ρ-p scattering is purely diffractive, we get by applying the optical theorem:

$$\left.\frac{d\sigma}{dt}\right|_{t=0} (\gamma p \to \rho p) = \frac{\alpha}{16\gamma_\rho^2} \cdot \sigma_{tot}^2 (\rho p) \qquad (3.11)$$

Equ. (3.11) depends on $\sigma^2(\rho p)$, which is not yet accurately enough known. Similar considerations can be made for the ω and ϕ mesons. Table 7 lists experimental values for $\left.\frac{d\sigma}{dt}\right|_{t=0}$ for all three vector mesons

and gives values for the coupling constants $\gamma_V^2/4\pi$ for various assumptions about the vector-meson-nucleon cross sections, using Equ. (3.11).
Furthermore these values of $\gamma_V^2/4\pi$ are compared with the values for the coupling constants given in the summary Table 5, to see whether they are equal.
Comments: The test is inconclusive for the ρ meson, due to the large uncertainties for the ρ N-cross section. Inserting the quark model value of 28 mb would give good agreement. For the ω meson, the good agreement with the vector dominance model cannot be taken to be significant, since both $d\sigma/dt$ (diffractive) and $\sigma(\omega N)$, which enter, are mere guesses. It is very interesting that we get approximate agreement for the ϕ meson, using a rather small value for the ϕ-nucleon cross section, which comes out from the quark model and from measurements on ϕ production on heavy nuclei by the DESY-MIT group (75).
Equation (3.11) can also be applied to ρ' production on heavy nuclei. The difficulty here is again the sensitivity on $\sigma(\rho'$-Nucleus), which must be calculated from an optical model of the nucleus. The results of the analysis from three experiments are given in Table 6. One result agrees with $\gamma_{\rho'}^2/4\pi \approx 0.5$ obtained from the leptonic ρ' decay and the storage ring experiments. The other two results give $\gamma_{\rho'}^2/4\pi \approx 1.0$ and disagree by about a factor two. At least a part of the discrepancy is most likely due to the uncertainties in the treatment of the nuclear physics of the experiments. This treatment was different in all three experiments. There might also be discrepancies in the absolute normalization of the three experiments, also this is difficult to ascertain, because they were done at different energies. In view of these difficulties, it is not yet possible to draw firm conclusions on the validity of the vector dominance model from the results of Table 6.

3.6 Total Hadronic Cross Section for Photoproduction.

The total cross section for the protoproduction of hadrons on protons has been measured at DESY and SLAC at various energies in a series of experiments. The SLAC hydrogen bubble chamber made a measurement at 7.5 GeV in an almost monochromatic photon beam derived from the annihilation of positrons (76). The other experiments used tagged photon beams together with bubble chambers (77) or counter arrangements (78) to detect photoproduction events. The total cross section on the deuteron has also been determined (78). Fig. 10 shows a summary of these data. The cross sections fall slightly with increasing energy. The energy behavior is consistent with the one of $\sigma(\pi^+ p) + \sigma(\pi^- p)$, which is connected with $\sigma(\gamma p)$ via the vector dominance and the quark model. Below 2 GeV there appear inconsistencies in the data, which indicate the presence of systematic errors. This requires further experimental study. The vector dominance model allows one to derive the following relation by applying the optical theorem for forward compton scattering on the proton (79):

$$\sigma_{tot}(\gamma p) = \sqrt{4\pi\alpha} \sum_{V=\rho,\omega,\phi} \left[\frac{d\sigma}{dt}(\gamma p \to V p)\Big|_{t=0} \cdot \left(\frac{\gamma_V^2}{4\pi}\right)^{-1} \right]^{1/2} \quad (3.12)$$

This is an exact relation without further assumptions, if the amplitudes for photoproduction of vector mesons in the forward direction were purely diffractive. Fortunately, the main contribution in the sum comes from the ρ meson, where this assumption seems well justified. Equ. (3.12) has been evaluated with vector meson cross sections $d\sigma/dt$ from Figs. 7 and 8 for ρ and ϕ, and making the guess $\frac{d\sigma}{dt}(\text{diffractive})\Big|_{t=0} \approx 20\,\mu b/\text{GeV}^2$ for the ω. Values for γ_V were taken from Table 5 and the contributions from all three vector mesons added with the same sign.

The resulting prediction for $\sigma(\gamma p)$ is included in Fig. 10. There is agreement with the experimentally measured cross section, with $\gamma_\rho^2/4\pi$ = 0.5.

3.7 Photoproduction of Pseudoscalar Mesons at High Energies-Survey.

Reactions:

$\gamma p \to n\pi^+$
$p\pi^0$
$\Delta^{++}\pi^-$
$p\eta$
pX^0

$\gamma p \to K^+\Lambda$
$K^+\Sigma^0$

$\gamma n \to p\pi^-$

Figure 11 shows a survey of total cross sections. The data at high energies from SLAC (86, 87, 102) are actually measurements in the forward direction only. The total cross section was inferred from these measurements by a reasonable extrapolation of the differential cross section. This should not introduce a large error, since the contribution at large angles is small. Above a few GeV the cross sections depend on photon energy roughly like $\sigma(k) \sim$ const./k^2 (80). It reminds one of the $\bar{\sigma} \sim$ const/$p_L^{1.6}$-dependence found by Morrison (82) for quasi two-body hadron collisons proceeding by non-strange meson exchange.

3.8 The Reactions $\gamma p \to h\pi^+$ and $\gamma h \to p\pi^-$:

The differential cross sections for both reactions at high energies are presented in Figs. 12 and 13.

The sharp peak of the differential cross section in the forward direction has drawn wide attention in connection with the Regge pole model. The sharpness of the peak indicates that it has something to do

with pion exchange. Since pion exchange alone would give a dip in the forward direction, the peak was taken as evidence for Regge conspiracy. A number of fits to the data were made, which included a reggeized pion and a pion conspirator (89). The difficulty of these models is, that via factorization they predict (90) a forward dip of the differential cross section in the reaction $\pi^+ p \rightarrow \Delta^{++} \rho^0$, which was experimentally not found (91). This difficulty is avoided by introducing more Reggepoles or by introducing cuts. For example, Froyland and Gordon (83) made a fit to the data, which used evading π and ρ trajectories, an evading ρP cut and a conspiring πP cut. The results of this model are included in Figs. 12 and 13. It gives also a good fit to the asymmetry parameter for π^+, obtained with polarized photons, which are shown in Fig. 14. The model has a large number of parameters, however, it describes quite well all differential cross sections, both π^+ and π^-, at all energies and also the polarization data π^+. It will be interesting to see the result for the π^- polarization, which might require a further refinement of the model. Another approach, using also Regge cuts, was made by Blackmon et al. (92). They have a smaller number of parameters, since they introduce the cuts via absorptive corrections to π and A_2 exchange. They get also reasonable fits to the data. Their result for the polarization is included in Fig. 14.

3.9 Comparison of charged Pion Production with the Vector Dominance Model

Single pion photoproduction and ρ^0 and ω production in pion-nucleon collisions are connected by the following relation, which uses besides vector dominance only detailed balance and isospin invariance in strong interactions (95, 96):

$$\sigma\begin{pmatrix}\gamma p \rightarrow n\pi^+ \\ \gamma n \rightarrow p\pi^-\end{pmatrix} = \frac{\alpha\pi}{\gamma_\rho^2} \cdot \frac{\vec{p}_\pi^{\,2}}{\vec{p}_\rho^{\,2}} \left[\sigma(\pi^- p \rightarrow \rho^0 n) \cdot \xi_{\pi}^{\rho} + \frac{1}{q}\sigma(\pi^+ n \rightarrow \omega p) p_\pi^\omega\right]$$

$$\pm \text{ interference terms} \qquad (3.13)$$

In Equ. (3.13) the SU_3 relation between γ_ρ^2 and γ_ω^2 is assumed, and the ϕ contribution is neglected. The quantities ρ_{11}^ρ and ρ_{11}^ω are the elements of the ρ and ω decay matrix in the reactions $\pi^- p \to \rho^0 n$ and $\pi^+ n \to \omega p$.

For a practical application of Equ. (3.13) it is advantageous to consider the sum $[\sigma(\gamma p \to n\pi^+) + \sigma(\gamma n \to p\pi^-)]$ because then the poorly known ρ-ω interference term cancels.

Using polarized photon beams allows one to check also a relation for the asymmetry A:

$$A = \frac{(\sigma_\perp(\pi^+) + \sigma_\perp(\pi^-)) - (\sigma_{\parallel}(\pi^+) + \sigma_{\parallel}(\pi^-))}{(\sigma_\perp(\pi^+) + \sigma_\perp(\pi^-)) + (\sigma_{\parallel}(\pi^+) + \sigma_{\parallel}(\pi^-))}$$

$$= \frac{\sigma(\rho) \cdot \rho_{1-1}^\rho + 1/9\, \sigma(\omega)\, \rho_{1-1}^\omega}{\sigma(\rho)\, \rho_{11}^\rho + 1/9\, \sigma(\omega)\, \rho_{11}^\omega} \qquad (3.14)$$

$\sigma_\perp$ and $\sigma_{\parallel}$ refer to pion production with the production plane perpendicular and parallel to the photon polarization vector, respectively.

In Equ. (3.13) and (3.14) the left hand sides are completely known from photoproduction experiments, and the right hand sides from bubble chamber experiments. For the evaluation of the decay matrix elements ρ_{ik} one has to consider the ambiguity in the choice of the quantization axis discussed in Sec. (3.1). The intuitive choice of the ρ direction of flight in the overall CMS for this axis leads to complete disagreement with Equ. (3.14). Bialas and Zalewski (97) pointed out the ambiguity in the choice of the quantization axis and suggested the used of the Donohue-Högaasen system (98).

This is a system, in which Re $\rho_{10} = 0$ and ρ_{1-1} / ρ_{11} = maximum, i.e. A = maximum. This is the best one can do in trying to overcome the disagreement mentioned above.

Figures 15 and 16 show a test of Equ. 3.13 and 3.14 with a compilation of data made by Krammer and Schildknecht (96, 99). Considering the difficulties of extracting the required data from bubble chamber measurements, the prediction of Equ. 3.14 for the asymmetry appears well fulfilled - see Fig. 16. The cross section $\sigma_\perp(\pi^+) + \sigma_\perp(\pi^-)$ is plotted in Fig. 15. By this choice one eliminates the ambiguity due to the choice of the quantization axis, since this cross section depends on the combination $\rho_{11} + \rho_{1-1}$. From Fig. 15 it is evident, that there is a disagreement for the choice $f_\rho^2/4\pi = 0.5$. In order to bring the two sets of data into approximate agreement one must choose $f_\rho^2/4\pi \approx 0.3$.

In the meantime new accurate bubble chamber data $\pi^- p$ at 4 GeV have become available (100). An evaluation of these same data by different authors (100) gave conflicting results for the value of $f_\rho^2/4\pi$. This situation requires further study, however, it is safe to say, that also these new data require a $f_\rho^2/4\pi < 0.5$, maybe $f_\rho^2/4\pi \gtrsim 0.3$.

3.10 The Reaction $\gamma p \to \pi^o p$

Figure 17 shows the differential cross section for π^o photoproduction for a number of photon energies (101, 102). In contrast to π^+ and π^- photoproduction the cross section drops in the forward direction.
(A sharp peak at zero degrees is due to the Primakoff effect and can be quantitatively related to the π^o life time (103).

Invariance under charge conjugation C excludes a number of particle exchanges in the t-channel. Among the well established meson only the following can contribute: ρ, ω, ϕ, B .

If one estimates coupling constants from SU_3 one finds, that the ω should make the biggest contribution, with a small contribution from ϕ and B, and a negligible contribution from the ρ. Regge pole fits with a Regge ω + some background from a ϕ or B Regge trajectory gave acceptable fits to the data of Ref. (101), and accounted very nicely for the dip in the data at $|t| \approx 0.5$ $(GeV/c)^2$ in terms of a zero of the trajectory $\alpha(t)$ of the ω meson. However, high energy data (102) showed, that the dip becomes less pronounced at high energy. This is hard to understand in a simple pole model, because the ω trajectory, being the highest, should become more and more important at high energies and make the dip more and more pronounced. An even more serious difficulty for this model is seen in Fig. 18 which shows π^0 production with polarized photons (104). Even at the position of the dip the exchange of natural spin-parity dominates (R = 1). According the simple pole model the ω contribution should vanish at the dip, and leave one with exchange of natural spin-parity. According to an argument by Stichel (105) this should lead to a value for the polarization R = -1, in obvious disagreement with the data.

In consequence, Regge pole models using cuts have been made for this process. The results of two such calculations are included in Figs. 17 and 18 as examples. Blackmon et al. (106) use a Regge model with ω and B-meson exchange with absorptive corrections. Fryland (107) uses an ω trajectory and an ωP cut. The authors succeed in reproducing the trend of the data reasonably well.

3.11 The Reaction $\gamma p \to \Delta^{++} \pi^-$:

Fig. 19 shows the differential cross section for this reaction for various energies. At high energies the data are quite consistent with a universal dependence of the cross section on photon energy k and momentum

transfer t of the form: $d\sigma/dt = f(t)/k^2$. For small momentum transfers $/t/ < 0.04\ GeV^2$ there is reasonable agreement with an OPE model with minimal gauge invariant extensions (110).

3.12 The Reactions $\gamma p \to K^+\Lambda$ and $K^+\Sigma^0$

Fig. 20 shows the differential cross section at high energies (111). The reactions allow interesting applications from SU_3 and the quark model: assuming SU_3 invariance and U-spin zero for the photon, one obtains relations between photoproduction amplitudes. One of them is shown in the form of a triangle inequality between cross sections in Fig. 21.

It is satisfied, if $-1 \leq \cos\phi \leq +1$. Fig. 21 shows $\cos\phi$ as a function of momentum transfer. At large values of $|t|$ the data are consistent with SU_3, but at small values there is a violation. A possible reason might be the SU_3 breaking due to the mass differences of mesons exchanged in the t-channel. Fig. 21 shows also the ratio of the cross sections $\sigma(\Lambda K^+)/\sigma(\Sigma^0 K^+) = R$. The quark model predicts R = 27 in the forward direction, and $R > 3$ at non-forward angles, assuming additivity (112). This prediction is apparently not fulfilled. Maybe this can be attributed to strong final state interactions.

3.13 Low Energy Data.

It is unfortunate, that most of the very interesting low energy data cannot be covered here. This shortcoming should be partly compensated by a number of excellent review papers on low energy pion production (113). I shall mention only Walker's recent compilation of data on single π^+, π^- and π^0 photoproduction up to photon energies of 1.3 GeV (114). He fitted all differential cross sections and the polarization in terms of a simple model, in which the amplitude consists of three contributions: 1) Born terms with electric coupling only 2) Breit-Wigner resonances 3) additional background contributions in the low partial waves J = 1/2, 3/2, 5/2. Table 8 shows the strengths of

the contributions of the various resonances according to these fits. It is not clear, how unique these fits are. Further polarization measurements should be very useful to settle this question. One important question, which is still not settled, concerns the photo-excitation of the P_{11} (1470). Up to now, no indication of this resonance in the reaction $\gamma n \to p\pi^-$ was found, which indicates that the P_{11} is not the member of an (exotic) $\overline{10}$ decuplet.

The importance of this work is, among others, demonstrated by its use in a number of applications for sum rules. As an important example we quote the application to finite energy sume rules, which connect low-energy with high energy data.

In a number of applications to π^+ photoproduction the low energy data were connected with Regge model parametrizations of high energy data. It was shown (116), that Regge fits with a pion conspirator are consistent with low energy data. However, Jackson and Quigg (117) have pointed out, that consistency within the FESR can be obtained for a wide class of models parametrizing the high energy data. Therefore the use of FESR cannot discriminate between different high-energy models. As a matter of fact, Jackson and Quigg used a very simple phenomenological parametrization of the high energy data and showed, that then the low energy data predict the high energy data very well via FESR. This is exemplified by a prediction of the polarization, which is shown in Fig. 14 and is seen to deviate very little from Fjyland's and Gordon's fit.

3.14 Survey of Tests of the Vector Dominance Model.

A simple but of course not sufficient way to state these tests consists in listing the value of the photon-Vector meson coupling constant f_V ,

which is required to fit various processes and to see, whether the coupling constant comes out the same in all cases. Table 9 gives a survey of those tests which use reasonably few additional assumptions.

Comments: Process No. 1 (ρ leptonic-decay) may be considered to define $\gamma_\rho^2/4\pi \approx 0.5$. Test No. 2 depends strongly on the value of the ρ -nucleon cross section used, which is not known with sufficient precision. Until the nuclear physics entering in this determination is better understood, process No. 2 may not provide an unambiguous test. The same is true for process No. 6. Process No. 3 is free from this uncertainty and is unambiguous. Its accuracy is limited by the ω and ϕ contributions, which amount to about 20 % and which are poorly known. Process No. 4 is unambiguous. It requires a coupling constant which is smaller than the one following from process No. 1 by about a factor 1.6. This might give one an indication of the accuracy with which the VDM is expected to hold in practical applications. Process No. 5 requires the assumption of ρ dominance of the pion form factor:

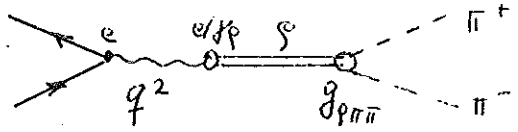

This form factor, evaluated according to standard Feynman rules, is

$$F_\pi(q^2) = \frac{g_{\rho\pi\pi}}{2\gamma_\rho} \cdot \frac{m_\rho^2}{m_\rho^2 - q^2}$$

$F_\pi(0) = 1$ by definition, therefore

$$g_{\rho\pi\pi}^2/4\gamma_\rho^2 = 1$$

The coupling constant $g_{\rho\pi\pi}$ can be evaluated from the ρ width and Equ. (3.6). With Γ_ρ = 110 MeV one gets $g_{\rho\pi\pi}^2/4\pi = 2.1 \pm 0.1$

With the value $\gamma_\rho^2/4\pi$ from Table 5 one gets for the ratio

$$g_{\rho\pi\pi}^2/4\gamma_\rho^2 = 1.03 \pm 0.16$$

This agrees well with the predicted ratio of one.

Process No. 7: This requires the assumption of ρ dominance in the ω decay:

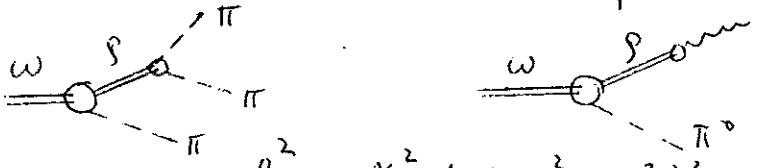

$$\Gamma(\omega \to \pi\gamma) = \frac{\alpha}{96} \cdot \frac{f_{\rho\omega\pi}^2}{4\pi} \cdot \left(\frac{\gamma_\rho^2}{4\pi}\right)^{-1} \cdot \frac{(m_\omega^2 - m_\pi^2)^3}{m_\omega^3}$$

$$\Gamma(\omega \to 3\pi) = \frac{g_{\rho\pi\pi}^2}{16\pi} \cdot \frac{f_{\rho\omega\pi}^2}{4\pi} \cdot \frac{(m_\omega - 3m_\pi)^4}{(m_\rho^2 - 4m_\pi^2)^2} \cdot \frac{m_\omega m_\pi^2}{\sqrt{27}} \cdot W(m_\omega)$$

W (ω) = correctionfactor for relativistic kinematics = 3.56

The branching ratio $\Gamma(\omega \to \pi\gamma)/\Gamma(\omega \to 3\pi)$ is independent of the coupling constant $f_{\rho\omega\pi}$. From the experimentally known value of the branching ratio (52) the value of $\gamma_\rho^2/4\pi$ can be calculated. It does not agree well with Reaction No. 1, 3 and 4. However, the test is at most as reliable as the doubtful assumptions needed for the ω-decay mechanism.

If one is willing to admit even further leading assumptions, one can make a number of further tests. However, if the tests fail, it is not clear if the VDM is to blame. Examples:

One can compare the following reactions:

$\gamma p \to p\pi^0$ with $\pi^- p \to \rho^- p$, $\pi^+ p \to \rho^+ n$, $\pi^- p \to \rho^0 n$, $\pi^- p \to \omega n$ / $\pi^+ n \to \omega p$ (118)

$\gamma p \to \Delta^{++}\pi^-$ with $\pi^+ p \to \Delta^{++}\rho^0$ (108)

$\gamma p \to$ many pions with $\pi^\pm p \to$ many pions (57)

It is well known, that the simplest application of the VDM to the nucleon form factors leads to trouble (see sect. 4.2). Maybe this is because the proton is more complicated than the pion and the assumption of a simple pole model for the form factors are just not valid. All these applications give results which range from agreement with the VDM to obvious, but never order of magnitude disagreement. This does not mean too much. The only reasonably reliable tests should be No. 3 and No. 4.

4. Elastic and Inelastic Electron-Nucleon Scattering

4.1 Survey of Elastic Scattering

Elastic electron-nucleon scattering is des cribed , in lowest order of the electromagnetic interaction, by the Rosenbluth formula:

$$\frac{d\sigma}{d\Omega} = \sigma_{NS} \cdot \left[\frac{G_E^2(q^2) + \tau G_M^2(q^2)}{1+\tau} + 2\tau G_M^2(q^2) \tan^2 \theta/2 \right] \quad (4.1)$$

$$\sigma_{NS} = \left(\frac{e^2}{2E_0}\right)^2 \cdot \frac{\cos^2 \theta/2}{\sin^4 \theta/2} \cdot \frac{1}{1 + \frac{2E_0}{M} \sin^2 \theta/2}$$

$$\tau = q^2/4M^2$$

$$q^2 = \frac{4E_0^2 \sin^2 \theta/2}{1 + \frac{2E_0}{M} \sin^2 \theta/2}$$

E_0, θ = energy, scattering angle of the electron in the laboratory system.

The validity of the Rosenbluth formula has been tested by: 1) checking the dependence of the square bracket in Equ. (4.1) on $\tan^2 \theta/2$ (Rosenbluth plot), 2) by comparing e^-p scattering with e^+p scattering (sensitive to the real part of a two photon contribution), 3) by looking for a polarization of the recoil proton (sensitive to the imaginary part

of a two photon contribution). These tests have up to now not shown any significant inconsistency with the Rosenbluth formula (120)(119).

The quantities G_E^p, G_E^n and G_M^p, G_M^n are the electric and magnetic formfactors of the proton and neutron, respectively. They can also be decomposed in terms of an isovector and an isoscalar formfactor:

$$G_V = 1/2 \ (G^P - G^n)$$

$$G_S = 1/2 \ (G^P + G^n)$$

For $q^2 = -4M^2$, which is of course not accessible by elastic scattering, one has the constraint

$$G_E^{p,n}(-4M^2) = G_M^{p,n}(-4M^2) \qquad (4.2)$$

The electric or magnetic charge radius is obtained from the mean square radius:

$$\langle r_{E,M}^2 \rangle = -6 \cdot \frac{dG_{E,M}(q^2)}{dq^2}\Big|_{q^2=0} \qquad (4.3)$$

As a first orientation the behavior of the form factors is given by the 'scaling law':

$$G_E^p(q^2) \approx \frac{G_M^p(q^2)}{\mu_p} \approx \frac{G_M^n(q^2)}{\mu_n} \qquad (4.4)$$

The universal function of q^2, which these three form factors obey, is roughly given by

$$G_E^p(q^2) \approx \frac{1}{(1 + q^2/0.71\ GeV^2)^2} \qquad (4.5)$$

('dipole formula').

The data can be conveniently discussed in terms of deviations from Equ. (4.4) and (4.5).

One also notices, that a strict validity of Equ. (4.4) would contradict Equ. (4.2), which is believed to be exact.

One gets the q^2 dependence of G_E^n near $q^2 = 0$ from scattering of thermal neutrons on atoms. The value of the slope is given by (121)

$$\left.\frac{dG_E^n(q^2)}{dq^2}\right|_{q^2=0} = (0.50 \pm 0.01)\ \mathrm{GeV}^{-2}$$

This value is very close to the one expected from the Foldy-term:

$$\left.\frac{dG_E^n}{dq^2}\right|_{q^2=0} = \frac{G_M^n(0)}{4M^2} = 0.539$$

Figures 22 - 26 show the electric and magnetic form factors of proton and neutron (122). Figures (22 - 25) show the data for that range of q^2, for which a separation of G_E and G_M was possible. Figure 26 shows G_M^P out to very large values of q^2. It was obtained (123) with the assumption, that G_E^P contributes negligibly to the cross section in the experiment. This assumption is very probably well satisfied. The data for $G_M^{P,n}$ and for G_E^P are plotted normalized to the dipole fit. In this way deviations from the dipole fit become obvious. A fit of the form

$$G(q^2)\ (1 + q^2/0.71\ \mathrm{GeV}^2)^2 = (1 + a\,q^2 + b\,q^4 + \ldots) \cdot G(0)$$

was made (122) to the data at small q^2. (Dashed line in Figs. 22 - 25), from this fit and from Equ. (4.3) the magnetic and electric radii can be obtained.

$$\langle r_E^2(\text{proton}) \rangle = 0.672 \pm 0.025 \ f^2$$

$$\langle r_M^2(\text{proton}) \rangle = 0.712 \pm 0.013 \ f^2$$

$$\langle r_M^2(\text{neutron}) \rangle = 0.610 \pm 0.14 \ f^2$$

There are small apparent differences between these three radii which may, however, not yet be significant. If true they would mean a deviation from the scaling law at small q^2. It should be noted, that for G_M^n the analysis of the measurements requires large and somewhat uncertain corrections due to the nuclear physics of the deuteron. Therefore there may be additional systematic errors in the data, and the question of a significant deviation from the scaling law at small q^2 appears not yet settled.

At larger values of q^2 definite deviations from the scaling law for G_M^p are indicated. Very little is known at present about the electric form factor G_E^n of the neutron, apart from the slope at $q^2 = 0$.
For larger values of q^2 its value is consistent with being close to zero everywhere.

4.2 Interpretation of the Nucleon Formfactors:

Any interpretation should at least reproduce the most important gross properties of the form factors given in Equ. (4.2) - (4.5) and the smallness of G_E^n . The most obvious starting points are dispersion relations of the type

$$G(q^2) = 1/\pi \int \frac{\rho(x)}{q^2 + x} \, dx$$

Approximating the spectral functions in the dispersion integrals by δ-functions at the positon of the vector mesons leads to the following ansatz for the isoscalar and isovector form factors, which satisfies automatically the constraint Equ. (4.2):

$$G^{S}_{E,M} = \frac{a_1^{\omega} + \varepsilon a_2^{\omega}}{1 + q^2/m_{\omega}^2} + \frac{a_1^{\phi} + \varepsilon a_2^{\phi}}{1 + q^2/m_{\phi}^2} \qquad (4.6)$$

$$G^{V}_{E,M} = \frac{a_1^{\rho} + \varepsilon a_2^{\rho}}{1 + q^2/m_{\rho}^2}$$

$$\varepsilon = \begin{cases} -\tau & \text{FOR } G_E^{S,V} \\ 1 & \text{FOR } G_M^{S,V} \end{cases}$$

This simple ansatz has the most obvious fault, that it fails to reproduce the dipole fit behavior $G(q^2) \sim 1/q^4$ at large q^2. If one modifies Equ. (4.6) and goes to more complicated schemes, this difficulty can be avoided. Examples: 1) Introducing additional form factors for the three vector mesons (129, 35). A fit to the data is possible with three more form factors chosen to fit the data (130, 122). 2) Introducing a finite width for the vector mesons - leads to a moderately successful fit (126) - see Fig. 26. 3) Höhler et al. (131) have improved upon the pole approximation by considering a more realistic spectral function for the isovector form factor. They show, that the pole approximation is not adequate and they connect the pion form factor and π-N scattering with the nucleon form factor. They were able to fit the isovector form factor up to $q^2 \sim 1$ GeV^2 and reproduce the slope dG_E/dq^2 at $q^2 = 0$. Similarly, Di Vecchia and Drago (132), by considering higher mass states, as suggested by a Regge model, get reasonable fits for the function $G(q^2)$ defined in Equ. (4.4).

A second line of approach connects ep-scattering with p-p-scattering, as first suggested by Wu and Yang (133).

The simplest conjecture is

$$d\sigma/dt\Big|_{pp} \approx d\sigma/dt\Big|_{pp,\,t=0} \cdot \left(\frac{G_M^p(q^2=-t)}{G_M^p(0)}\right)^4$$

which might become exact for very large energies. For finite energies there are deviations. For more detailed considerations see e.g. Cho and Yang (128) and Drell et al. (134).

Models of this sort do not a priori satisfy Equ. (4.2).
There appear to be at least two riddles in the interpretation of the form factors:

1) How to understand intuitively the very steep q^2 dependence, as given approximately by the dipole fit, which is in contrast to the most naive expectation of Equ. (4.6). Drell has pointed out, that in the nonrelativistic limit, where one can work with the Schrödinger equation, the steep q^2 dependence follows rather naturally (135). Several authors have considered models for the proton, assuming a composite structure, which can also lead to a steep q^2 dependence (136).

2) Difficulty with the quark model:
In the non relativistic Fermi quark model of the proton the nucleon wave function is the product of a symmetric spin- U-spin wave function for the three quarks and of an antisymmetric wave function for the space part with S = O. In this model $|\psi(r_1, r_2, r_3)|^2$ at the origin is zero because of the antisymmetric space part of the wave function. It then follows that *

$$\int G(q^2) \cdot q^2 \, dq = 0$$

which means that the form factor has a zero somewhere, which, however, has not been seen experimentally so far. Three ways out of this difficulty have been suggested so far.

* It should be remembered, that this follows in a non relativistic quark theory.

(i) Quarks obey parastatistics. This eliminates the need for an antisymmetric space wave function (137). (ii) The zero is at very large values of q^2, which have not yet been reached (138). (iii) R.F. Meyer has shown (139), that one can find an antisymmetric wave function, which can be chosen singular enough in the origin in order not to lead to a zero in the form factor, and which on the other hand does not lead to physically unacceptable consequences.

4.3 Inelastic Electron-Scattering - Kinematics and Definitions

One of the difficulties encountered for inelastic electron-nucleon scattering are the many types of notation. We therefore start with a collection of useful formulae and consider the case that the inelastically scattered electron only is detected.

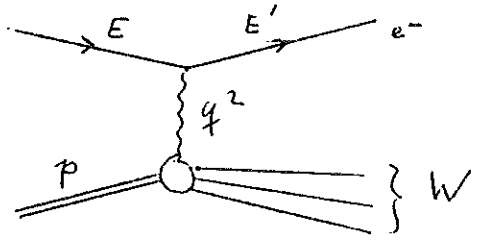

Let E and E^1 be initial and final electron energies, and θ its scattering angle (all in the lab. system). The differential cross section can be expressed in terms of two structure functions W_1 and W_2:

$$\frac{d^2\sigma}{dq^2 d\nu} = \frac{E'}{E} \cdot \frac{4\pi\alpha^2}{q^4} \cdot \left(\cos^2\theta/2 \; W_2(q^2,\nu) + 2\sin^2\theta/2 \; W_1(q^2,\nu) \right)$$

$$\frac{d^2\sigma}{dE' d\Omega} = \frac{4\alpha^2}{q^4} \cdot E'^2 \left(\cos^2\theta/2 \; W_2(q^2,\nu) + 2\sin^2\theta/2 \; W_1(q^2,\nu) \right) \qquad (4.7)$$

$\nu = E - E^1$

$q^2 = 4 EE' \sin^2 \theta/2$

M = nucleon mass

(Some people do not absorb a factor M into the definition of the W_1, W_2).
A few more important quantities are:
Total CMS energy of the final state hadrons W:

$$W = (M^2 + 2\,MK)^{1/2}$$

Equivalent photon energy K:

$$K = \nu - q^2/2\,M$$

Momentum transfer:

$$q^2 = |\vec{q}^{\,2}| - \nu^2$$

(Virtual) photon polarization:

$$\varepsilon = \left[\, 1 + 2\,(1 + \nu^2/q^2)\,\tan^2 \theta/2 \,\right]^{-1}$$

(Virtual) photon flux:

$$\Gamma_t = \frac{\alpha}{2\pi^2} \cdot \frac{K}{q^2} \cdot \frac{E'}{E} \cdot \frac{1}{1-\varepsilon}$$

The differential cross section can also be expressed by what is equivalent to the total cross sections for transversely and for longitudinally polarized photons σ_T and σ_S respectively:

$$\frac{d^2\sigma}{d\Omega\, dE'} = \Gamma_t \left(\sigma_T + \varepsilon\, \sigma_S \right) \qquad (4.8)$$

In the limiting case $q^2 \to 0$ σ_T goes towards the photoproduction cross section and $\sigma_S \to 0$.
This is the notation of Hand (140). One has also the notation (141)

$$\sigma_T = \frac{|\vec{q}|}{K} \sigma_{TRANS} \quad , \quad \sigma_S = - \frac{|\vec{q}|}{K} \sigma_{LONG}$$

The structure functions are related to the cross sections by

$$W_1(q^2,\nu) = \frac{K}{4\pi^2\alpha} \sigma_T(q^2,\nu) \qquad (4.9)$$

$$W_2(q^2,\nu) = \frac{q^2}{|\vec{q}|^2} \frac{K}{4\pi^2\alpha} (\sigma_T + \sigma_S)$$

4.4 Inelastic Scattering in the Region of the Nucleon Resonances:

Many experiments were made to study the inelastic electron spectrum at high energies (142, 143). Fig. 27 shows an example (143). The excitation of nucleon resonances near 1238 MeV, 1525 MeV, 1700 MeV and possibly 1920 MeV is evident.
Fig. 38 shows the quantity $\frac{i}{\Gamma_t} \cdot \frac{d^2\sigma}{d\Omega\, dE'} = \sigma_T + \varepsilon \sigma_S$ as a function of q^2 for various values of the total CMS energy W. To the extent to which $\varepsilon\sigma_S$ can be neglected compared with σ_T, it measures the q^2 dependence of the photoproduction cross section.

Among the nucleon isobars, only the Δ (1236) has up to now been closely examined. Bartel et al. (143) have parametrized the cross section around the Δ (1236) in a resonant (σ_R) and a non resonant (σ_B) part:

$$\frac{1}{\Gamma_t}\frac{d^2\sigma}{d\Omega\, dE'} = \sigma_R(q^2,\nu) + \sigma_B(q^2,\nu)$$

$$\sigma_R(q^2,\nu) = \frac{\alpha\pi}{W(W^2-M^2)}\,|\vec{q}|^2\,\frac{\Gamma_\Delta(W)}{(W-M_\Delta)^2+\Gamma_\Delta^2(W)/4}\cdot G_\Delta^2(q^2)$$

The quantity $G_\Delta(q^2)$ can be regarded as the magnetic dipole transition form factor for the excitation of the $\Delta(1236)$. It is shown in Fig. 29, together with the dipole fit and a prediction from Gutbrod and Simon (148) who have used a dispersion theoretic approach. Although the theory seems to account very well for the measured form factor, it is not clear to me, why it is so good, in view of the approximations made. Similar measurements, which also agree well with this theory have been made by Albrecht et al. (149).

A more detailed investigation of the $\Delta(1236)$ will require coincidence measurements to investigate the Δ decay.

Such measurements have been started and will allow in future a much more detailed analysis (150, 147).

For the $N^*(1520)$ and the $N^*(1688)$ cross sections as a function of q^2 were measured at SLAC (151).

4.5 Inelastic Scattering in the Deep Inelastic Region:

By deep inelastic region we will understand inelastic scattering for large values of q^2 and large values of the excitation energy W (above the resonance region). The main difficulty for evaluating the data in this region are the radiative corrections, which require the knowledge of the differential cross sections in a certain region of the (q^2, ν) plane for their application. The incomplete knowledge of these cross sections and the doubtful validity of the approximations in the formulae make final experimental data slow in coming and may eventually limit in principle the accuracy one can get.

In spite of these cautious remarks I shall present first results in this field, because they appear to be of the highest importance.

Presentation of the data has been affected by a paper by Bjorken (152), who conjectured that for large values of q^2 and ν the structure functions may essentially depend only on one variable $\omega = \nu / q^2$:

$$M W_1(q^2, \nu) \to F_1(\omega), \quad \nu W_2(q^2, \nu) \to F_2(\omega)$$

$$W_2 = 1/\sigma_{Mott} \cdot d^2\sigma/d\Omega dE' \cdot \left[1 + [2/(1+R)] \cdot (\nu^2/q^2 + 1) \cdot \tan^2 \vartheta/2\right]^{-1}, \text{ with}$$

$$R = \sigma_S / \sigma_T$$

$$\sigma_{Mott} = \frac{a^2 \cos^2 \vartheta/2}{4E^2 \sin^4 \vartheta/2}$$

For R = o and R = ∞ one has upper and lower limits of W_2:

$$\frac{\varepsilon}{\sigma_{Mott}} \cdot \frac{d^2\sigma}{d\Omega dE'} \leq W_2 \leq \frac{1}{\sigma_{Mott}} \cdot \frac{d^2\sigma}{d\Omega dE'}$$

In many practical cases $\mathcal{E} \approx 1$ and measurements at a single (small) angle give a good estimate for W_2. Fig. 30 shows a summary of preliminary measurements made at SLAC at high energies (151). They have plotted the quantity $\nu \cdot W_2$ for two extreme assumptions about R, showing that the uncertainty of its value makes a small effect.

Data at lower energies have been contributed by Albrecht et al. (154). They have succeeded in separating W_1 and W_2 (see Fig. 31). Unfortunately, the data do not go far into the region of interest, but they seem qualitatively consistent with the SLAC data (solid and dashed line in Fig. 32a). The data show the following features:

1) They seem to indicate that $\nu \cdot W_2 \approx$ const and $\frac{q^2}{\nu} \cdot W_1 \approx$ const, which behavior was suggested by Abarbanel et al. (155).

2) The data are in agreement (see Fig. 32b) with the prediction

$$W_1 / \nu \cdot W_2 = \nu / q^2$$

coming from a very interesting field theoretic model of Drell et al. (156).

It is very remarkable, that $\nu \cdot W_2$ seems indeed a function of ω only for $\omega = \nu / q^2 > 2\ \mathrm{GeV}^{-1}$, and moreover, seems to tend to a constant. This has a simple interpretation in terms of cross sections, if we assume for simplicity $\nu^2 \gg q^2$, leading to $K \approx \nu \approx |\vec{q}|$. We have then from Equ. (4.9)

$$\nu \cdot W_2 \ (q^2, \nu) \approx \frac{q^2}{4\pi^2 \alpha} \cdot (\sigma_T + \sigma_S) \approx \text{const.}$$

It means, that at high energies the cross sections are fairly independent of energy, which seems reasonable, and that they have a dependence like $1/q^2$

for large values of q^2, which seems very remarkable. This dependence on q^2 is much weaker than the $1/q^8$ dependence of the nucleon form factors, and also weaker than a $(m_\rho^2/(m_\rho^2+q^2))^2 \sim 1/q^4$ dependence from a naive vector dominance model.

Unfortunately, from the many comments made on this remarkable situation, we can mention here only two: 1) it has been pointed out, that in a vector dominance model σ_S depends on q^2 like $(m_\rho^2/(m_\rho^2+q^2))^2 \cdot q^2 \approx 1/q^2$ (157). If σ_S makes a big contribution to the measured cross sections, this could explain their relatively slow dependence on q^2. Sakurai's prediction:

$$R = \frac{\sigma_S}{\sigma_T} = \frac{\sigma_{\rho p}^{\parallel}(k)}{\sigma_{\rho p}^{\perp}(k)} \cdot \frac{q^2}{m_\rho^2} \cdot \left[1 - \frac{1}{2\omega m_\rho}\right]^2$$

The ratio $\sigma_{\rho p}^{\parallel} / \sigma_{\rho p}^{\perp}$ is expected to be ≈ 1, so Sakurai predicts a large longitudinal cross section σ_S for large values of q^2 and ω. The data (154) are at present compatible with this relation but it seems too early to say whether the measurements really support the model.

2) Drell et al.'s field theoretic model (156) can be adjusted, with a very plausible assumption on the maximum transverse momentum $p_\perp$ transmitted in a reaction to give the relation $\nu W_2 \approx$ const., from which follows $W_1 \approx \nu/q^2$, which seems consistent with the present data.

Sum rules for $W_2(\nu, q^2)$: Bjorken's derived from Adler's sum rule for inelastic neutrino scattering, says (158):

$$\int_0^\infty \left[W_2^{\text{proton}}(q^2,\nu) + W_2^{\text{neutron}}(q^2,\nu)\right] d\nu \geq 1/2$$

If νW_2 would really $\approx$ const, the intregral would diverge logarithmically and the sum rule would be trivially satisfied. Nevertheless, it is interesting to see, at which maximal energy it is saturated. If $W_2^{\text{neutron}} \approx W_2^{\text{proton}}$, this seems to be the case if one integrates in energy up to a few GeV (154).

Gottfried's sum rule is derived from an uncorrelated quark model of the nucleon (159). It reads:

$$\int_0^\infty W_2(q^2,\nu)\, d\nu = 1$$

A recipe has it (160), that one should take only the non diffractive part of W_2. This makes the test of the sum rule somewhat ambiguous. Inserting best guesses for W_2 gives values for the integral significantly smaller than one. A specialization of the equation for photoproduction seems consistent with the data.

Acknowledgement:

I am very thankful to Drs. R.D. Felst and P. Joos for making the results of their data compilation available to me.

I also thank Drs. M. Krammer, D. Schildknecht, R.D. Felst and Prof. S.C.C. Ting for many useful discussions.

Table 1

Values of the Fine Structure Constant α

Method	Ref.	Comments	$1/\alpha$
Deuterium fine Structure	4	If the recent measurement of the Lamb shift in D by Cosens[5] is taken, together with ref. 4 , one gets $1/\alpha$ = 137.0373 (6)	137.0388 (6)
Muonium hfs	12	Main uncertainty from μ magnetic moment	137.0368 (12)
Josephson effect	8		137.0359 (4)
Hydrogen Maser hfs splitting	10	Uncertain nuclear corrections	137.0359
Hydrogen fine structure $2S_{1/2} - 2P_{1/2}$ interval and Lamb shift	6	Metcalf et al.	137.0353 (8)
	7	Kaufman et al.	137.0350 (4)
dto.	7 Shyn et al.	α^{-1} calculated from their value $\Delta E_H - S_H$ = 9911.213 ± .053 MHZ	137.0361 (6)

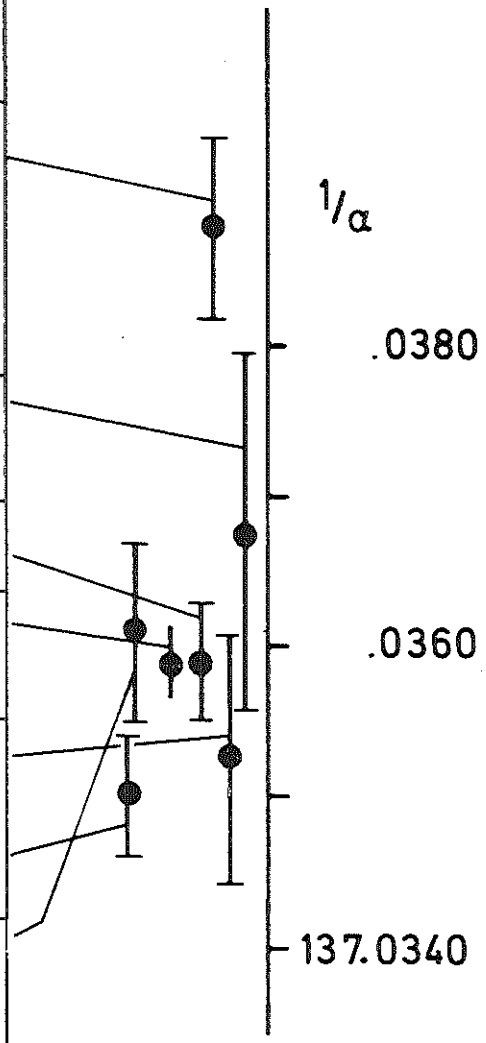

Table 2

Lamb shift

$S = (2\,S_{1/2} - 2\,P_{1/2})$ interval

	ref.	S (MHz)	Remarks
Experiment:			
Lamb and collaborators	14	1057.77 ± 0.05	'average' = 1057.81 ± 0.05
Robiscoe	15	1057.86 ± 0.05	
Theory	13	1057.57 ± 0.08	using a value $\alpha^{-1} = 137.0359$

Table 3

Anomalous Magnetic Moment

Author	$\frac{g-2}{2}$ experimental	$\frac{g-2}{2}$ theoretical	theoretical expression
CERN muon storage ring muon (16)	$(116616 \pm 31) \times 10^{-8}$	116560×10^{-8}	$\frac{\alpha}{2\pi} + 0.7658\frac{\alpha^2}{\pi^2} + 2.49\frac{\alpha^3}{\pi^3}$ + strong interaction corrections
Rich (17) electron	$(115956 \pm 3) \times 10^{-8}$	115964×10^{-8}	$\frac{\alpha}{2\pi} - 0.328\frac{\alpha^2}{\pi^2} + \sim 0.15\frac{\alpha^3}{\pi^3}$

Table 4

Leptonic Decays of Vector Mesons.

Particle	Ref.		$B = \frac{\Gamma(\ell^+\ell^-)}{\Gamma_{tot}} \times 10^5$	'average' B $\times 10^5$
ρ	42	Novosibirsk storage ring	5.0 ± 1.0	6.2 ± 0.5
	41	Orsay storage ring	6.63 ± 0.85	
	43	lept.decay e^+e^- : DESY-MIT	6.5 ± 1.4	
		lept.decay $\mu^+\mu^-$:		
	44	Wehmann et al. at AGS	5.6 ± 1.1	
	45	de Pagter et al. at CEA	$4.4 \; {}^{+2.1}_{-0.9}$	
	46	Lütjens et al. at CERN	$9.7 \; {}^{+2.0}_{-2.3}$	
ω	47	Orsay storage ring	7.6 ± 1.4	6.9 ± 1.4
	48	lept.decay e^+e^- CERN	4.0 ± 1.5	
ϕ	49	Orsay storage ring	39.6 ± 6.2	
	50	lept.decay DESY-MIT	29 ± 8	37 ± 6
	51	lept.decay CERN	61 ± 26	

Table 5

Summary of Results on Coupling Constants

Particle	$\Gamma(e^+e^-)/\Gamma_{tot}$ from Table 4 $\times 10^5$	Γ_{tot} used (MeV)	$\gamma_V^2/4\pi$ (Equ. 3.3)	γ_V^{-2} normalized to $\gamma_\varphi^{-2} = 9$	Predictions for γ_V^{-2}			$\Gamma(V \to e^+e^-)$ [keV]	
					SU_3	Sakurai (53)	DMO (54)	experimental	Ref. 55 Quark Model
φ	6.2 ± 0.5	110	0.50 ± 0.07	9	9	9	9	6.8 ± 1.0	5.7
ω	6.9 ± 1.4	12.6*	4.0 ± 0.9	1.1 ± 0.3	1	0.65	1.21	0.87 ± 0.19	0.61
ϕ	37 ± 6	3.9**	3.1 ± 0.7	1.5 ± 0.4	2	1.33	1.34	1.44 ± 0.32	0.95

* Ref. 52

** Average of Ref. 49 and Ref. 52

Table 6

Rho Production on Heavy Nuclei

Reference	Photon Energy GeV	Range of Nuclei investigated	σ_{tot} (ρ-Nucleon) mb	Comments	$\gamma_\rho^2/4\pi$
Cornell (71)	6.2	D - Pb	37.5 ± 1.4	Nuclear radius deduced from analysis of π-Nucleus cross sections (72).	
			35.0 ± 1.5	Nuclear radius deduced from e^--Nucleus cross sections.	
			39.0 ± 2.0	assuming vector dominance model	1.1 ± 0.15
DESY-MIT (73)	2.7 - 4.5	Be - Pb	31.3 ± 2.3	Nuclear radius deduced from analysis of the data themselves.	0.5 ± 0.1
SLAC (74)	8.8	Be - Pb	30^{+6}_{-4}	using hard-sphere nuclear model to get t=o cross sections, using Woods-Saxon form of nuclear density.	1.1 ± 0.2

Table 7

Test of Vector Dominance Model according to Equ. 3.11

Reaction	$d\sigma/dt\|_{t=0}$ [μb GeV^{-2}]	$\sigma_{V/N}$ assumed	Source of $\sigma_{V/N}$	$\gamma_V^2/4\pi$ from Equ. (3.11) (Vector Dominance)	$\gamma_V^2/4\pi$ from Table 5 (leptonic Decay)
$\gamma p \to \rho p$	140	30 mb	Table 6	0.59	0.50
		38 mb	Table 6	0.94	
$\gamma p \to \omega p$	≈ 20 *	30 mb	Quark Model	4.1	4.0
$\gamma p \to \phi p$	3	12 mb	Quark Model and Ref. 75	4.4	3.1

* estimate of diffractive part

Table 8

Isobars in Single Pion Photoproduction (114)

Resonant Helicity Element	Isobar	Isospin I, J^P	Mass GeV	Amplitude (μb)$^{1/2}$ for $\gamma p \rightarrow$		
				$\pi^+ n$	$\pi^0 n$	$\pi^- p$
A_{1+}	P_{33}	$3/2, 3/2^+$	1.236	1.000	1.414	1.000
B_{1+}	P_{33}	$3/2, 3/2^+$	1.236	-2.43	-3.43	-2.43
A_{2-}	D_{13}	$1/2, 3/2^-$	1.519	-0.20	0.14	0
B_{2-}	D_{13}	$1/2, 3/2^-$	1.519	-1.32	0.94	-1.15
B_{3-}	F_{15}	$1/2, 5/2^+$	1.672	-0.60	0.43	-0.50
A_{0+}	S_{11}	$1/2, 1/2^-$	1.561	-0.65	0.46	-0.80
A_{1-}	P_{11}	$1/2, 1/2^+$	1.471	-0.25	0.18	0
B_{2+}	D_{15}	$1/2, 5/2^-$	1.652	-0.14	-0.10	-0.14

Table 9

Test of Vector Meson Dominance Model

Process	$\gamma_\rho^2/4\pi$ obtained	m_ρ	No.	Remarks, Section
$B = \Gamma_\rho(e\bar{e})/\Gamma_\rho$ from storage ring and ρ leptonic decay	0.5	on mass shell	1	See Table 5, (3.2)
$d\sigma/dt\,(\gamma p \to \rho p)$ vs. $\sigma_{tot}\,(\rho p)$	0.5-1.0	0	2	depends on value used for $\sigma_t(\rho p)$ - still in doubt, (3.5)
$\sigma_{tot}(\gamma p)$ vs. $\sum\left[d\sigma/dt(\gamma p \to \rho,\omega,\phi)\right]^{1/2}$	0.5 ± 0.1	0	3	Accuracy limited by uncertainty of ω, ϕ contributions, (3.6)
$\sigma_\perp(\gamma p \to \bar{\pi}^+ n) + \sigma_\perp(\gamma n \to \bar{\pi}^- p)$ vs. $\sigma(\bar{\pi}^- p \to n\rho^0)$	~ 0.3	0	4	(3.9)
Pion formfactor $F_\pi(0)$	≈ 0.5	0	5	Assumes rho dominance of pion form factor (3.14)
$d\sigma/dt\,(\gamma A \to \rho A)$	0.5-1.0	0	6	Sensitive to value of $\sigma_t(\rho N)$ used and to details of nuclear physics, (3.5)
$\Gamma(\omega \to \pi\gamma)/\Gamma(\omega \to 3\pi)$	≈ 0.85	different in the two decay modes	7	Assumption of ρ dominance of ω decay, ρ-width Γ_ρ = 110 MeV, (3.14)

References

1) Proceedings 1967 International Symposium on on Electron and Photon Interactions at High Energies, Stanford

2) Proceedings of the Heidelberg International Conference on Elementary Particles, 1967

3) International Conference on High-Energy Physics Vienna 1968

4) E.S. Dayhoff, S. Triebwasser and W.E. Lamb Phys. Rev. 89, 106 (1953)

5) B.L. Cosens, Phys. Rev. 173 , 49 (1968)

6) H. Metcalf, J.R. Brandenberger and J.C. Baird Phys. Rev. Letters 21, 165 (1968)

7) S.L. Kaufman et al., Phys. Rev. Letters 22, 507 (1969)
T.W. Shyn et al. , Phys. Rev. Letters 22, 1273 (1969)

8) W.H. Parker, B.N. Taylor and D.N. Langenberg, Phys. Rev. Letters 18, 287 (1967)

9) J.C. Clarke, quoted by W.K.H. Panofsky in Ref. 3)

10) s.B. Cramton, D. Kleppner and N.F. Ramsey, Phys. Rev. Letters 11 , 338 (1963)

- see also reevaluation made in Ref. 6
- see summary by E.R. Cohen and J.W.M. Du Mond, Rev.Mod. Phys. 37, 537 (1965)

11) S.D. Drell and J.D. Sullivan, Phys. Rev. 154, 1477 (1967)

12) P.A. Thompson et al., Phys. Rev. Letters 22, 163 (1969)

13) G.W. Erickson and D.R. Yennie, Ann. Phys. 35, 271, 447 (1965)
M.F. Soto Jr. Phys. Rev. Letters 17, 1153 (1966)
D.R. Yennie, quoted by S.J. Brodsky and R.G. Parsons, Phys. Rev. 163, 134 (1967)

14) S. Triebwasser, E.S. Dayhoff and W.E. Lamb, Phys. Rev. 89, 98 (1953)

15) R.T. Robiscoe, Phys. Rev. 168, 4 (1968)

16) J. Bailey et al., Phys. Letters 28 B, 287 (1968)

17) A. Rich, Phys. Rev. Letters 20, 967, 1221 (1968)

18) N.M. Kroll, Nuovo Cim. 45 A, 65 (1966)

19) H. Alvensleben et al., Phys. Rev. Letters 21, 1501 (1968)

20) E. Eisenhandler et al., Phys. Rev. Letters 18, 425 (1967)

21) K.J. Cohen, S. Homma, D. Luckey and L.S. Osborne, Phys. Rev. 173, 1339 (1968)

22) R. Weinstein, in Ref. 1) pge. 409 (CEA)
S. Hayes et al. Phys. Rev. Lett. 22, 1134 (1969) (Cornell)

23) R.H. Siemann et al., Phys. Rev. Letters 22, 421 (1969)

24) A.D. Liberman et al., Phys. Rev. Letters 22, 663 (1969)

25) W.C. Barber et al., quoted by S.C.C. Ting in Ref. 3, pge. 43

26) F.E. Low, Phys. Rev. Letters 14, 238 (1965)

27) C. Betourne et al., Phys. Letters 17, 70 (1965)

28) Budnitz et al., Phys. Rev. 141, 1313 (1966)
H.J. Behrend et al., Phys. Rev. Letters 15, 900 (1965)

29) C.D. Boley et al., Phys. Rev. 167, 1275 (1968)

30) S. Parker, H.L. Anderson and C. Rey, Phys. Rev. 133 B, 768 (1964)

31) S. Frankel, W. Fraiti and J. Halpern, Nuovo Cim. 27, 894 (1963)

32) W.C. Barber et al. Phys. Rev. Lett. 22, 902 (1969)

33) L.M. Lederman et al., quoted by W.K.H. Panofsky in Ref. 3, pge. 23

34) J.J. Sakurai, Ann. Phys. 11, 1 (1960)
M. Gell-Mann and F. Zachariasen, Phys. Rev. 124, 953 (1961)
Y. Nambu and J.J. Sakurai, Phys. Rev. Lett. 8, 79 (1962)
M. Gell-Mann, D. Sharp and W.G. Wagner, Phys. Rev. Lett. 8, 261 (1962)

35) N.M. Kroll, T.D. Lee and B. Zumino, Phys. Rev. 157, 1376 (1967)

36) W. Zimmermann, DESY-Reports 68/46 and 68/47

37) H. Joos, Schladming Lectures 1967, Acta Physica Austriaca, Suppl. IV, 1967

38) R. Haag, Phys. Rev. 112, 669 (1958)
K. Nishijima, Phys. Rev. 111, 995 (1958)

39) H. Fraas and D. Schildknecht, Nucl. Phys. B 6, 395 (1968)

40) G.J. Gounaris and J.J. Sakurai, Phys. Rev. Lett. 21, 244 (1968)

41) J.E. Augustin et al., Phys. Letters 28B, 508 (1969)

42) V.L. Auslander et al., quoted by S.C.C. Ting in Ref. 3, pge. 43

43) J.G. Asbury et al., Phys. Rev. Lett. 19, 869 (1967)

44) A.A. Wehmann et al., Phys. Rev. 178, 2095 (1969)

45) J.K. de Pagter et al., Quoted by S.C.C. Ting in Ref. 1, pge. 452

46) G. Lütjens et al., Phys. Letters 24 B, 634 (1967)

47) J.E. Augustin et al., Phys. Letters 28 B, 513 (1969)

48) D. Bollini et al., Nuovo Cim. 57 A, 404 (1968)

49) J.E. Augustin et al., Phys. Letters 28 B, 517 (1969)

50) U. Becker et al., Phys. Rev. Lett. 21, 1504 (1968)

51) D. Bollini et al., Nuovo Cim. 56 A, 1173 (1968)

52) Review of Particle Properties, Particle Data Group UCRL-8030 Pt. 1 (Jan. 1969)

53) R.J. Oakes and J.J. Sakurai, Phys. Rev. Lett. 19, 1266 (1967)

54) T. Das, V.S. Mathur and S. Okubo, Phys. Rev. Lett. 19, 470 (1967)

55) A. Dar and V.F. Weisskopf Phys. Letters 26 B, 670 (1968)
R. van Royen and V.F. Weisskopf, Nuovo Cim. 51 A, 583 (1967)
H. Pietschmann and W. Thirring, Phys. Letters 21, 713 (1966)

56) See Refs. 53) and 54)

57) Aachen - Berlin - Bonn - Hamburg - Heidelberg - München Collaboration, Phys. Rev. 175 , 1669 (1968)
Phys. Letters 27 B, 54 (1968)

58) Y. Eisenberg et al. Phys. Rev. Lett. 22 , 669 (1969)

59) J. Ballam et al. Phys. Rev. Lett. 21, 1541 (1968)

60) M. Davier et al. Phys. Rev. Lett. 21, 841 (1968)
Phys. Letters 28 B, 619 (1969)

61) Cambridge Bubble Chamber Group, Phys. Rev. 146, 994 (1966)
155, 1468 (1967)
155, 1477 (1967)

62) W.G. Jones et al. Phys. Rev. Lett. 21, 586 (1968)

63) G. Mc Clellan et al. Phys. Rev. Lett. 22, 374 (1969)

64) H. Blechschmidt et al. Nuovo Cim. 52 A, 1348 (1967)

65) J.D. Jackson Nuovo Cim. 34 , 1644 (1964)

66) J.G. Asbury et al., quoted by S.C.C. Ting in Ref. 3

67) M. Ross and L. Stodolsky, Phys. Rev. 149 , 1172 (1966)

68) L. Criegee et al. Phys. Lett. 28 B, 282 (1968)

69) L. Criegee and U. Timm, private communication

70) Aachen - Bonn - Hamburg - Heidelberg - München Collaboration, private communication by Dr. H. Spitzer

71) G.Mc Clellan et al. Phys. Rev. Lett 22, 377 (1969)

72) G. Belletini et al. Nuclear Phys. 79 , 609 (1966)
and R.J. Glauber and G. Matthiae, Report ISS 67/16
Instituto Superiore di Sanita, Roma 1967

73) J.G. Asbury et al., quoted by S.C.C. Ting in Ref. 3
see also Phys. Rev. Lett. 19, 865 (1967)

74) F. Bulos et al., Phys. Rev. Lett. 22 , 490 (1969)

75) J.G. Asbury et al., quoted by S.C.C. Ting in Ref. 3

76) J. Ballam et al., Phys. Rev. Lett. 21, 1544 (1968)

77) Aachen - Berlin - Bonn - Hamburg - Heidelberg - München Collaboration, Phys. Letters 27 B, 474 (1968)

78) H. Meyer et al., private communication

79) L. Stodolsky, Phys. Rev. Lett. 18, 135 (1967)

80) R. Diebold, quoted by B. Richter in Ref. 3

81) P. Joos, Compilation of Photoproduction data, private communication. X^0 data: Ref. 57; η data: Review by G. Salvini, Rivista Nuovo Cim. 1, 57 (1969), also Ref. 57 and D. Bellenger et al., Phys. Rev. Lett. 21, 1205 (1968) E.D. Bloom et al., Phys. Rev. Lett. 21, 1100 (1968)

82) D.R.O. Morrison, Phys. Letters 22, 528 (1966)

83) J. Froyland and D. Gordon, Phys. Rev. 177, 2500 (1969)

84) G. Buschhorn et al. Phys. Rev. Lett. 17, 1027 (1966)
Phys. Rev. Lett. 18, 571 (1967)
Phys. Letters 25 B, 622 (1967)

85) P. Heide et al., Phys. Rev. Lett. 21, 248 (1968)

86) A.M. Boyarski et al., Phys. Rev. Lett. 20, 300 (1968)

87) A.M. Boyarski et al. Phys. Rev. Lett. 21, 1767 (1968)

88) Z. Bar - Yam et al. Phys. Rev. Lett. 19, 40 (1967)

89) For list of References to this topic see e.g. Ref. 117

90) M. Le Bellac Phys. Letters 25 B, 524 (1967)

91) M. Aderholz et al. Phys. Letters 27 B, 174 (1968)

92) M.L. Blackmon, G. Kramer and K. Schilling Regge-Pole Model with Absorptive Correction Cuts for Photoproduction of charged Pions, Argonne Preprint 1969

93) Ch. Geweniger et al., Phys. Letters 29 B, 41 (1969)

94) Ch. Geweniger et al., Phys. Letters 28 B, 155 (1968)

95) D.S. Beder Phys. Rev. 149, 1203 (1966)

96) For details see Ref. 97 and M. Krammer and D. Schildknecht, Nucl. Phys. B 7, 583 (1968)

97) A. Bialas and K. Zalewski Phys. Letters 28 B, 436 (1969)

98) J.T. Donohue and H. Högaasen Phys. Letters 25 B, 554 (1967)

99) D. Schildknecht DESY 69/10

100) Data: P.B. Johnson et al. Phys. Rev. 176, 1651 (1968)
R. Diebold and J.A. Poirier, Phys. Rev. Lett. 22, 906 (1969)
find $\gamma_1^2/4\pi \approx 0.2$
Z.G.T. Guiragossian and A. Levy, SLAC-PUB-581 (1969)
find $\gamma_1^2/4\pi \gtrsim 0.4$

101) M. Braunschweig et al. Phys. Letters 26 B, 405 (1968)

102) R. Anderson et al. Phys. Rev. Lett. 21, 384 (1968)

103) M. Braunschweig et al., quoted by B. Richter in Ref. 3, see also Ref. 101.

104) D. Bellenger et al., quoted by B. Richter in Ref. 3

105) P. Stichel, Z. Physik 180, 170 (1964)

106) M.L. Blackmon, G. Kramer and K. Schilling
Preprint Argonne / Cal tech 1969

107) J. Froyland, Preprint Universitet Oslo 1969, a similar model was made by A. Capella and J. Tran Than Van, Lett. Nuovo Cim. 1, 321 (1969)

108) A.M. Boyarski et al. Phys. Rev. Lett. 22, 148 (1969)

109) Cambridge Bubble Chamber group, Phys. Rev. 163, 1510 (1967)

110) P. Stichel and M. Scholz, Nuovo Cim. 34, 1381 (1964)

111) A.M. Boyarski et al. Phys. Rev. Lett. 22, 1131 (1969)

112) J. Kupsch Phys. Letters 22, 690 (1966)
H.J. Lipkin and F. Scheck, Phys. Rev. Lett. 18, 347 (1967)

113) See e.g. Review by H. Rollnik in Ref. 2)
F.A. Berends, A. Donnachie and D.L. Weaver
Nucl. Phys. B 4, 1, 54, 103 (1967)

114) R.L. Walker CALT-68-158 preprint

115) J.L. Alberi et al. Phys. Rev. 176, 1631 (1968)

116) See compilation of recent papers in Ref. 117

117) J.D. Jackson and C. Quigg, Phys. Letters 29 B, 236 (1969)

118) A. Dar et al. Phys. Rev. Letters 20, 1261 (1968)

119) Rosenbluth plot:K.W. Chen et al. Phys. Rev. 141, 1267 (1965), K. Berkelman et al. Phys. Rev. 130, 2061 (1963), T. Jansens et al. Phys. Rev. 142, 922 (1966), W. Bartel et al Phys. Letters 25 B, 236 (1967), see also compilation Ref. 122

120) e^+/e^- : D.H. Coward et al. Phys. Rev. Lett. 20, 292 (1968)
W. Bartel et al. Phys. Lett. 25 B, 242 (1967)
D. Yount and J. Pine Phys. Rev. 128, 1842 (1962)
A. Browman et al. Phys. Rev. 139, B 1079 (1965)
R.L. Anderson et al. Phys. Rev. Lett. 17, 407 (1966)

Recoil polarization: G. v. Giorgio et al. Nuovo Cim. 39, 474 (1965)

121) V.E. Krohn and G.R. Ringo, Phys. Rev. 148, 1303 (1966)
and references quoted there.

122) W. Schmidt DESY Internal Report F 22 - 69/2
R. Felst, private communication.

123) D.H. Coward et al. Phys. Rev. Lett. 20, 292 (1968)

124) W. Bartel et al., Phys. Rev. Lett. 17, 608 (1966)
W. Albrecht et al. Phys. Rev. Lett. 17, 1192 (1966), 18, 1014 (1967)
H.J. Behrend et al. Nuovo Cim. 48, 140 (1967)
M. Goitein et al. Phys. Rev. Lett. 18, 1016 (1967)
D.J. Drickey and L.N. Hand, Phys. Rev. Lett. 9, 521 (1962)
Chr. Berger et al. Phys. Letters 28 B, 276 (1968) and papers of Ref. 119

125) For a compilation see also R.J. Budnitz et al., Phys.Rev. 173, 1357 (1968)
D. Benaksas et al. Phys. Rev. Lett. 13, 353 (1964)
B. Grossetete et al. Phys. Rev. 141, B 1435 (1966)
E.B. Hughes et al. Phys. Rev. 139, B 458 (1965)
C.W. Akerloff et al. Phys. Rev. 135, B 810 (1965)
P.Stein et al. Phys. Rev. Lett. 16, 592 (1966)

Theory: D. Braess and G. Kramer Z. Physik 189, 242 (1966)
D. Hasselmann and G. Kramer DESY 67/2

126) V. Wataghin Nuovo Cim. 54 A, 805, 840 (1968)

127) G. Morpurgo Phys. Letters 27 B, 378 (1968)

128) T.T. Chou and C.N. Yang, Phys. Rev. 170, 1591(1968)
Phys. Rev. Lett. 20, 1213 (1968)

129) T. Massam and A. Zichichi Nuovo Cim. 43, 1137 (1966)

130) King Yuen Ng Phys. Rev. 170, 1435 (1968)

131) G. Höhler, R. Strauss and H. Wunder, preprint,
quoted by W.K.H. Panofsky and by N.M. Kroll, Ref. 3

132) P.D. Vecchia and F. Drago Preprint LNF-69/25

133) T.T. Wu and C.N. Yang Phys. Rev. 137 B, 708 (1965)

134) H.D.I. Abarbanel, S.D. Drell and F.J. Gilman,
Phys. Rev. Lett. 20, 280 (1968)

135) S.D. Drell, in Ref. 1

136) See Review by N.M. Kroll, Ref. 3
D. Amati et al. Phys. Letters 27 B, 38 (1968)
M. Ciafaloni and P. Menotti, Phys. Rev. 173, 1575 (1968)

137) H.S. Green, Phys. Rev. 90, 270 (1953)
O.W. Greenberg Phys. Rev. Lett. 13, 598 (1964)

138) See Ref. 127 for a model with a zero in the form factor

139) R.F. Meyer, DESY 69/17 - he uses the wave function
$\psi(\vec{r}_1, \vec{r}_2, \vec{r}_3) = R^{-6}(\vec{r}_1^{\,2} - \vec{r}_2^{\,2})(\vec{r}_2^{\,2} - \vec{r}_3^{\,2})(\vec{r}_3^{\,2} - \vec{r}_1^{\,2}) \cdot f(R)$
$R = (\vec{r}_1^{\,2} + \vec{r}_2^{\,2} + \vec{r}_3^{\,2})^{1/2}$
$f(R) = \text{prop. } R^{-3/2} e^{-6R/2}$

140) L.N. Hand, Phys. Rev. 129, 1834 (1963)

141) J.D. Bjorken and J.D. Walecka Annals of Phys. 38, 35 (1966)

142) F.W. Brasse et al. Nuovo Cim. 55, 679 (1968) and DESY 67/34
see also Ref. 145, 146, 149 and 151

143) W. Bartel et al. Phys. Letters 28 B , 148 (1968) and DESY 68/53

144) H. Dorner, thesis Hamburg 1969

145) H.L. Lynch, J.V. Allaby and D.M. Ritson Phys. Rev. 164, 1635 (1967)

146) A.A. Cone et al., Phys. Rev. 156, 1490 (1967)

147) S. Galster et al., preprint, contribution to this conference, measured $e + p \to e' + N^* \to e' + p + \pi^0$

148) F. Gutbrod and D. Simon, Nuovo Cim. 51 A , 602 (1967)

149) W. Albrecht et al., Phys. Letters 28 B , 225 (1968) and DESY 68/48

150) C. Mistretta et al. Phys. Rev. Lett. 20 , 1070 (1968)

151) E. Bloom et al. quoted by W.K.H. Panofsky in Ref. 3

152) J.D. Bjorken, SLAC-PUB-510 (1968)

153) W.W. Ash et al. Phys. Letters 24 B , 165 (1967), D. Imrie et al. Phys. Rev. Lett. 20 , 1074 (1968)

154) W. Albrecht et al. DESY 69/7

155) H.D.I. Abarbanel, M.L. Goldberger and S.B. Treiman Phys. Rev. Lett. 22, 500 (1969)

156) S.D. Drell, D.J. Levy and Tung-Mow Yan Phys. Rev. Lett. 22, 744 (1969)

157) J.J. Sakurai Phys. Rev. Lett. 22 , 981 (1969)
H. Fraas and D. Schildknecht, DESY preprint 1969

158) J.D. Bjorken, Phys. Rev. Lett. 16, 408 (1966)

159) K. Gottfried, Phys. Rev. Lett. 18 , 1174 (1967)

160) J.D. Bjorken in Ref. 1, page 109

Figure Captions

Fig. 1 Electron-Positron large angle pair experiment by DESY - MIT group (19).

Fig. 2 Large angle $\mu^+\mu^-$ experiment from Cornell (22)
(a) Ratio of experimental yield to that expected from elastic BH production as a function of momentum transfer q^2 to the carbon nucleus.

(b) Ratio of experimental yield to yield expected from sum of BH elastic + inelastic $\mu^+\mu^-$ pair production + ϱ and ϕ leptonic decay + contribution from $\pi \rightarrow \mu\,\nu$ decays.

(c) Total yield minus yield expected from elastic BH pair production, showing the rho peak.

$M_{\mu\mu} = \mu^+\mu^-$ invariant mass.

Fig. 3 Large angle bremsstrahlung. Abszissa = $e\gamma$ or $\mu\gamma$ invariant mass. Data on electron BS from Ref. 23, muon BS from Ref. 24.

Fig. 4 Comparison of Muon and electron form factors of the proton (from Ref. 33).

Fig. 5 Comparison of leptonic decay rates of vector mesons with Weinberg's first sum rule (56).

Fig. 6 Total cross section for vector meson production on hydrogen
a) for ϱ b) for ω c) for ϕ .

References: ABBHHM (57), Eisenberg (58), Ballam (59), Davier (60), Blechschmidt (64), CEA (61), Jackson (65), Ross-Stodolsky (67)

Fig. 7 Fit of rho production $\gamma p \rightarrow \varrho p$ to: $d\sigma/dt = d\sigma/dt|_{t=0} \exp[-B|t|]$

a) $d\sigma/dt\,|_{t=0}$ b) B, both as a function of the primary photon energy.
Ref. as in Fig. 6

Fig. 8 $\gamma p \rightarrow \phi p$. Summary of data, taken from review paper of S.C.C. Ting in Ref. 3.
DESY -MIT: Ref. 66
DESY-Bubble Chamber: Ref. 57
SLAC: Ref. 62

Fig. 9 Asymmetry of rho production $\Sigma = (\sigma_{\parallel} - \sigma_{\perp})/(\sigma_{\parallel} + \sigma_{\perp})$ as a function of momentum transfer in the reaction $\gamma p \rightarrow p\varrho$.
$\Sigma = +1$ is value expected from diffraction model. Data from Ref. 69. Photonenergy 2.0 - 2.8 GeV.

Fig. 10 Total photoproduction Cross Section as a function of photon energy E_γ . Data below 2 GeV may be affected by systematic errors. References: ABBHHM: Ref. 77, DESY counter: Ref. 78, SLAC annihilation beam: Ref. 76, SLAC Laser beam: Preliminary results from a bubble chamber experiment with a reflected laser beam at SLAC by a SLAC-TUFTS-UC Berkeley-UCRL collaboration. The Vector dominance prediction is from Equ. 3.12.

Fig. 11 Compilation of Cross sections for photoproduction of Pseudoscalar mesons. (Lab.) photon energy = k . Taken from compilations by R. Diebold (80) and P. Joos (81).

Fig. 12 Differential cross section for the reaction $\gamma p \to \pi^+ n$, shown for energies of 2.0, 2.6, 5.0, 8, 11, 16 GeV. Data from Ref. 84, 86, Figure taken from Ref. 83. The curves are from model Ref. 83.

Fig. 13 Ratio of single π^-/π^+ photoproduction on deuterium as a function of momentum transfer, for photon energies of 3.4 GeV and 16 GeV. Data from CEA: Ref. 88, DESY: Ref. 85, SLAC: Ref. 87. Figure taken from Ref. 87. The curves are from Regge model Ref. 83.

Fig. 14 Asymmetry Parameter $\Sigma = (\sigma_\perp - \sigma_\parallel)/(\sigma_\perp + \sigma_\parallel)$ for the reactions $\gamma p \to \pi^+ n$ ($\times$) and for the average of $\sigma(\gamma p \to \pi^+ n) + \sigma(\gamma n \to \pi^- p)$ (ϕ).
$\sigma_\perp(\sigma_\parallel)$ = cross section for pion production with photons linearly polarized perpendicular (parallel) to the production plane. Data are at a photon energy of 3.4 GeV from Ref. 93, 94. Theoretical curves: Froyland Ref. 83, Blackmon Ref. 92, Jackson Ref. 117.

Fig. 15 Comparison of π^+ and π^- photoproduction (ϕ , ϕ) with rho and ω production in π — N collisions ($\perp$) via the vector dominance model. The evaluation was made for $f_\rho^2/4\pi = 0.5$ (Ref. 96, 99).

Fig. 16 Check of Equ. 3.14 . A = asymmetry in pion photoproduction with polarized photons. Photoproduction data: ϕ , Ref. 93, 94 ; $\perp$ compilation of bubble chamber data by Ref. 96, 99, evaluated in the Donohue-Högaasen system.

Fig. 17 Differential cross section for the reaction $\gamma p \to \pi^0 p$ at photon energies of 4, 5.8, 6, 11, 16 GeV. Data: DESY Ref. 101, SLAC Ref. 102. S = (CMS energy)^2. The curves are a Regge Model of Ref. 106.

Fig. 18 Asymmetry parameter Σ for π^0 production with polarized photons. The data are from CEA (Ref. 104). Curves are from Regge models with cuts: ——Ref. 107, — – —Ref. 106

Fig. 19 Differential cross section for the reaction $\gamma p \to \pi^- \Delta^{++}$ (from P. Joos, Ref. 81). k = photon energy. Bojarski (k = 5 - 16 GeV) Ref. 108; ABBHHM (k = 1.1 - 5.8 GeV and 0.6 - 1.1 GeV) Ref. 57; CEA (k = 0.7 - 1.1 GeV) Ref. 109

Fig. 20 Ref. 111:

a) Differential cross section for the reaction $\gamma p \to K^+ \Lambda$
b) Behavior of effective Regge trajectory $\alpha(t)$
c) Behavior of the differential cross section for small momentum transfers (S = (total CMS energy)^2).

Fig. 21 Ref. 111: a) The ratio $d\sigma/dt(K^+\Sigma^0)/d\sigma/dt(K^+\Lambda)$ vs. $-t$
b) $\cos\phi$ vs. $-t$, where $\cos\phi$ is defined in the triangle.
The amplitudes mean: $A(\pi^+ n) = A(\gamma p \to \pi^+ n)$, etc.

Fig. 22 Magnetic form factor of the proton, normalized to the dipole fit. Compilation by Ref. 122, using list of papers given in Ref. 124 (proton) and Ref. 125 (neutron). Dashed line: see text.

Fig. 23 Electric form factor of the proton (Ref. 122, 124) (See also Fig. 22).

Fig. 24 Magnetic form factor of the neutron (see also Fig. 22) Ref. 122, 125.

Fig. 25 Electric form factor of the neutron (Ref. 122, 125) VDM = Vector dominance model of Ref. 122 a) small q^2, Ref. 122, 125 b) large q^2 (note different ordinate!) from R.J. Budnitz et al., Ref. 125

Fig. 26 Magnetic form factor of the proton for large momentum transfers Ref. 122, 123, 124. Curves are theoretical models of Refs. 126, 127, 128, 122.

Fig. 27 An example of an electron spectrum for inelastic e - p scattering (Ref. 143).

Fig. 28 Dependence of $\sigma_T + \varepsilon\sigma_S$ on q^2.
W = total energy in the final state hadrons CMS. Figure taken over from Ref. 144, data from Refs. 142, 145, 146, 154.

Fig. 29 a) The transition form factor $G_M^*(q^2) = G_\Delta(q^2)$ as a function of the momentum transfer q^2. Figure taken from Ref. 143, additional data: Ref. 153.

b) Comparison of $G_\Delta(q^2)$ with dipole fit, $G(q^2) = 3\,(1 + q^2/0.71\ \mathrm{GeV}^2)^{-2}$

Fig. 30 Plot of $F(\omega) = \nu W_2(q^2, \nu)$ as a function of $\omega = \nu/q^2$, from Ref. 151.

Fig. 31 The structure functions W_1 and W_2 at $q^2 = 0.773$ and $q^2 = 1.935\ \mathrm{GeV}^2$ (Ref. 154).

Fig. 32 a) νW_2 for $q2 = 0.773$ and $1.935\ \mathrm{GeV}^2$ ($\theta = 47.8^\circ$) as a function of $\omega = \nu/q^2$ with the assumption $\sigma_S/\sigma_T = R = 0$. Solid line corresponds to the SLAC data (Ref. 151) with $R = 0$, dashed line derived from solid line with the assumption $R = 1$, $q^2 = 0.773$.

b) $q^2/\nu \cdot W_1$, for same q^2 and θ as a), as a function of ν/q^2, under the assumption $R = 0$

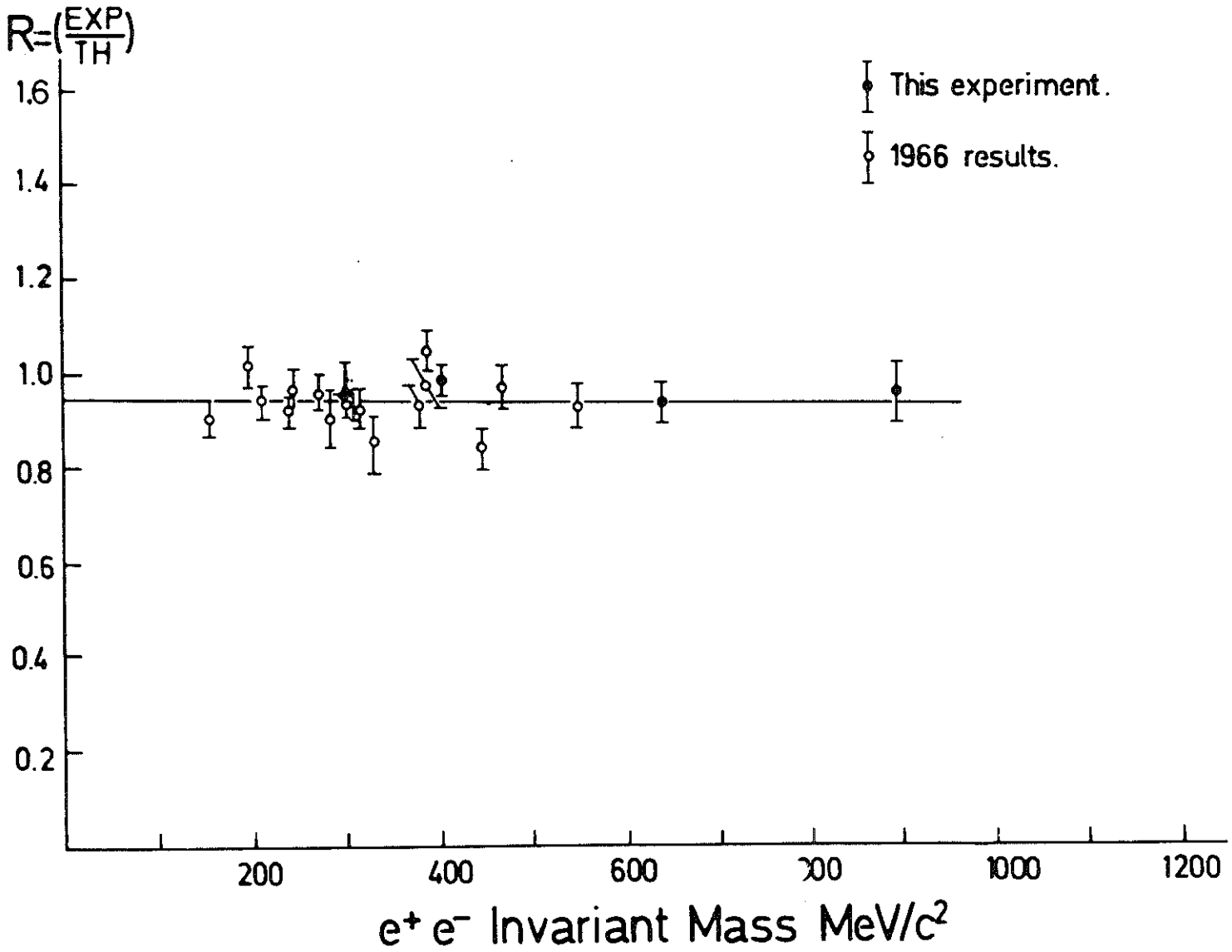
R=(EXP/TH)
1.6
1.4
1.2
1.0
0.8
0.6
0.4
0.2
This experiment.
1966 results.
200
400
600
1000
1200
e+ e- Invariant Mass MeV/c2

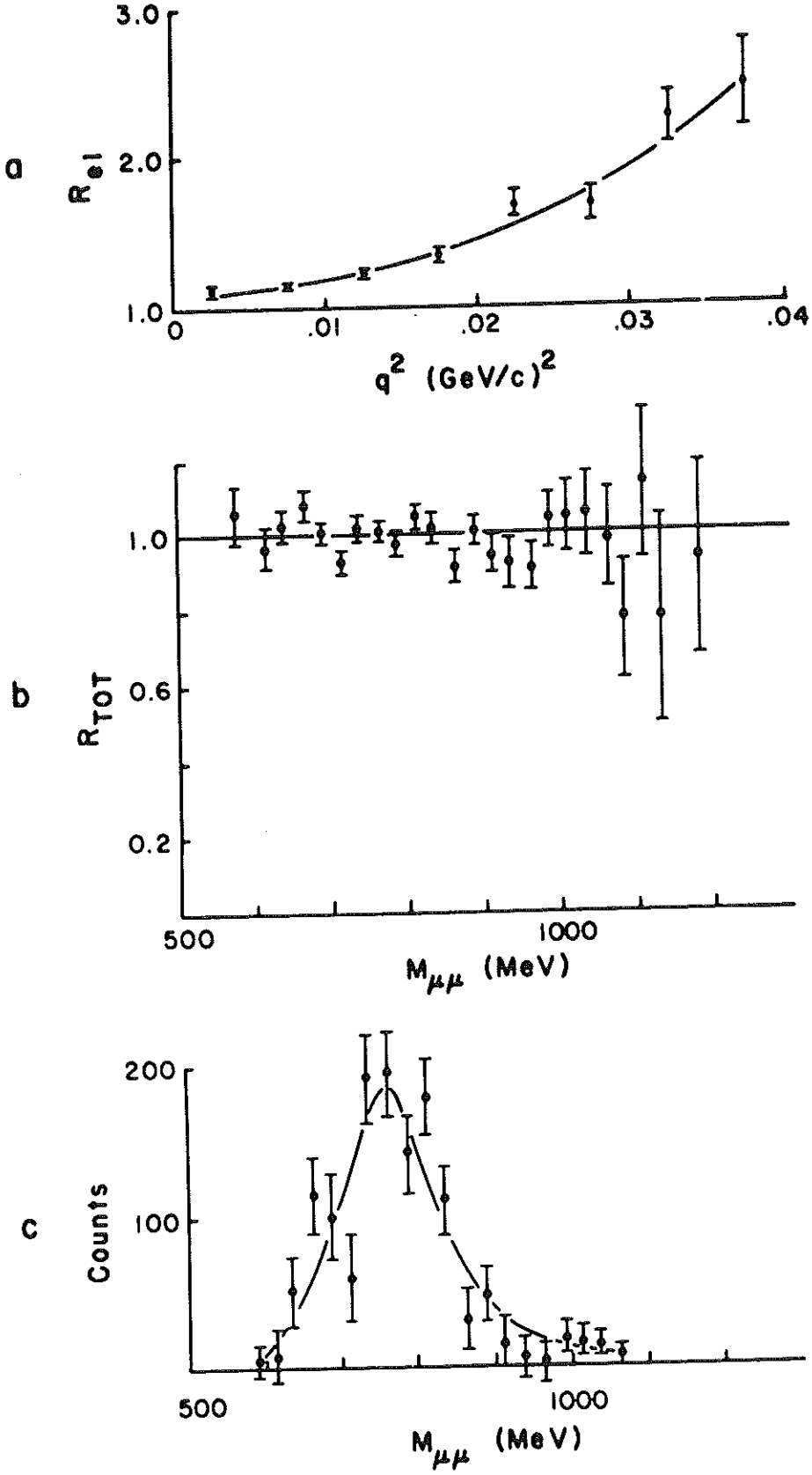
a
3.0
2.0
1.0
R_{el}
0
.01
.02
.03
.04
q^2 (GeV/c)^2
b
1.0
0.6
0.2
R_{TOT}
500
1000
$M_{\mu\mu}$ (MeV)
c
200
100
Counts
500
1000
$M_{\mu\mu}$ (MeV)

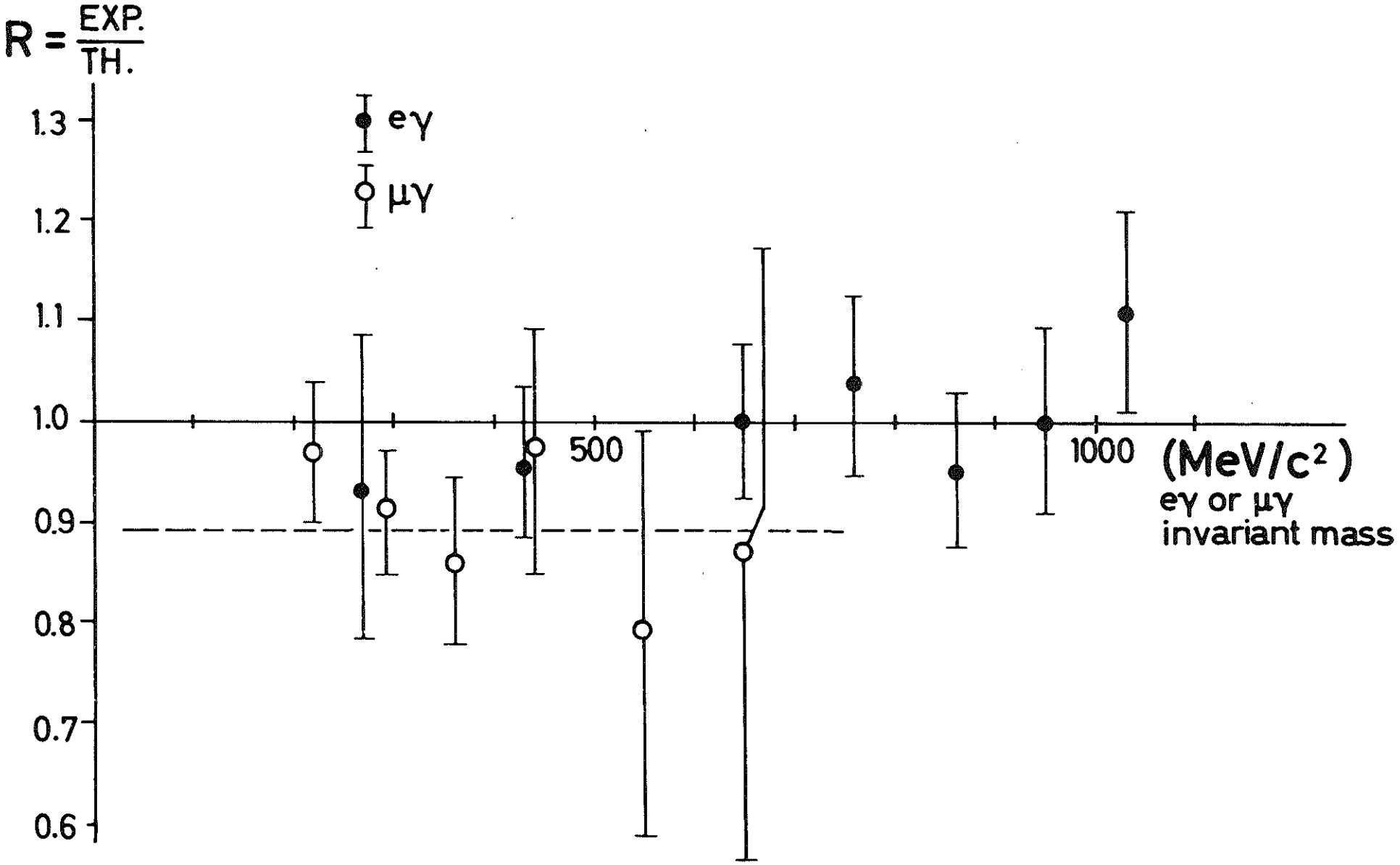
R = EXP./TH.
1.3
1.2
1.1
1.0
0.9
0.8
0.7
0.6
eγ
μγ
500
1000
(MeV/c²)
eγ or μγ
invariant mass

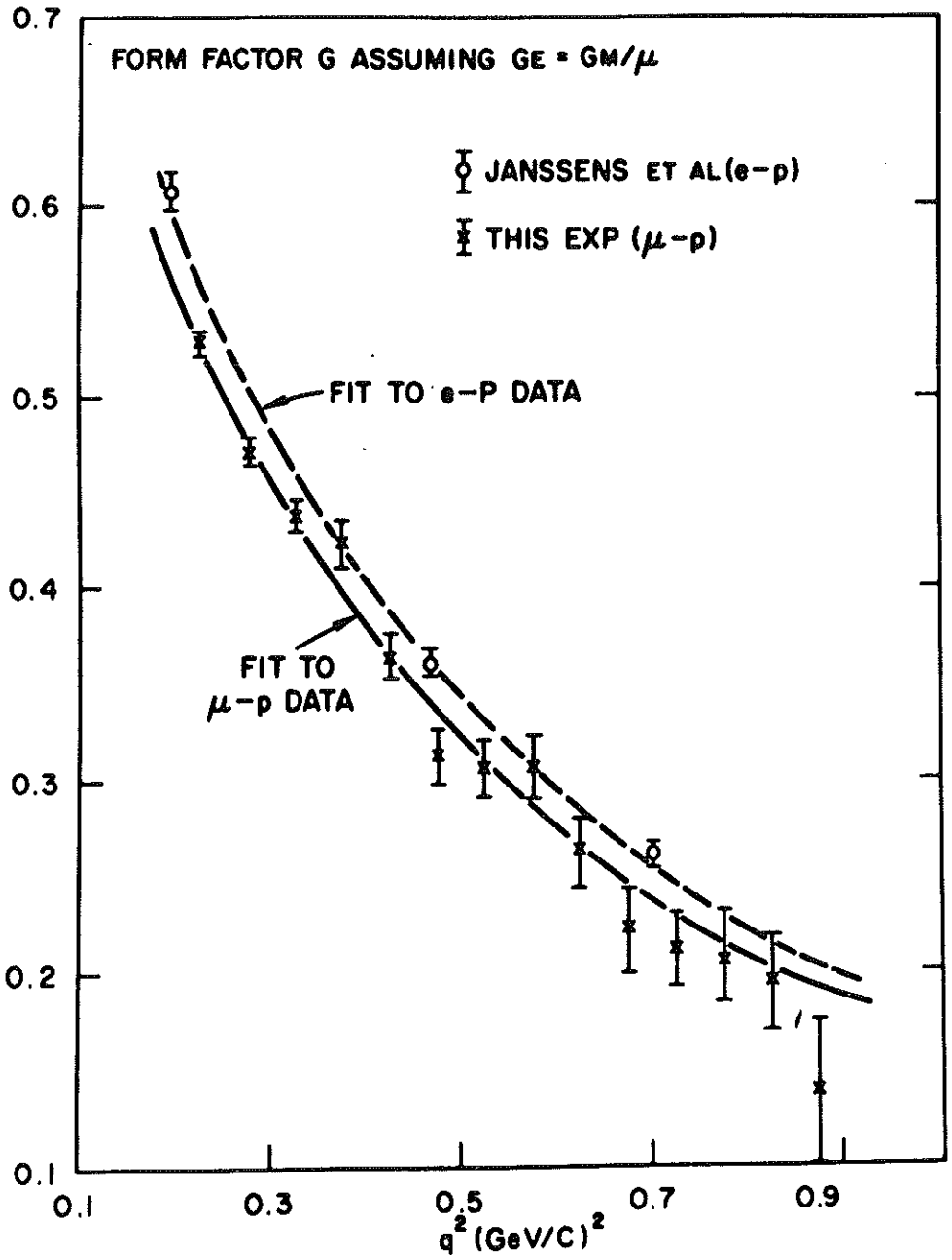

Fig. 4 Comparison of muon and electron form factors of the proton.

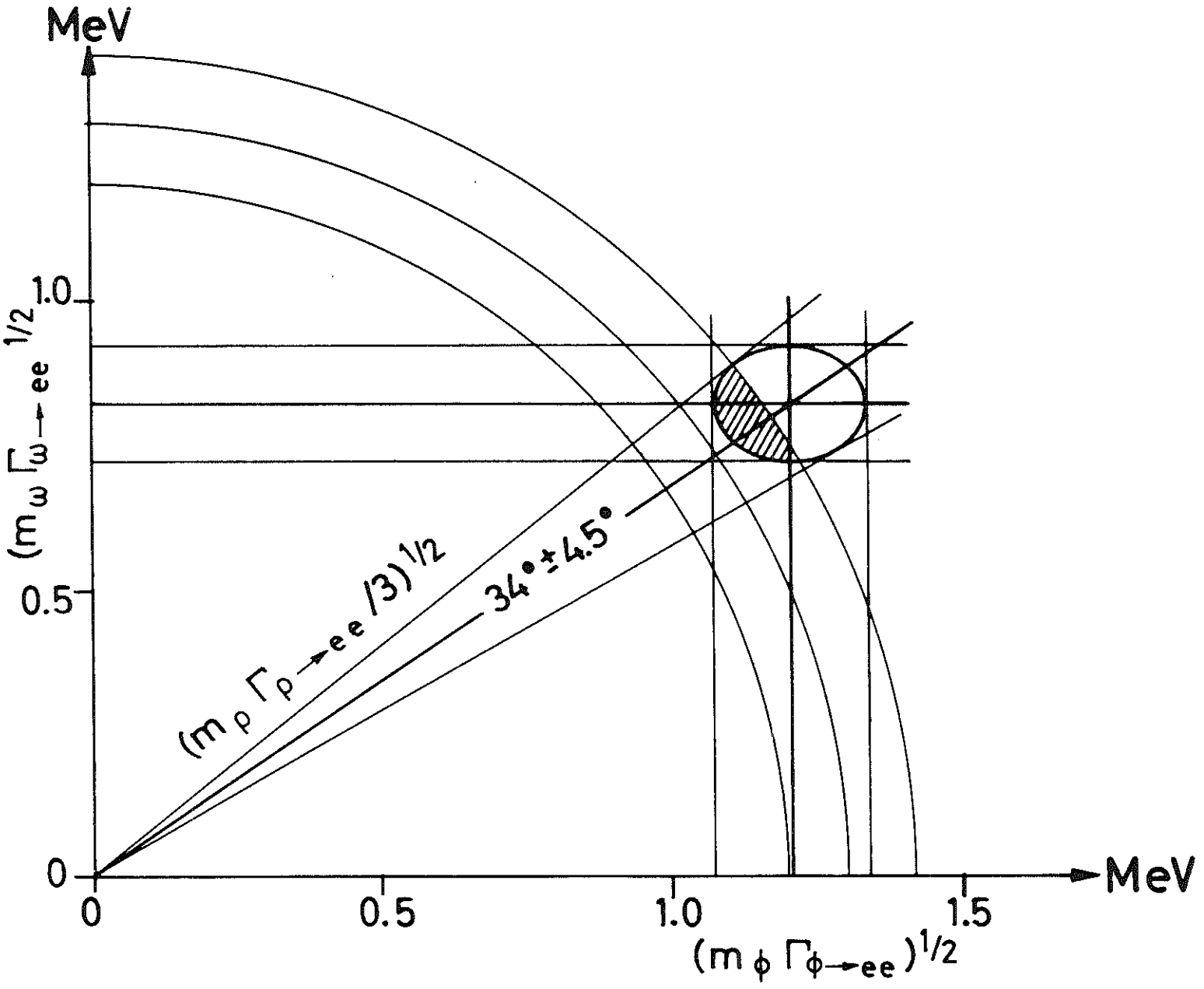
MeV
1.0
0.5
0
$(m_\omega \Gamma_{\omega\to ee})^{1/2}$
$(m_\rho \Gamma_{\rho\to ee}/3)^{1/2}$
$34° \pm 4.5°$
0
0.5
1.0
1.5
MeV
$(m_\phi \Gamma_{\phi\to ee})^{1/2}$

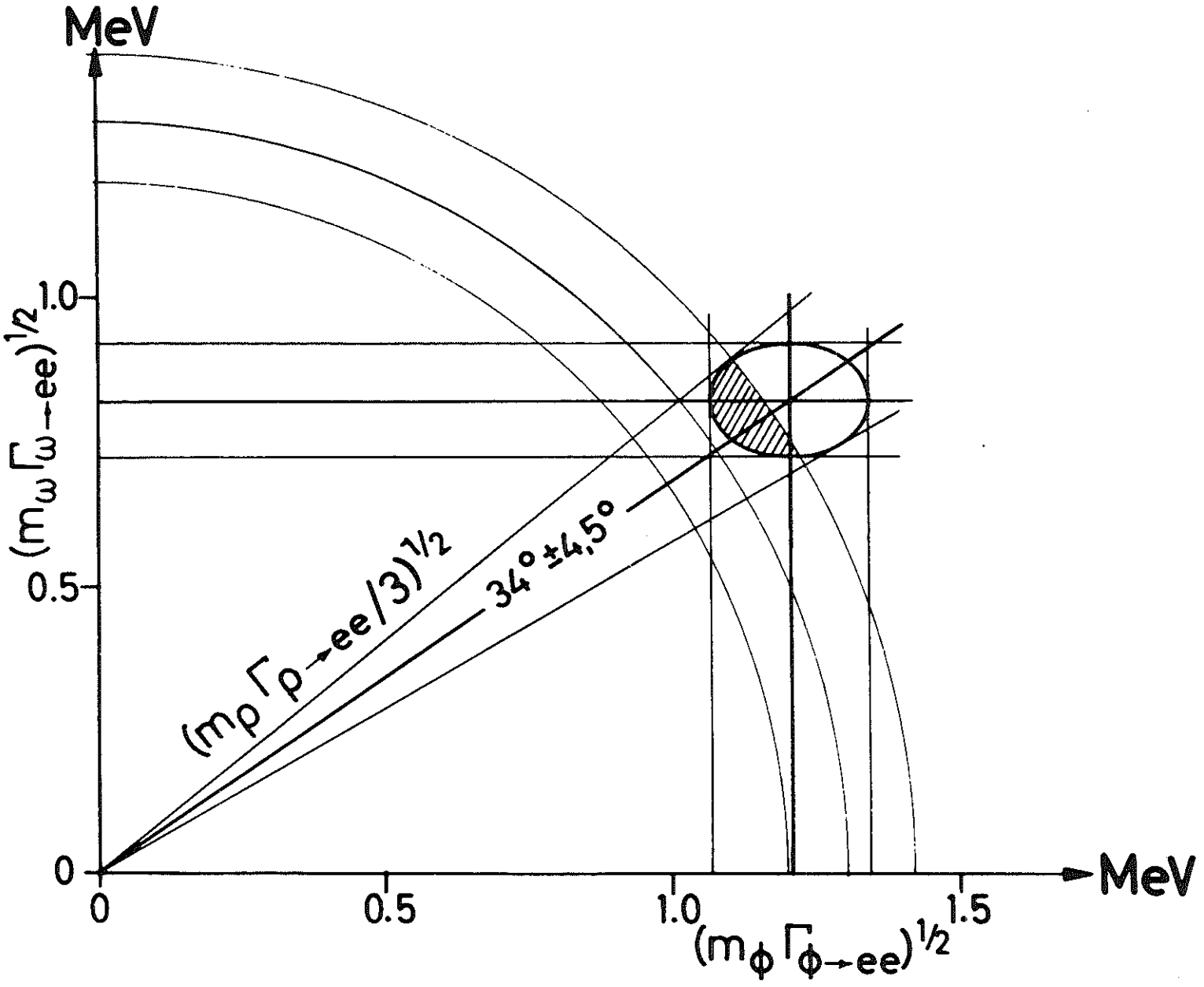
MeV
1.0
0.5
0
$(m_\omega \Gamma_{\omega\to ee})^{1/2}$
$(m_\rho \Gamma_{\rho\to ee}/3)^{1/2}$
$34° \pm 4,5°$
0
0.5
1.0
1.5
MeV
$(m_\phi \Gamma_{\phi\to ee})^{1/2}$

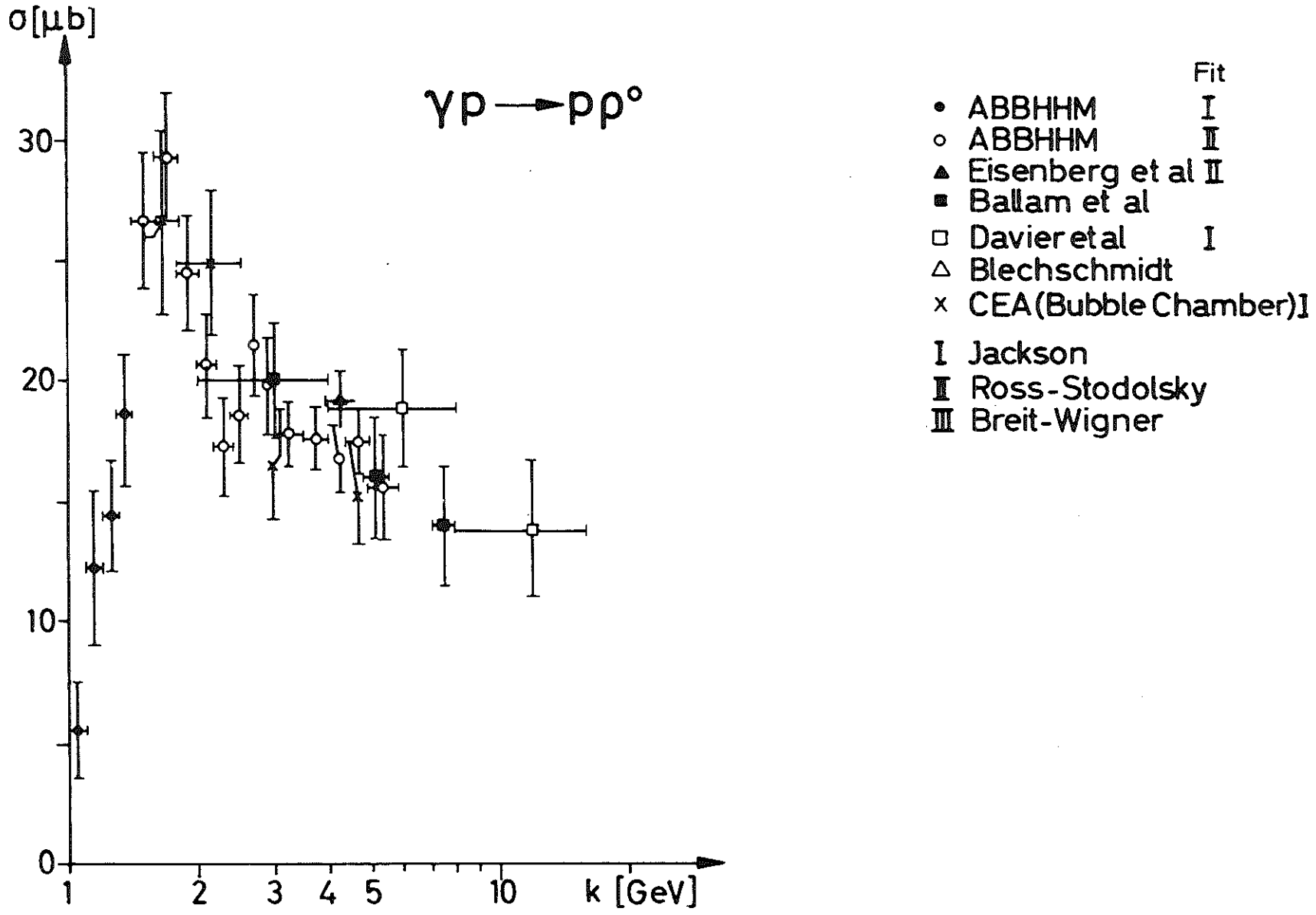
σ[μb]
γp → pρ°
30
20
10
0
1
2
3
4
5
10
k [GeV]
Fit
• ABBHHM I
○ ABBHHM II
▲ Eisenberg et al II
■ Ballam et al
□ Davier et al I
△ Blechschmidt
× CEA (Bubble Chamber) I
I Jackson
II Ross-Stodolsky
III Breit-Wigner

6a

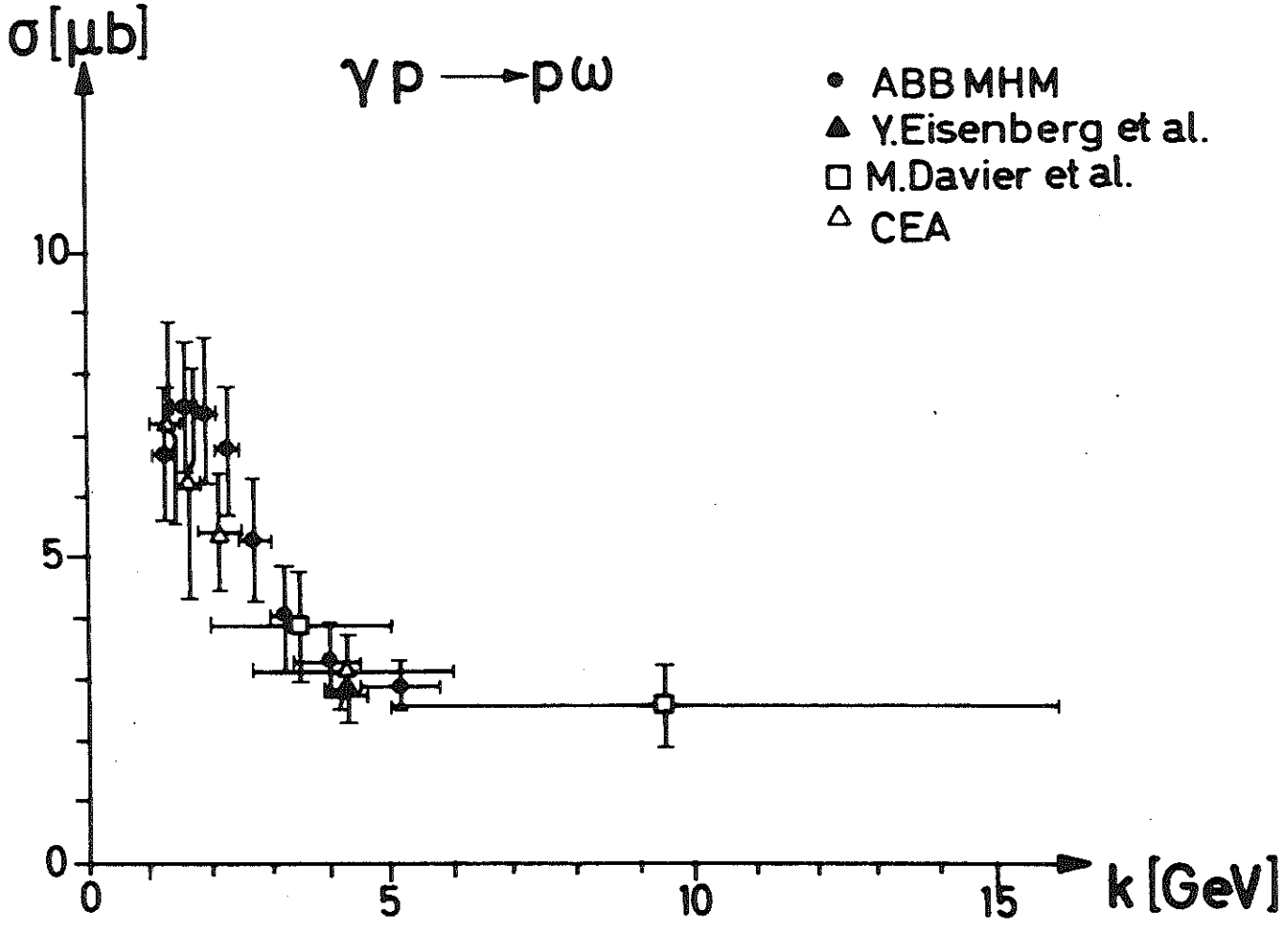
σ[μb]
γp → pω
ABB MHM
Y.Eisenberg et al.
M.Davier et al.
CEA
10
5
0
0
5
10
15
k [GeV]

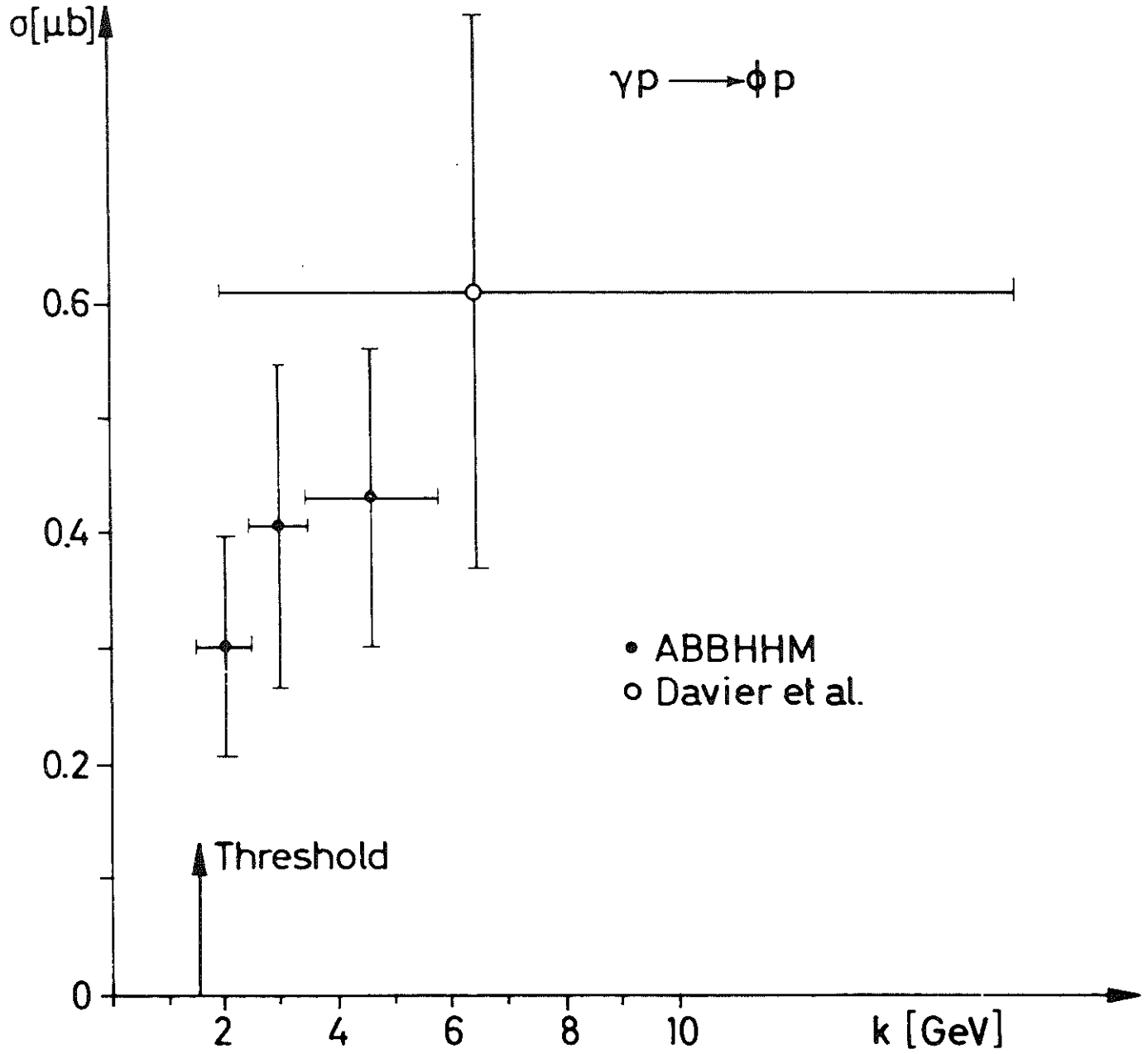
σ[μb]
γp ⟶ φp
0.6
0.4
0.2
0
• ABBHHM
o Davier et al.
Threshold
2
4
6
8
10
k [GeV]

7a

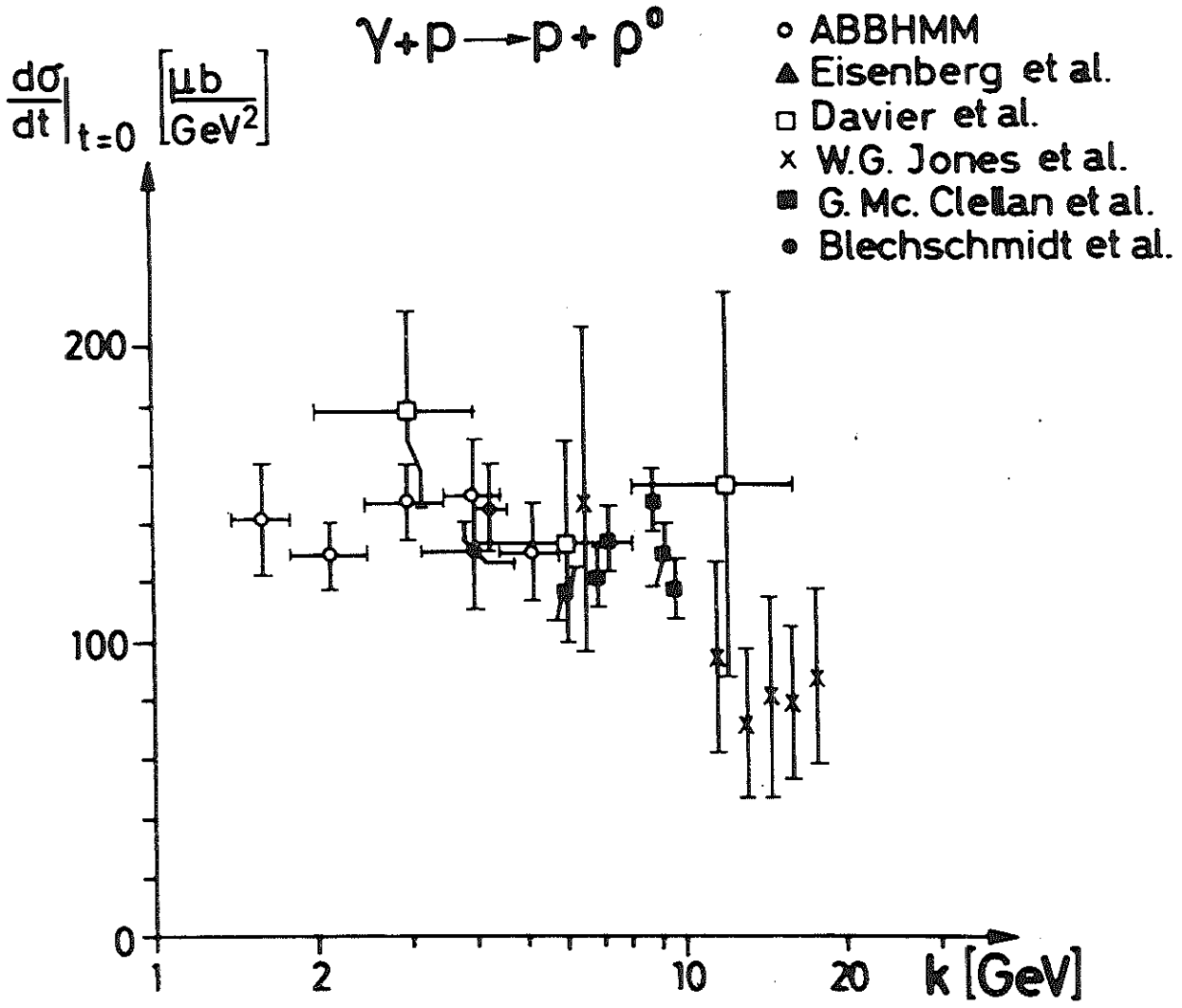
γ+p → p+ρ°
dσ/dt|t=0 [μb/GeV²]
ABBHMM
Eisenberg et al.
Davier et al.
W.G. Jones et al.
G. Mc. Clellan et al.
Blechschmidt et al.
200
100
0
1
2
10
20
k [GeV]

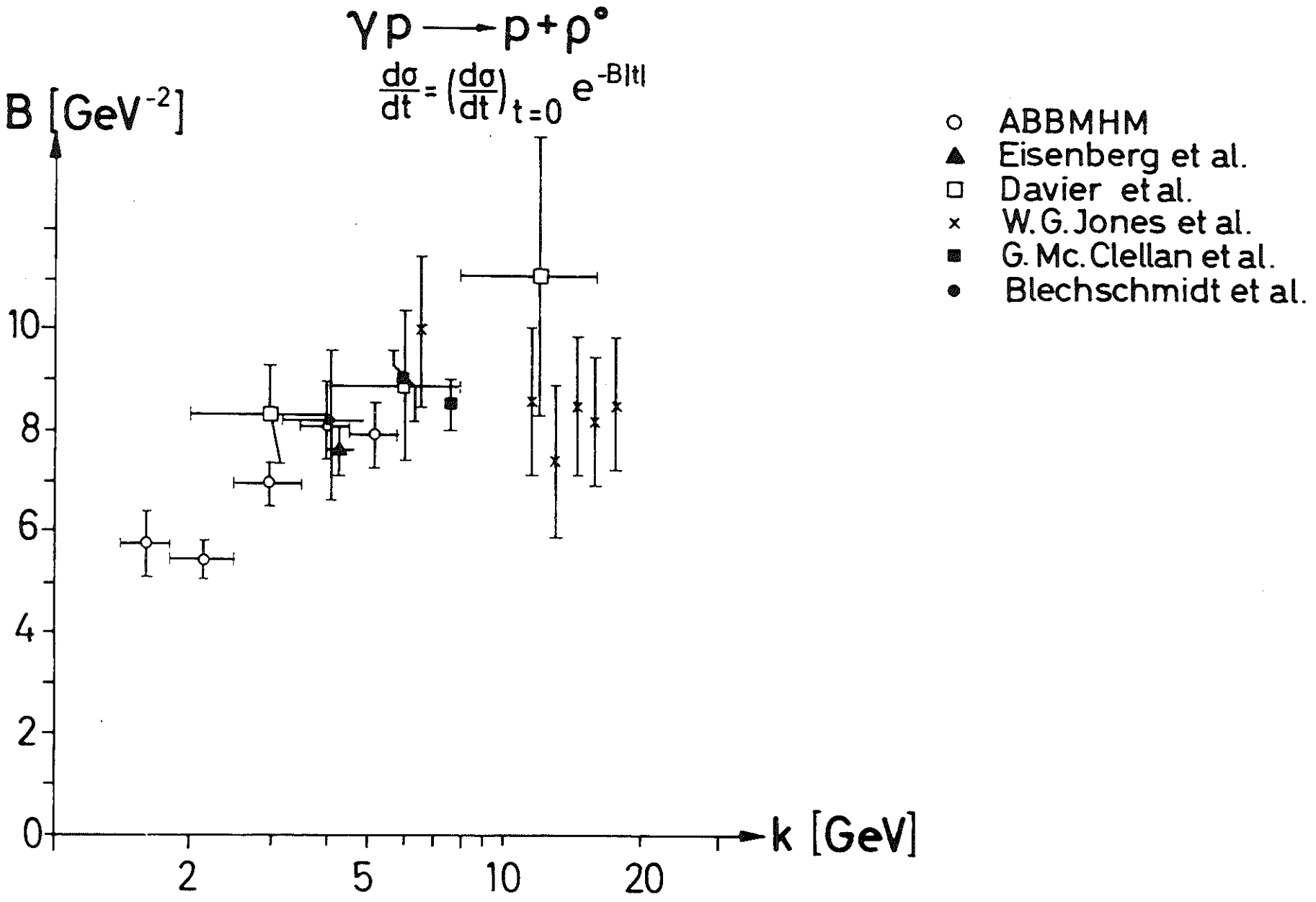
γp ⟶ p+ρ°
dσ/dt = (dσ/dt)t=0 e-B|t|
B [GeV-2]
10
8
6
4
2
0
2
5
10
20
k [GeV]
ABBMHM
Eisenberg et al.
Davier et al.
W.G.Jones et al.
G.Mc.Clellan et al.
Blechschmidt et al.

PRELIMINARY

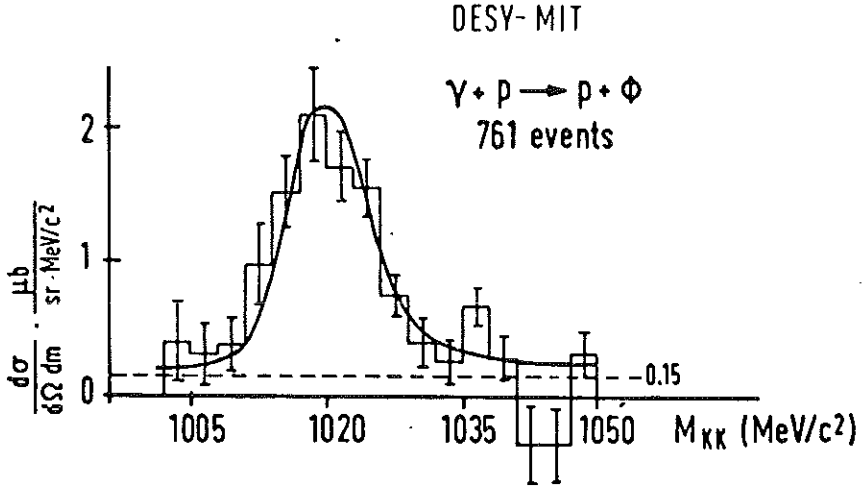

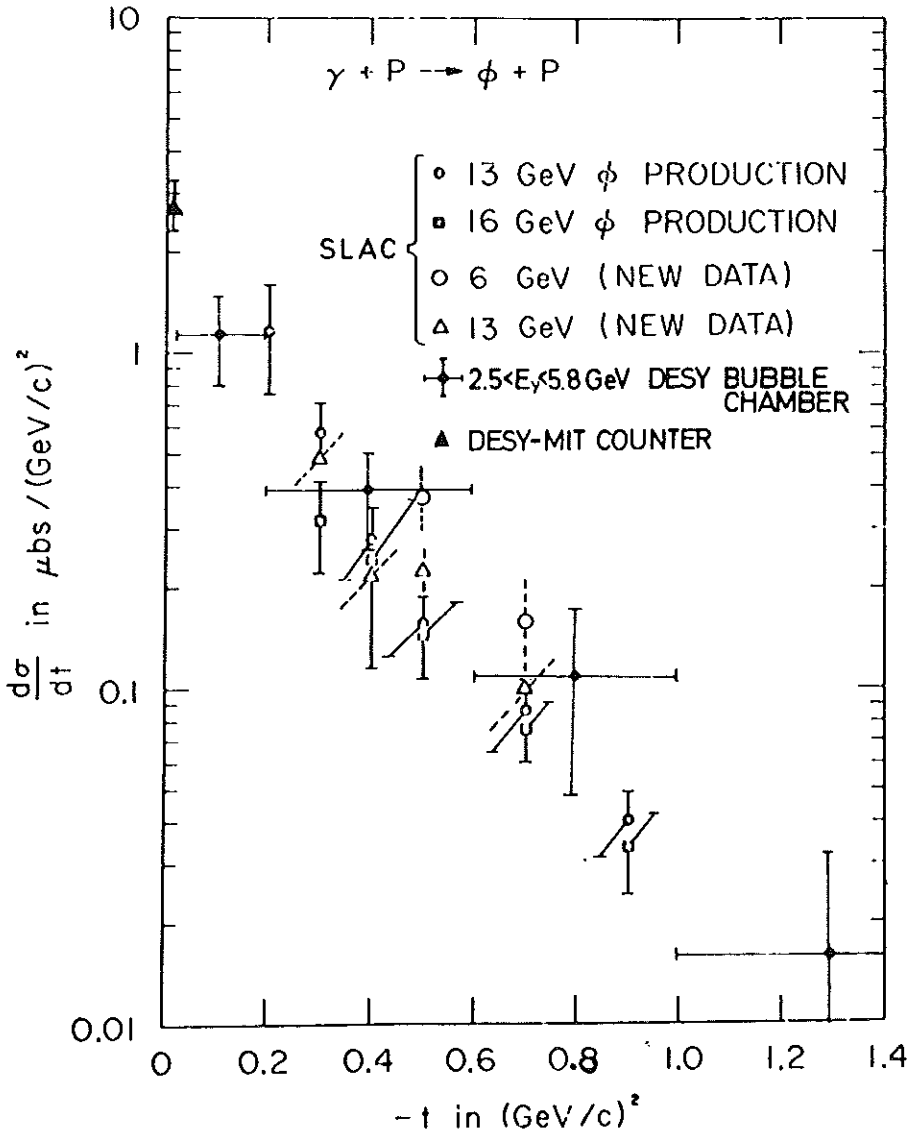

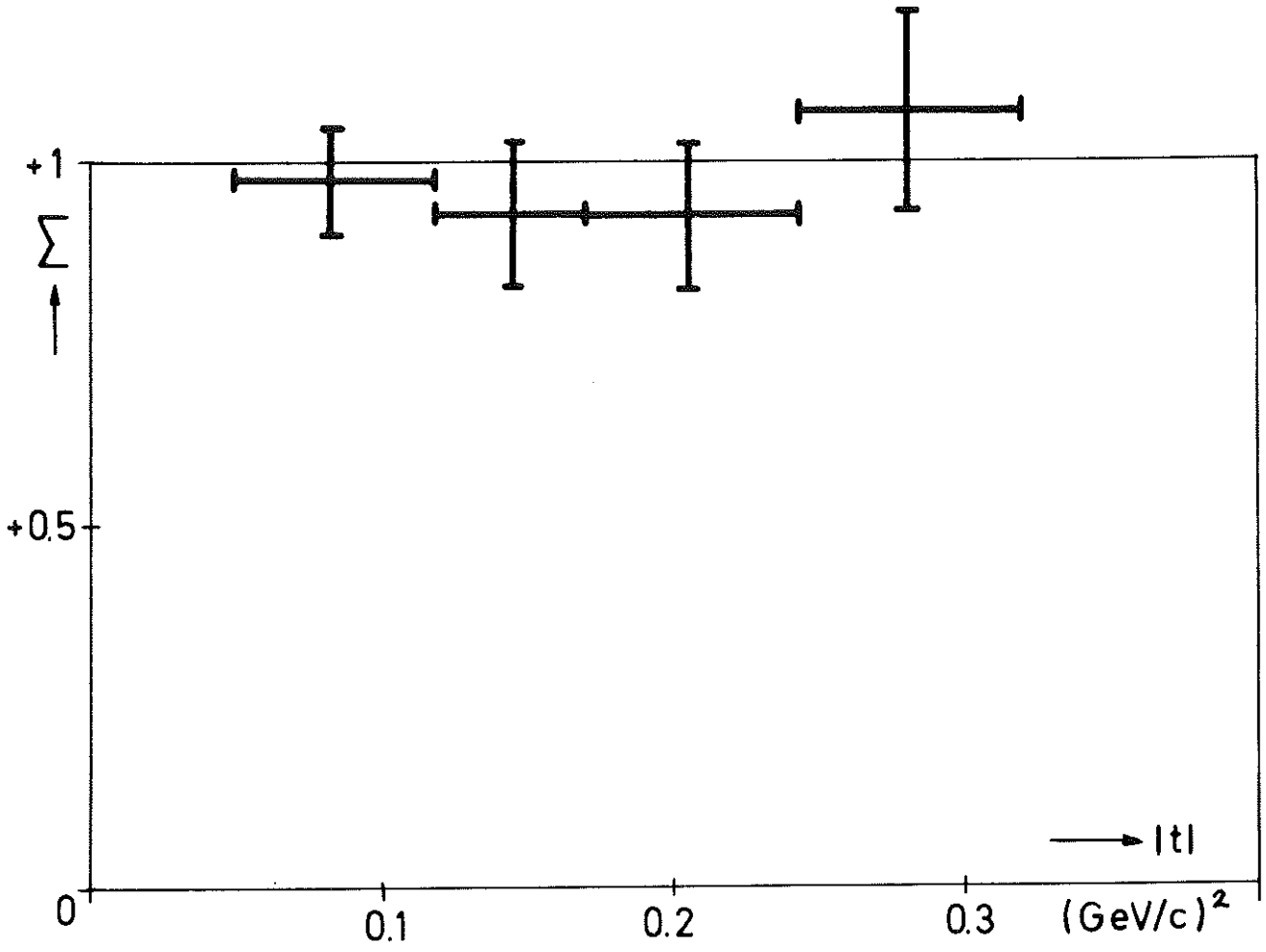

Asymmetry of ρ^0 Photoproduction

$2.0 \leq E_\gamma \leq 2.8$ GeV

$0.65 \leq m_{\pi\pi} \leq 0.90$ GeV/c²

Decay Solid Angle: 0.36 ster.

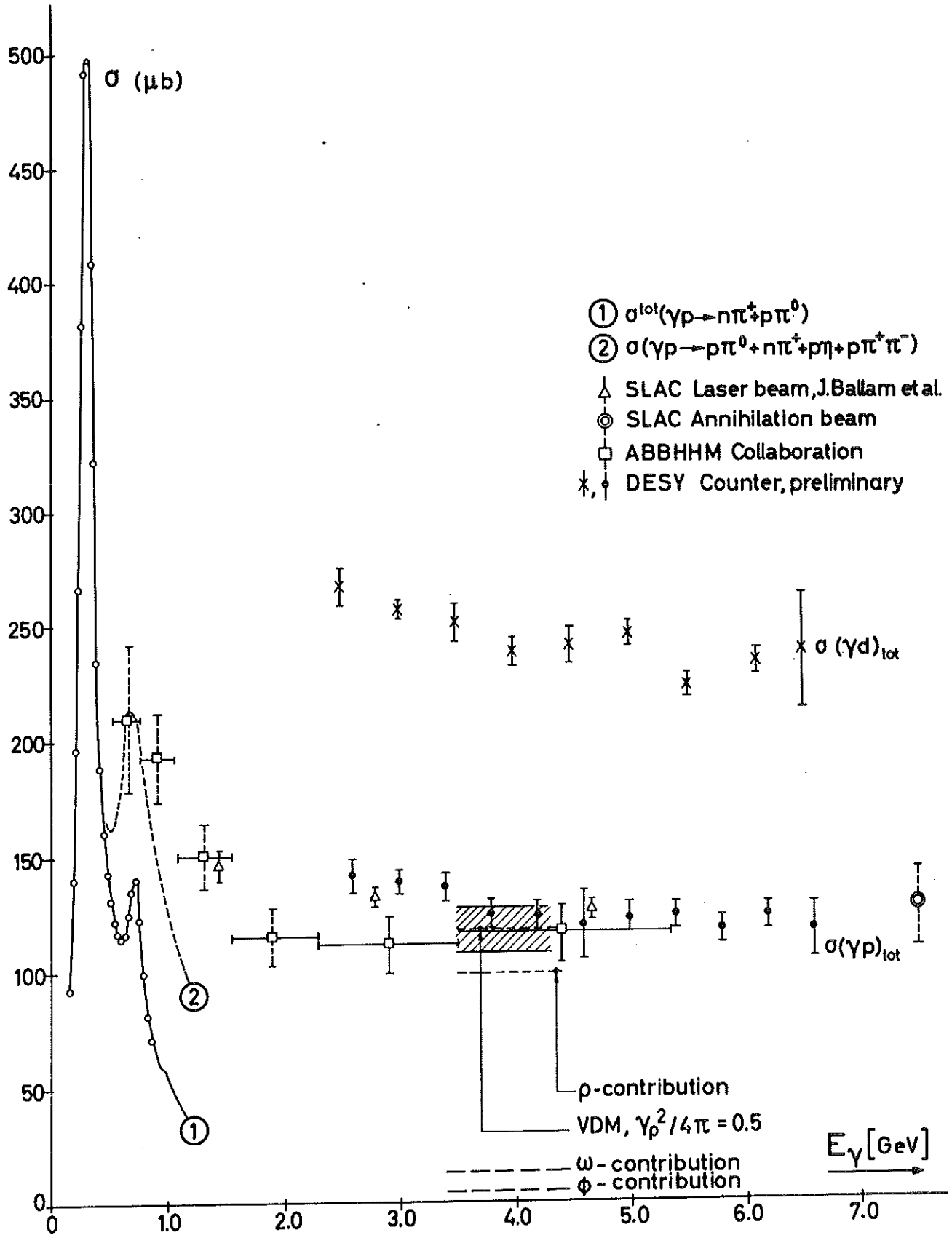
σ (μb)
500
450
400
350
300
250
200
150
100
50
0
0
1.0
2.0
3.0
4.0
5.0
6.0
7.0
① σ^tot(γp→nπ⁺pπ⁰)
② σ(γp→pπ⁰+nπ⁺+pη+pπ⁺π⁻)
SLAC Laser beam, J.Ballam et al.
SLAC Annihilation beam
ABBHHM Collaboration
DESY Counter, preliminary
σ (γd)tot
σ(γp)tot
ρ-contribution
VDM, γρ²/4π = 0.5
ω - contribution
φ - contribution
Eγ [GeV]

Fig. 10

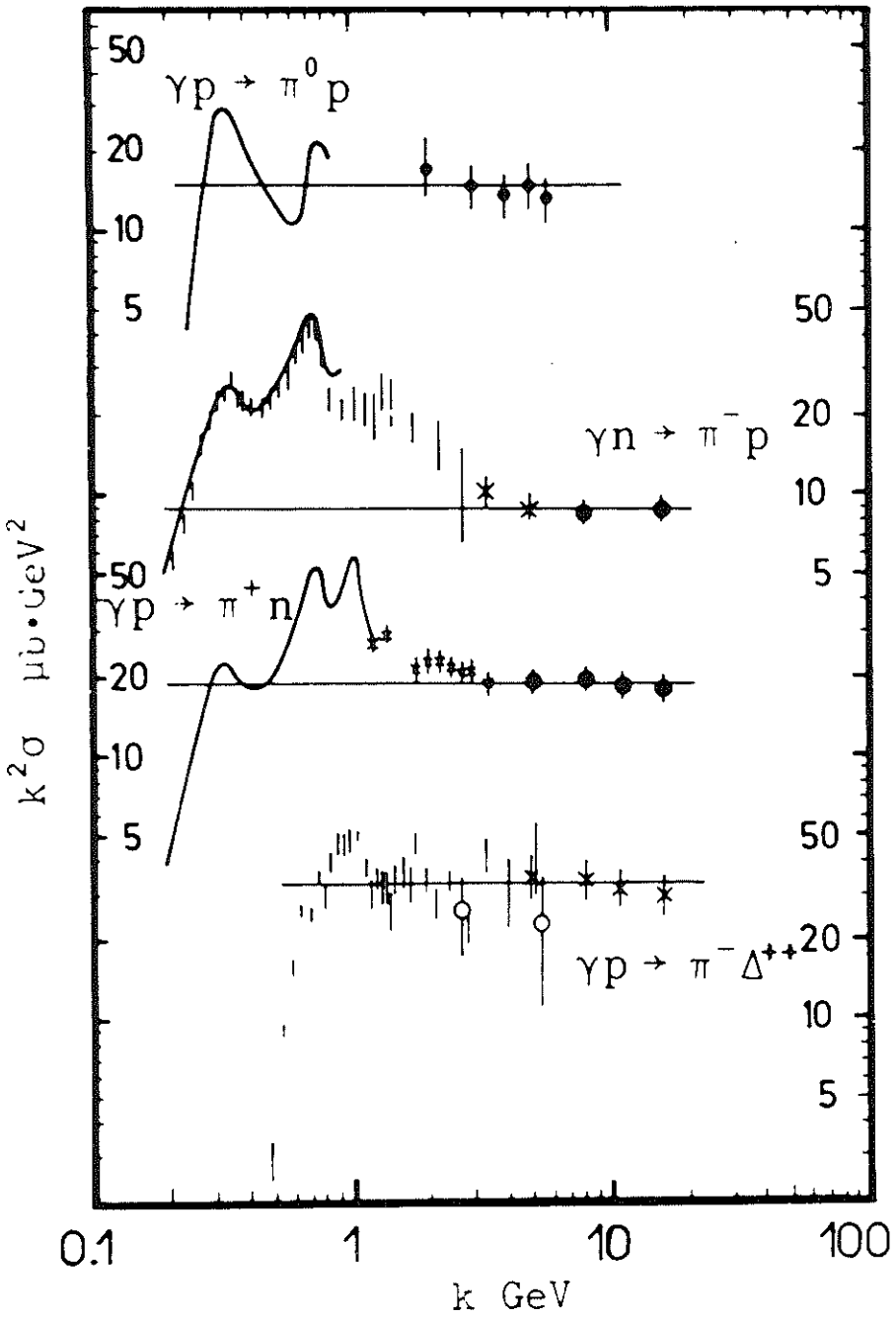
γp → π⁰p
γn → π⁻p
γp → π⁺n
γp → π⁻Δ⁺⁺
k²σ μb·GeV²
k GeV
0.1
1
10
100
50
20
10
5

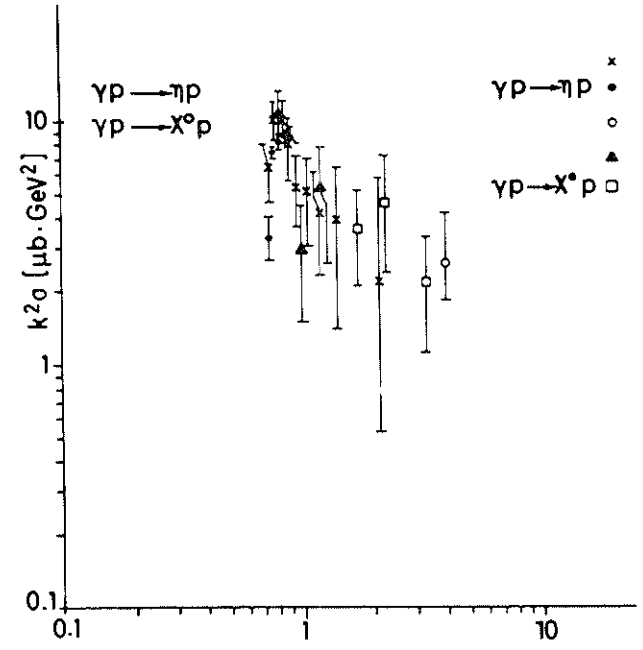
γp → ηp
γp → X°p
γp → ηp
γp → X°p
k²σ [μb·GeV²]
0.1
1
10

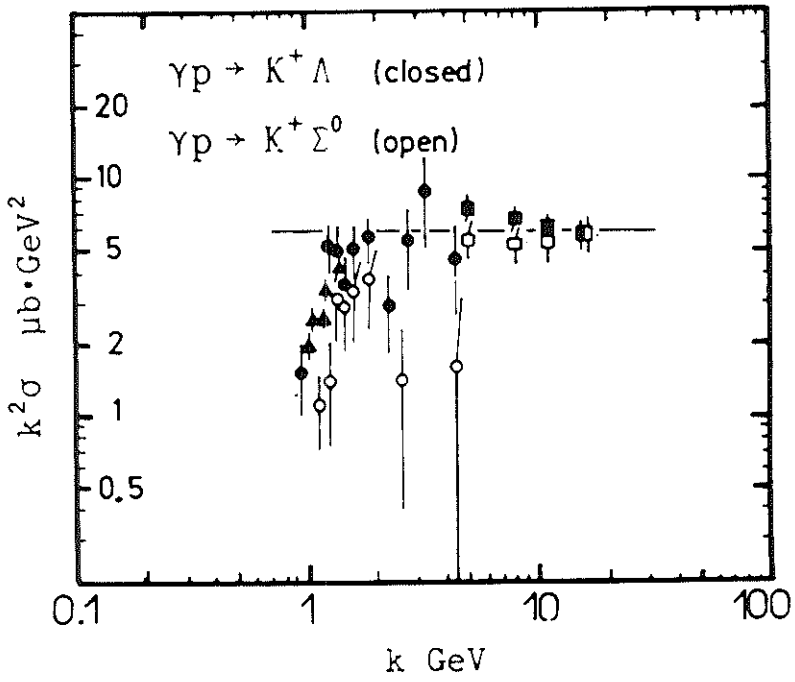
γp → K⁺Λ (closed)
γp → K⁺Σ⁰ (open)
k²σ μb·GeV²
k GeV
0.1
1
10
100
20
10
5
2
1
0.5

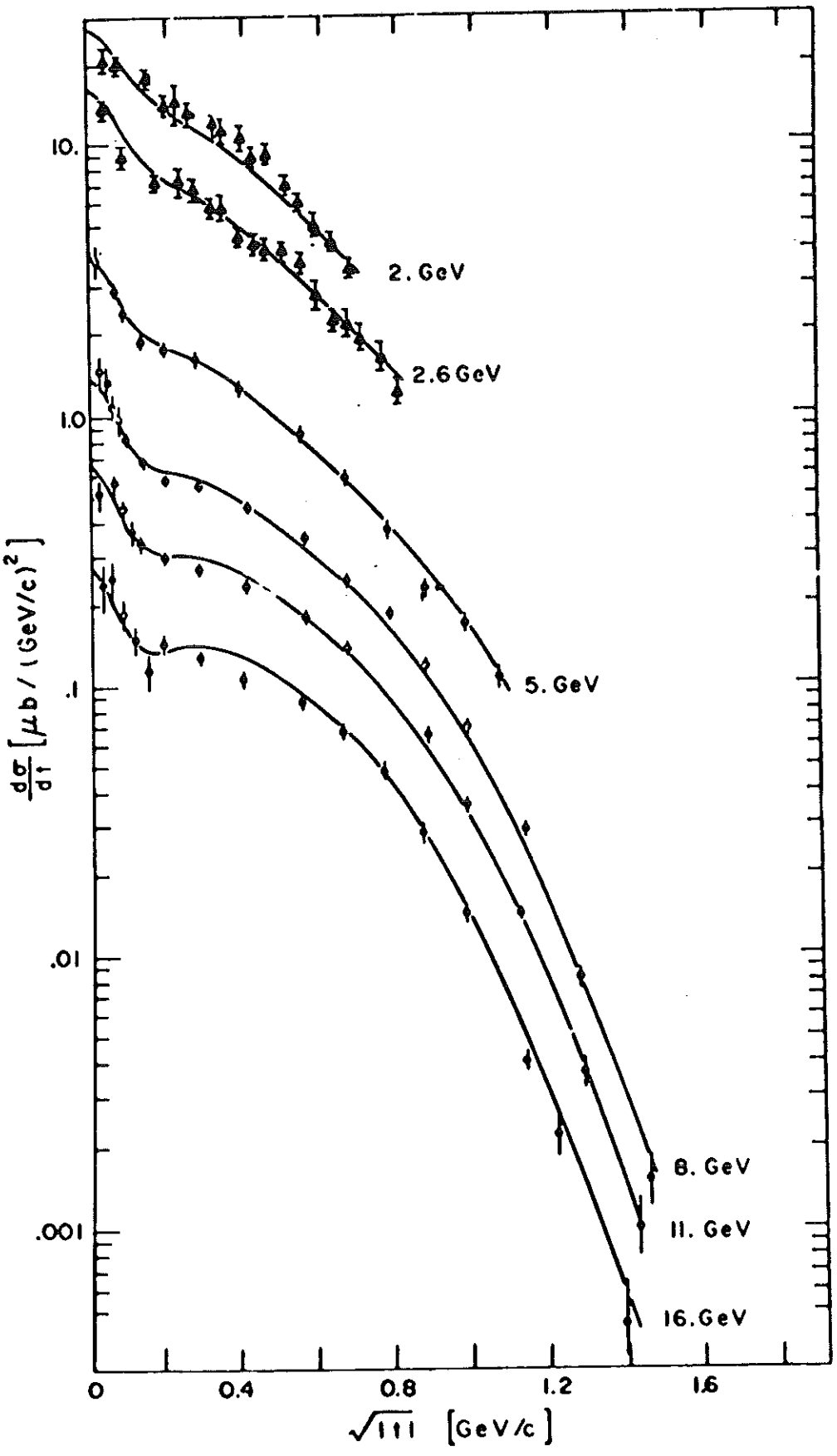
10.
1.0
.1
.01
.001
2. GeV
2.6 GeV
5. GeV
8. GeV
11. GeV
16. GeV
0
0.4
0.8
1.2
1.6
$\frac{d\sigma}{dt}$ [μb / (GeV/c)²]
$\sqrt{|t|}$ [GeV/c]

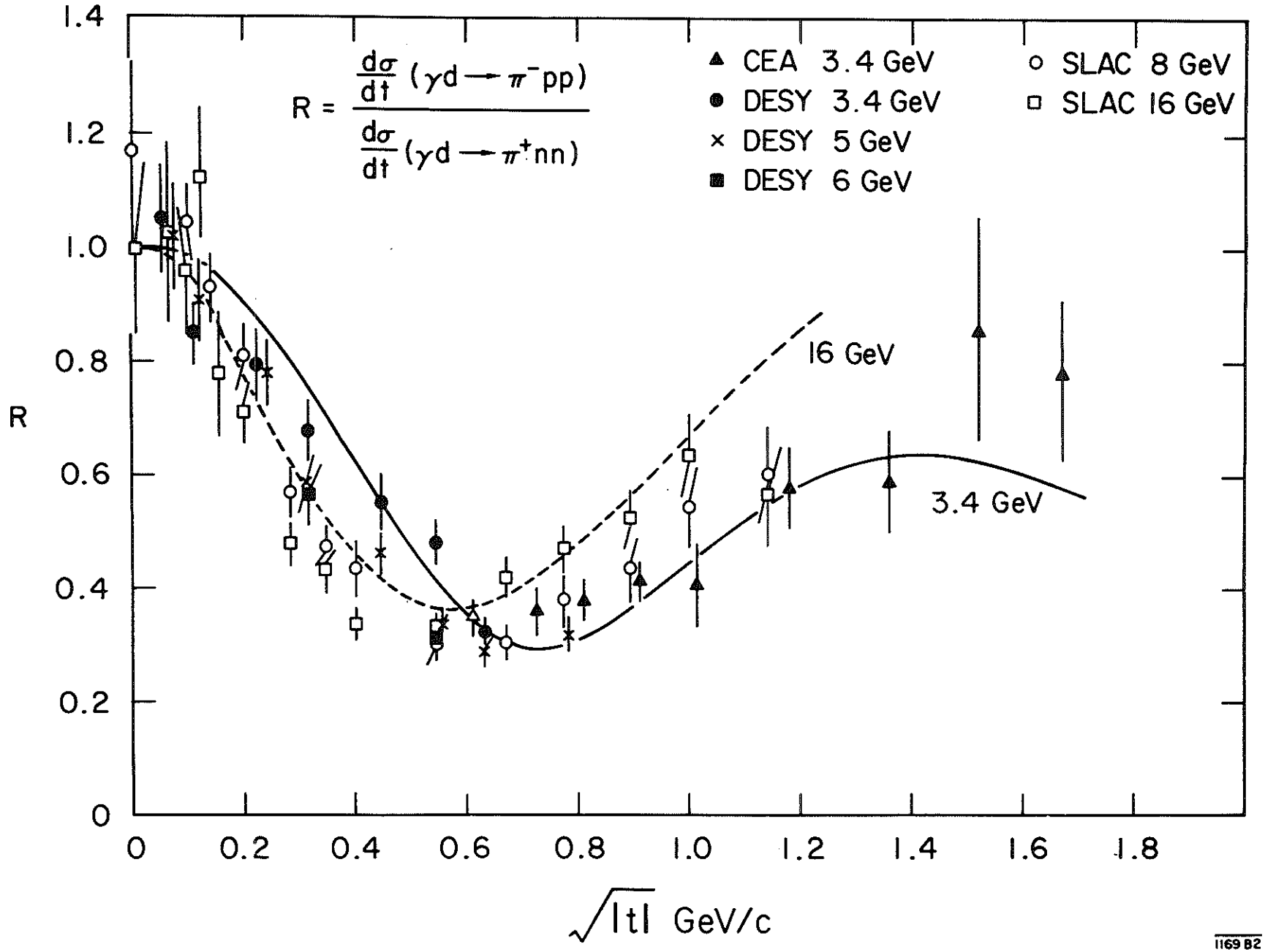
$R = \frac{\frac{d\sigma}{dt}(\gamma d \to \pi^- pp)}{\frac{d\sigma}{dt}(\gamma d \to \pi^+ nn)}$
CEA 3.4 GeV
DESY 3.4 GeV
DESY 5 GeV
DESY 6 GeV
SLAC 8 GeV
SLAC 16 GeV
16 GeV
3.4 GeV
R
$\sqrt{|t|}$ GeV/c
1169B2

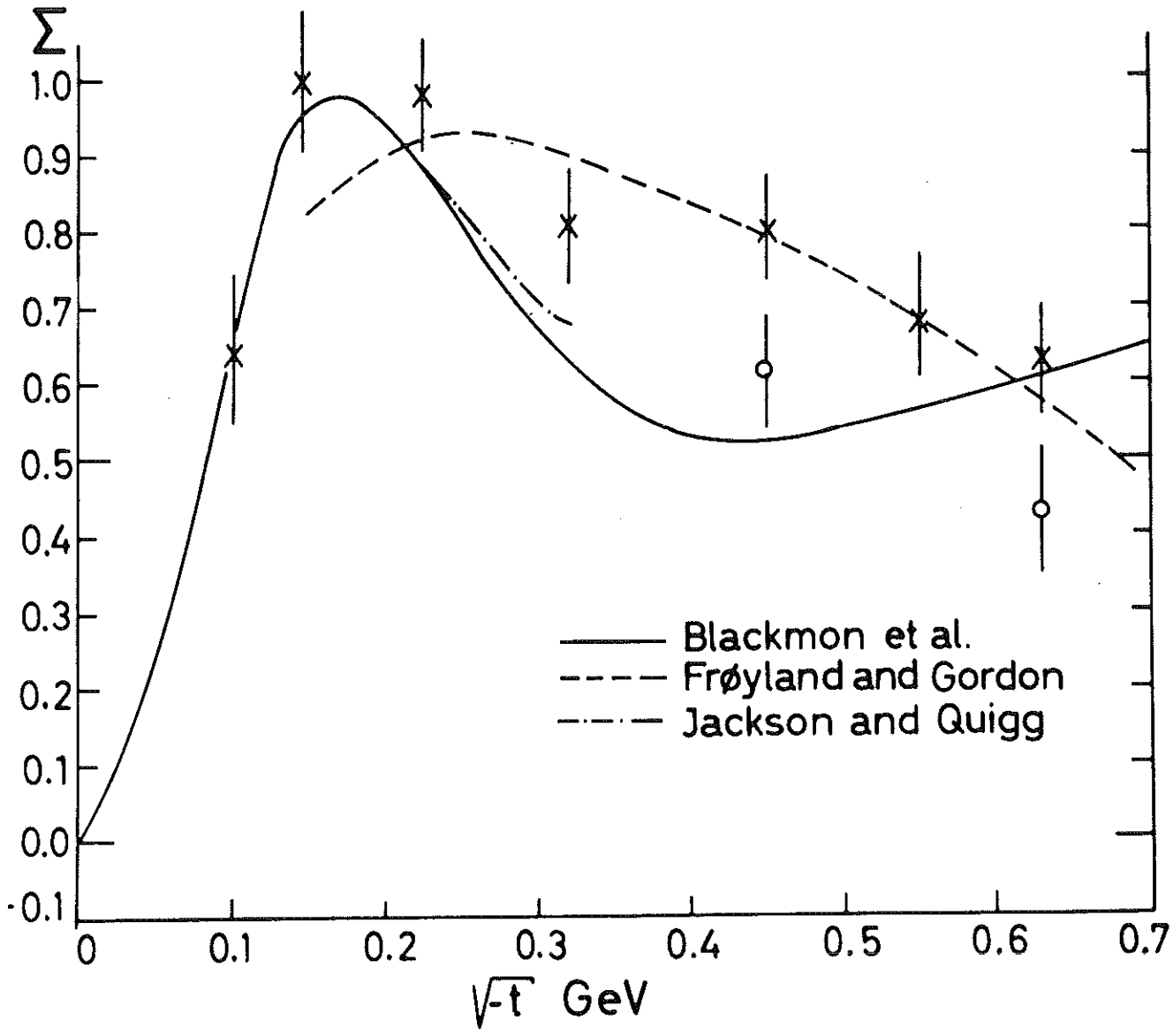
Σ
1.0
0.9
0.8
0.7
0.6
0.5
0.4
0.3
0.2
0.1
0.0
-0.1
0
0.1
0.2
0.3
0.4
0.5
0.6
0.7
√-t GeV
Blackmon et al.
Frøyland and Gordon
Jackson and Quigg

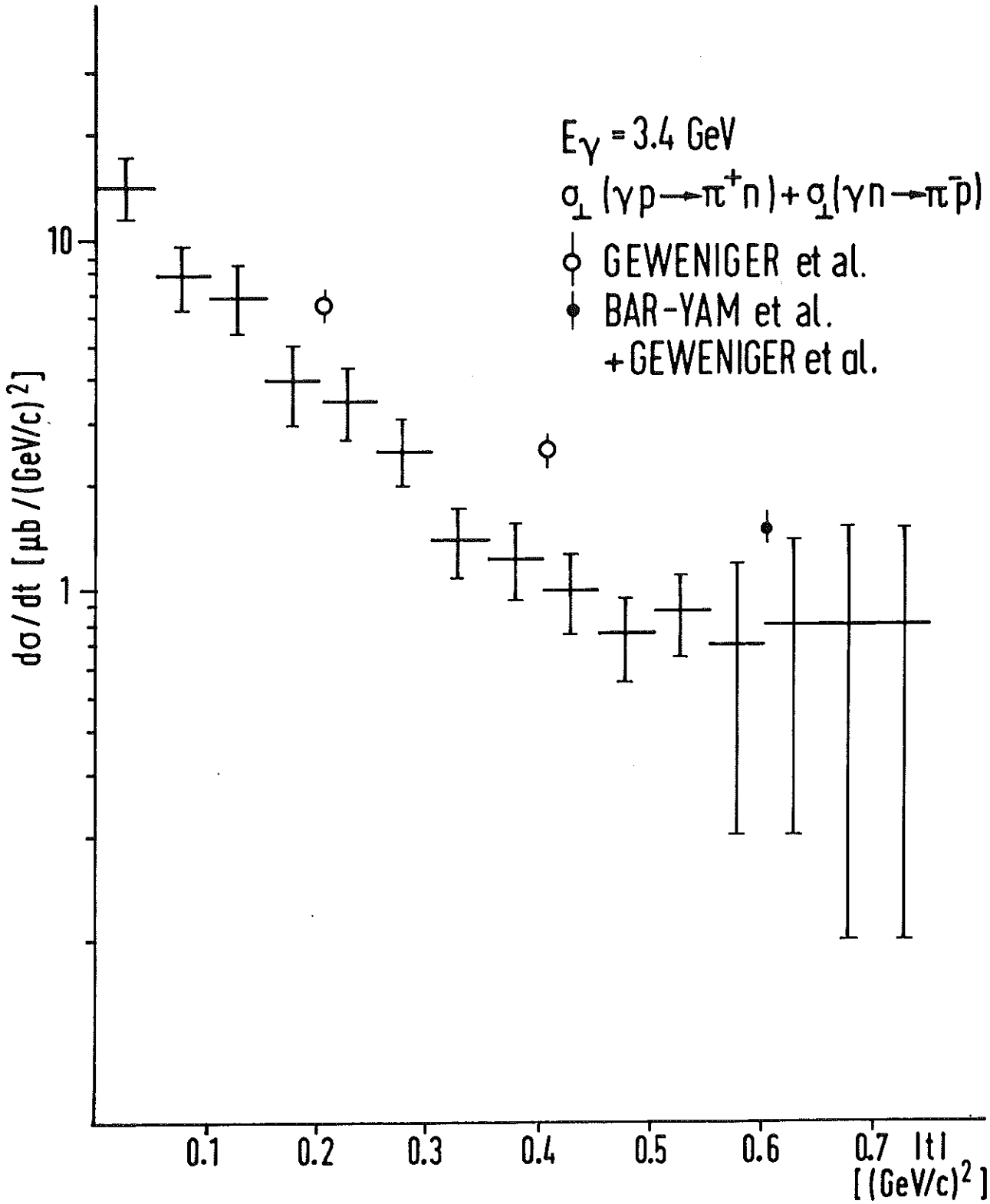
E_γ = 3.4 GeV
$\sigma_\perp(\gamma p \to \pi^+ n) + \sigma_\perp(\gamma n \to \pi^- p)$
GEWENIGER et al.
BAR-YAM et al.
+GEWENIGER et al.
10
1
$d\sigma/dt$ [$\mu b/(GeV/c)^2$]
0.1
0.2
0.3
0.4
0.5
0.6
0.7
$|t|$
[$(GeV/c)^2$]

Fig.4

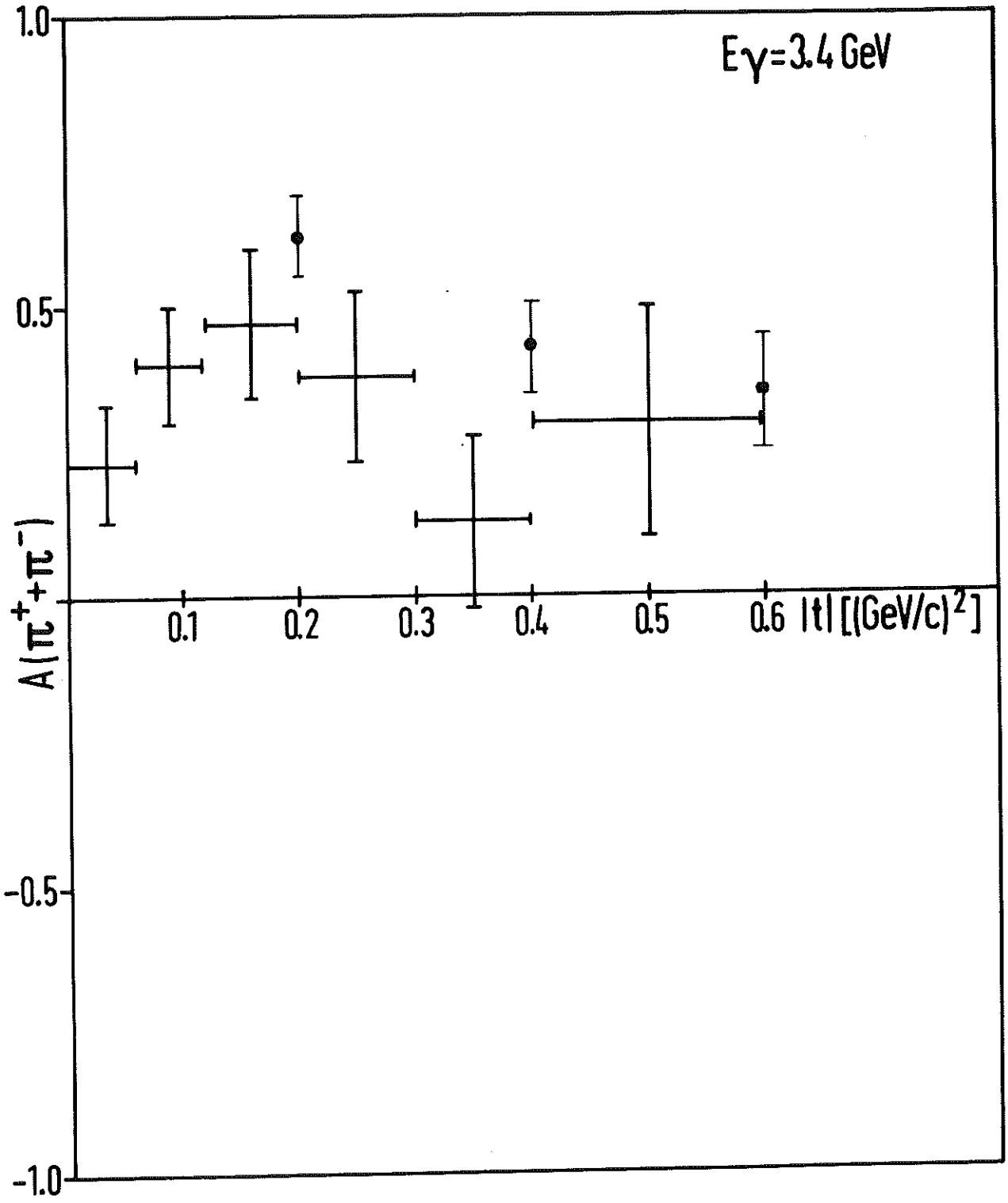
Eγ=3.4 GeV
1.0
0.5
-0.5
-1.0
0.1
0.2
0.3
0.4
0.5
0.6
|t| [(GeV/c)²]
A(π⁺+π⁻)

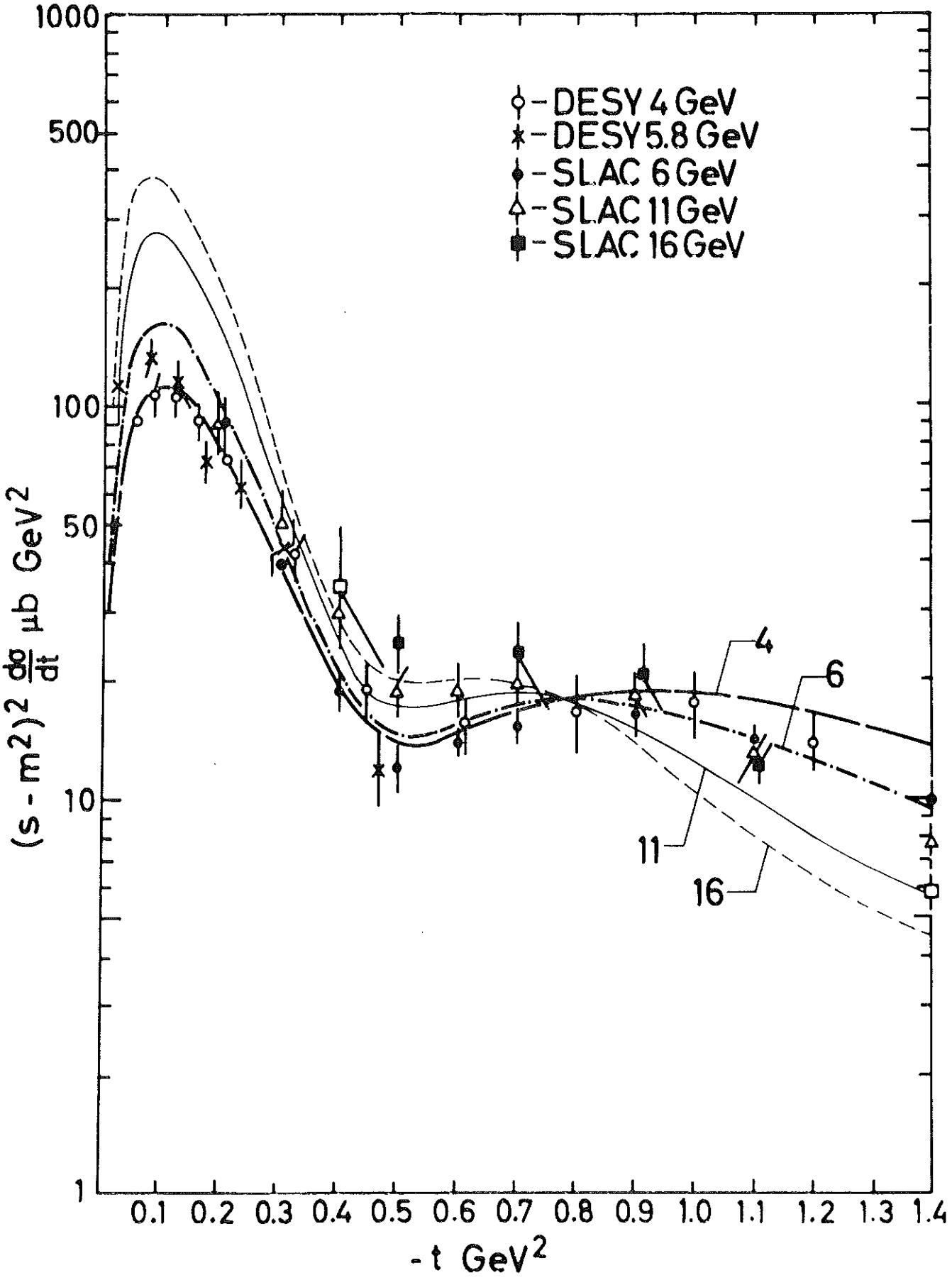
1000
500
100
50
10
1
$(s-m^2)^2 \frac{d\sigma}{dt}$ μb GeV^2
0.1 0.2 0.3 0.4 0.5 0.6 0.7 0.8 0.9 1.0 1.1 1.2 1.3 1.4
-t GeV^2
DESY 4 GeV
DESY 5.8 GeV
SLAC 6 GeV
SLAC 11 GeV
SLAC 16 GeV
4
6
11
16

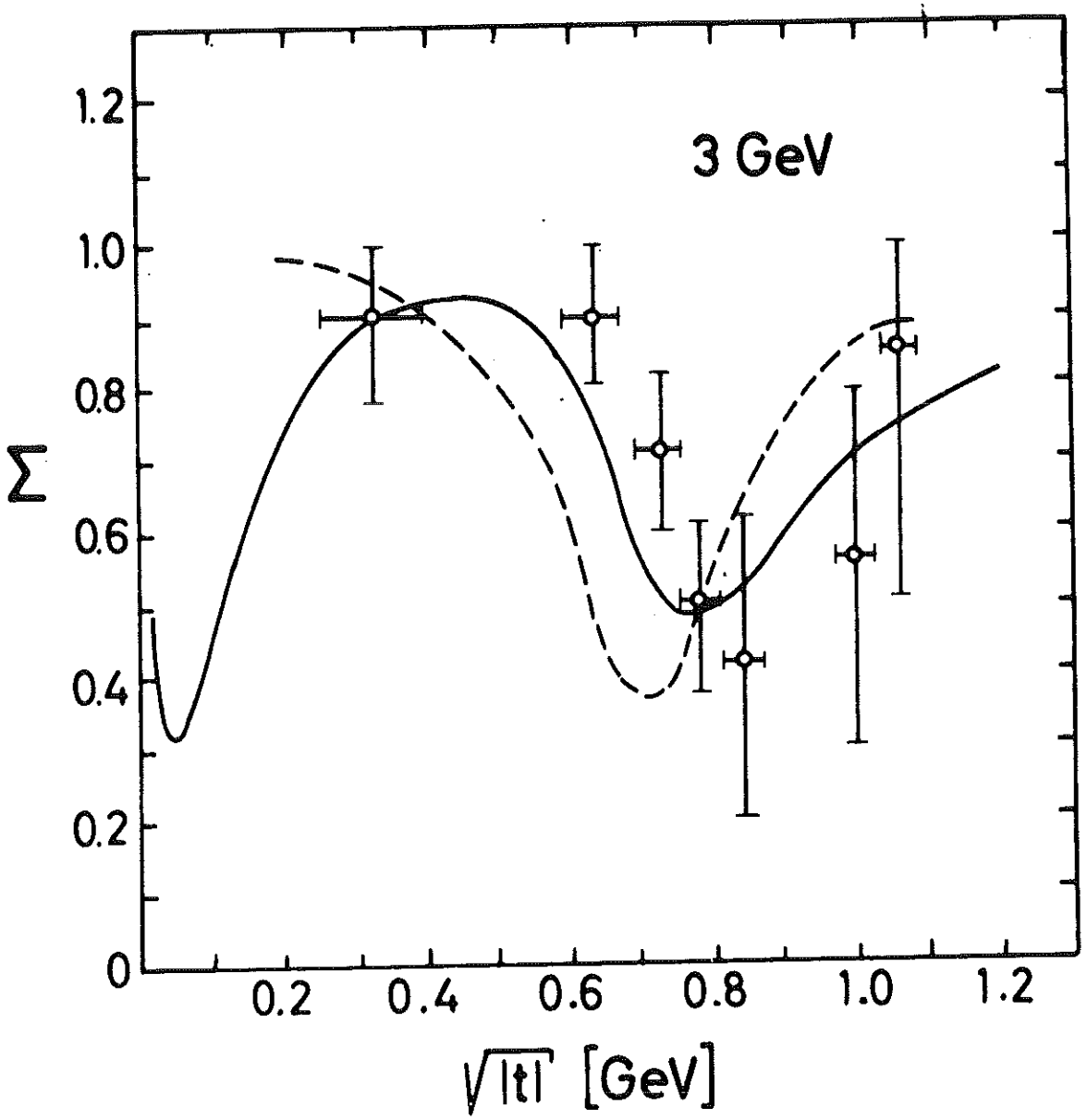
3 GeV
Σ
1.2
1.0
0.8
0.6
0.4
0.2
0
0.2
0.4
0.6
0.8
1.0
1.2
√|t| [GeV]

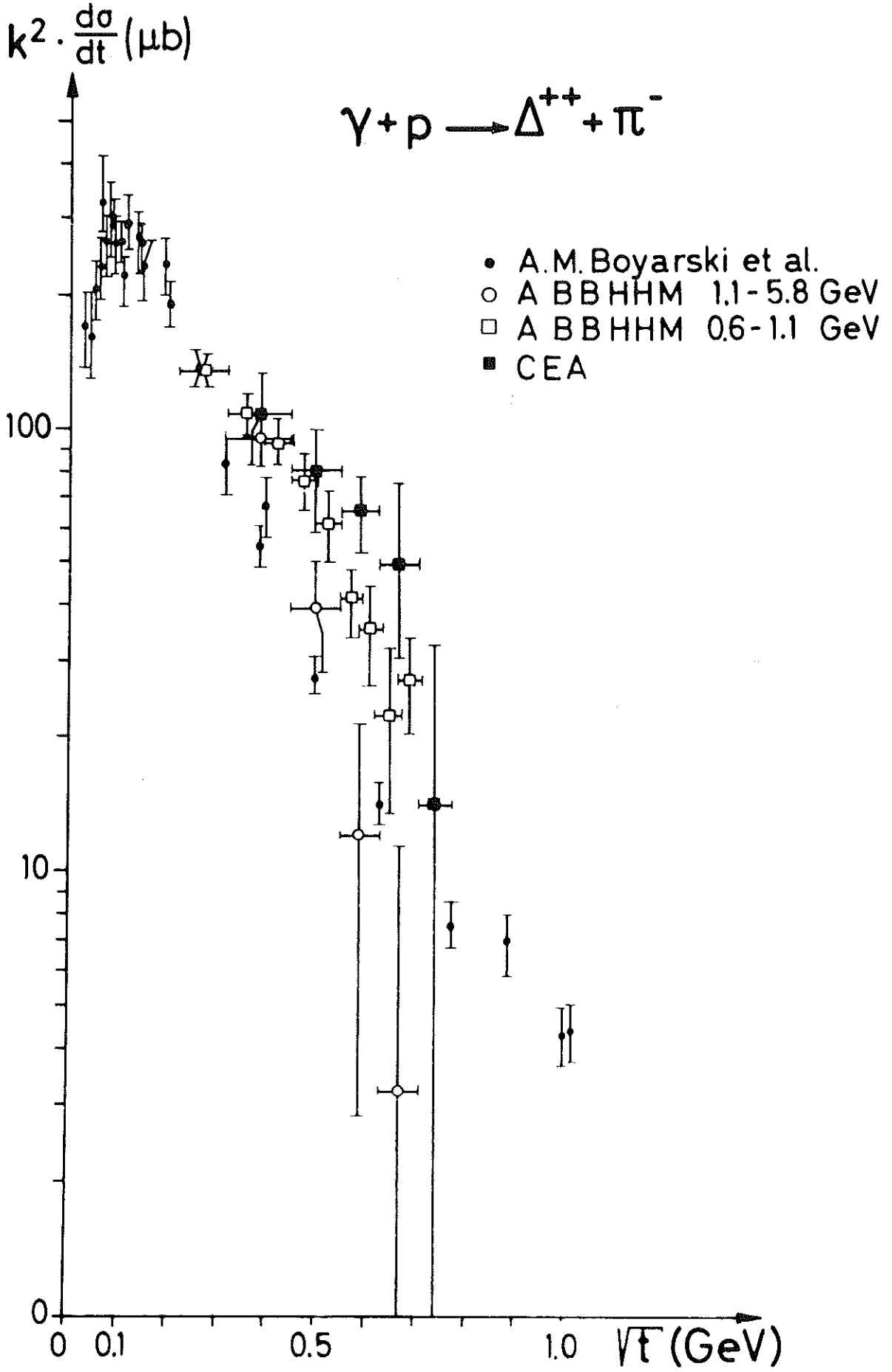
$k^2 \cdot \frac{d\sigma}{dt}$ (μb)
$\gamma + p \longrightarrow \Delta^{++} + \pi^-$
• A.M. Boyarski et al.
○ A B B H H M 1.1 - 5.8 GeV
□ A B B H H M 0.6 - 1.1 GeV
■ C E A
100
10
0
0
0.1
0.5
1.0
$\sqrt{t}$ (GeV)

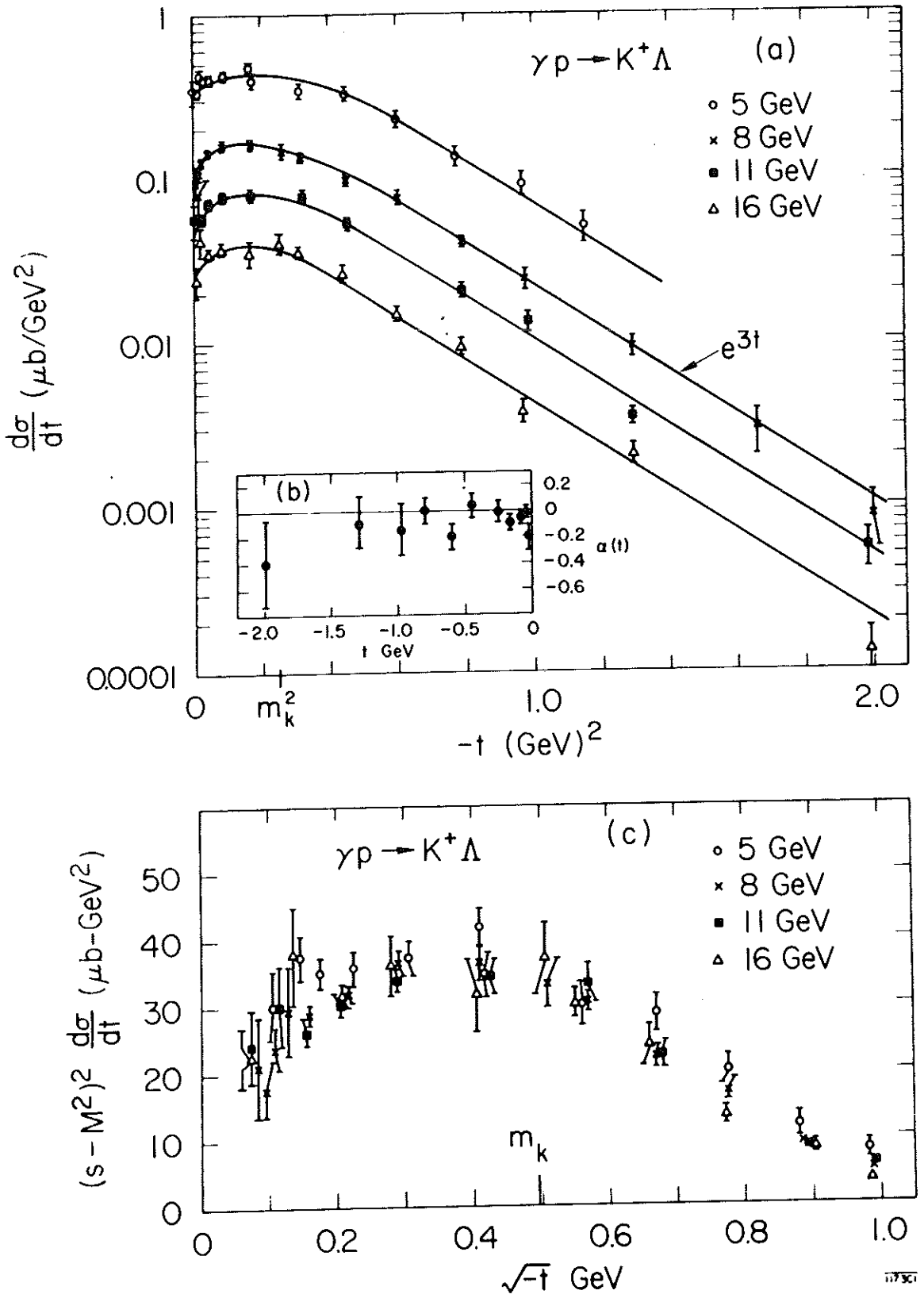
γp → K⁺Λ
(a)
5 GeV
8 GeV
11 GeV
16 GeV
e^{3t}
dσ/dt (μb/GeV²)
1
0.1
0.01
0.001
0.0001
0
m_k²
1.0
2.0
-t (GeV)²
(b)
0.2
0
-0.2
-0.4
-0.6
α(t)
-2.0
-1.5
-1.0
-0.5
0
t GeV
γp → K⁺Λ
(c)
5 GeV
8 GeV
11 GeV
16 GeV
(s-M²)² dσ/dt (μb-GeV²)
50
40
30
20
10
0
m_k
0
0.2
0.4
0.6
0.8
1.0
√-t GeV

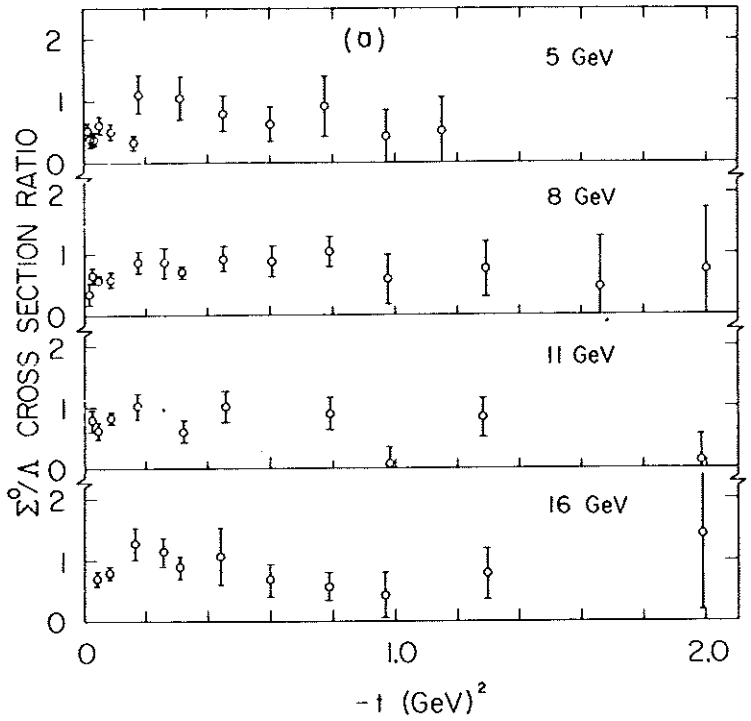
(a)
5 GeV
8 GeV
11 GeV
16 GeV
Σ^0/Λ CROSS SECTION RATIO
0
1.0
2.0
$-t$ (GeV)^2

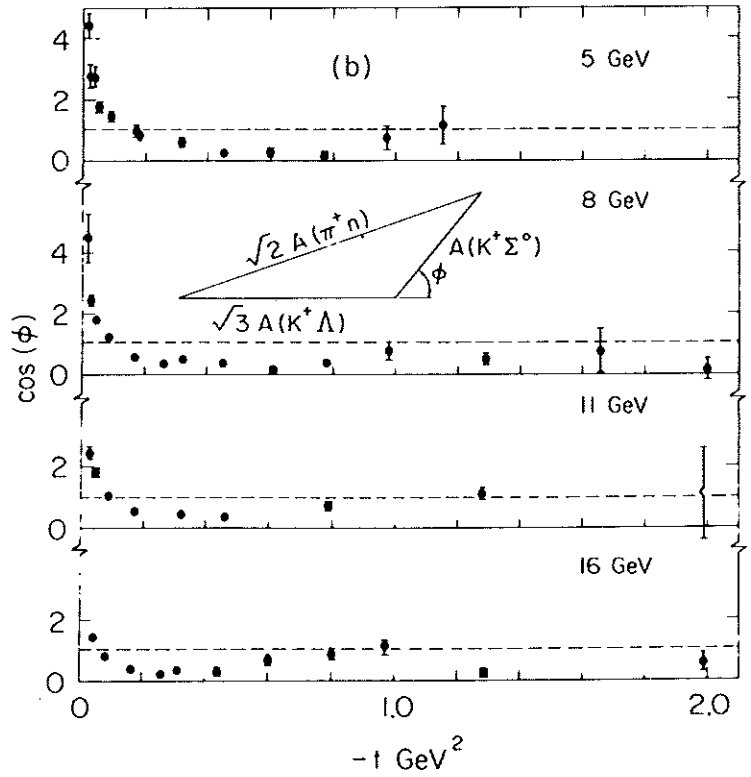
(b)
5 GeV
8 GeV
11 GeV
16 GeV
$\sqrt{2}\,A(\pi^+ n)$
$A(K^+\Sigma^0)$
ϕ
$\sqrt{3}\,A(K^+\Lambda)$
cos (ϕ)
0
1.0
2.0
$-t$ GeV^2

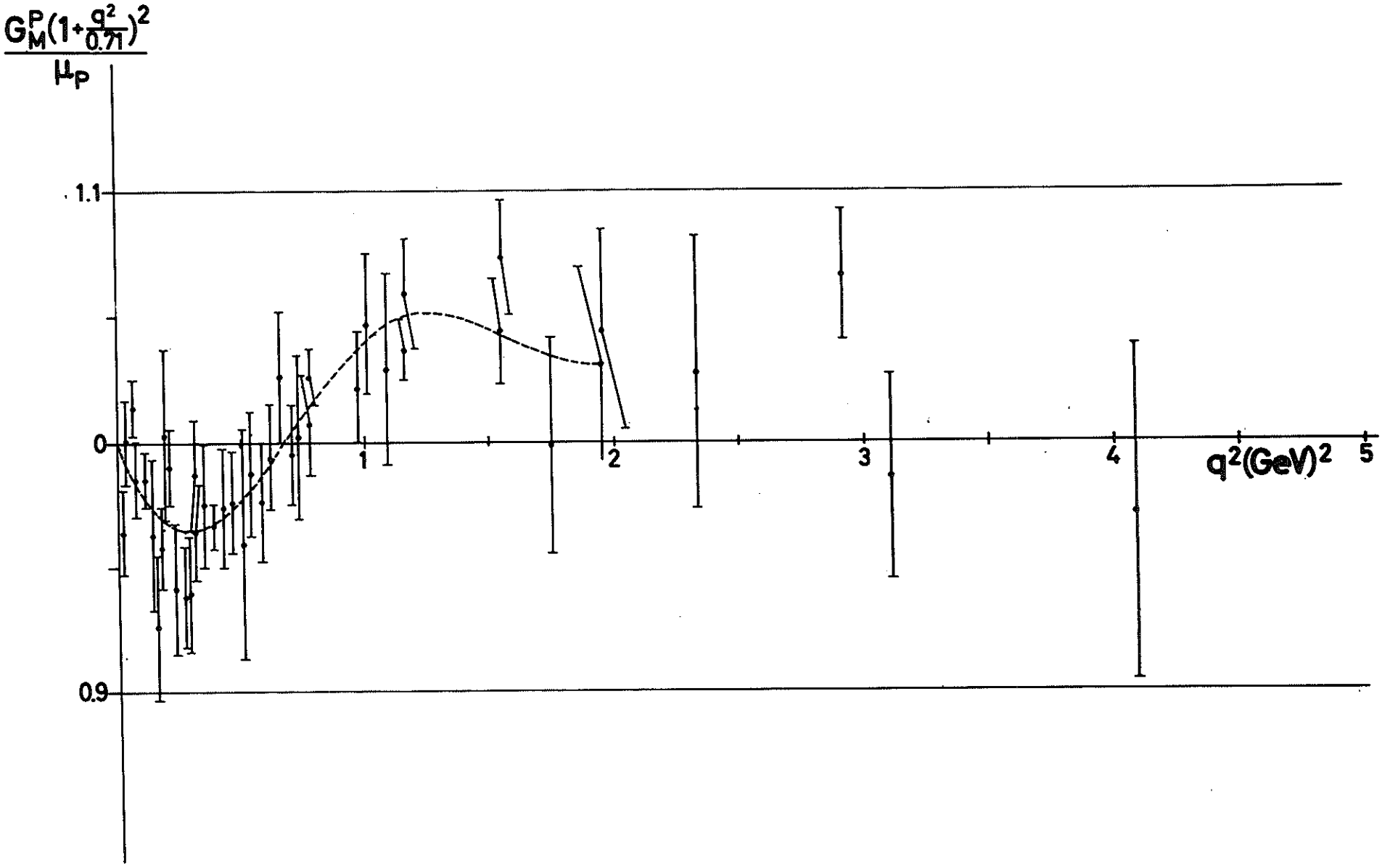
$\frac{G_M^p(1+\frac{q^2}{0.71})^2}{\mu_p}$
1.1
0
0.9
1
2
3
4
5
q^2(GeV)^2

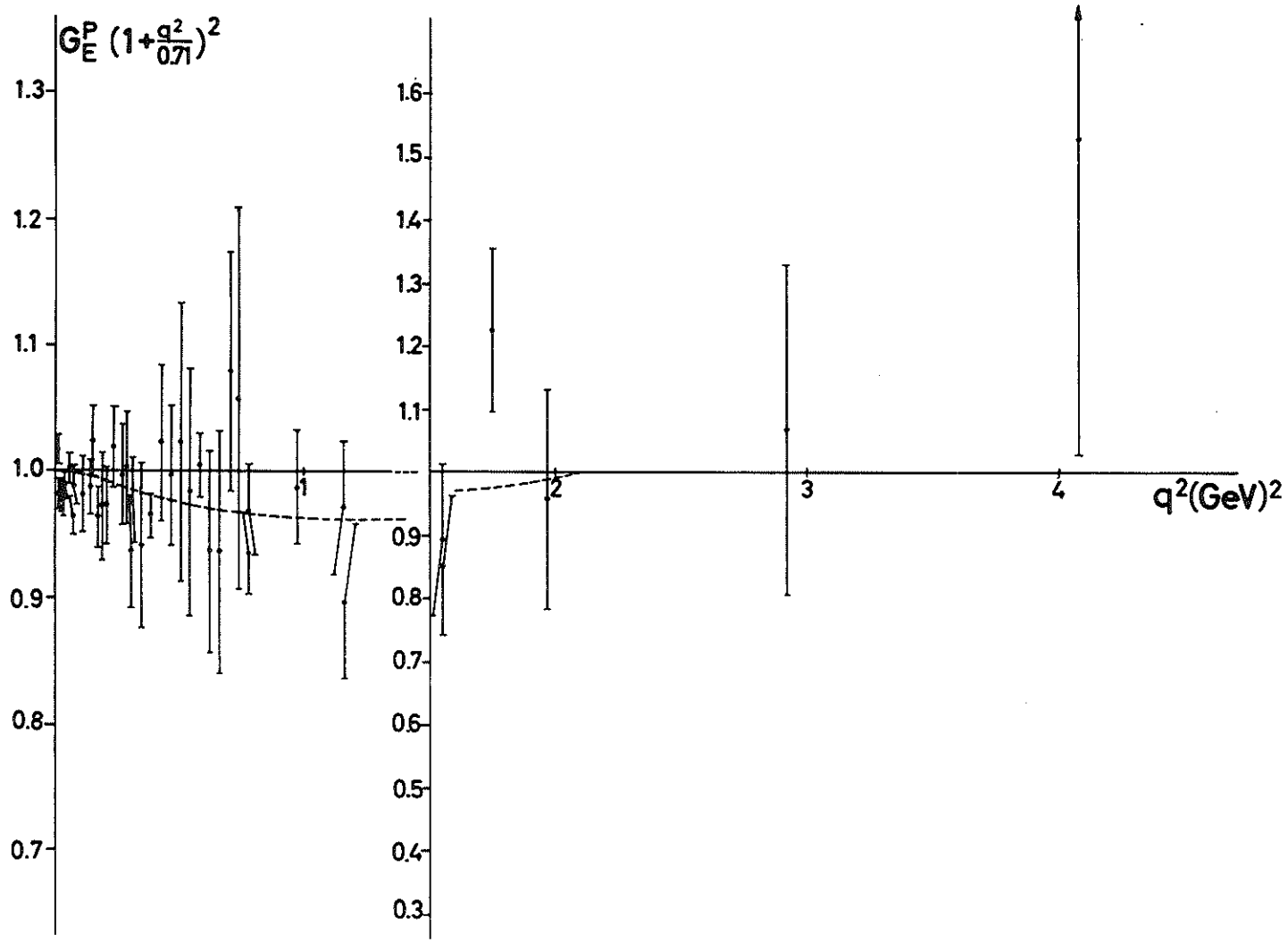
$G_E^P\,(1+\frac{q^2}{0.71})^2$
1.3
1.2
1.1
1.0
0.9
0.8
0.7
1.6
1.5
1.4
1.3
1.2
1.1
0.9
0.8
0.7
0.6
0.5
0.4
0.3
1
2
3
4
$q^2(GeV)^2$

$\frac{G_M^N(1+\frac{q^2}{0.71})^2}{\mu_N}$
1.5
1.4
1.3
1.2
1.1
1.0
0.9
0.8
0.7
0.6
0.5
0.4
0.3
0.5
1.0
1.5
2.0
$q^2(GeV)^2$ 25

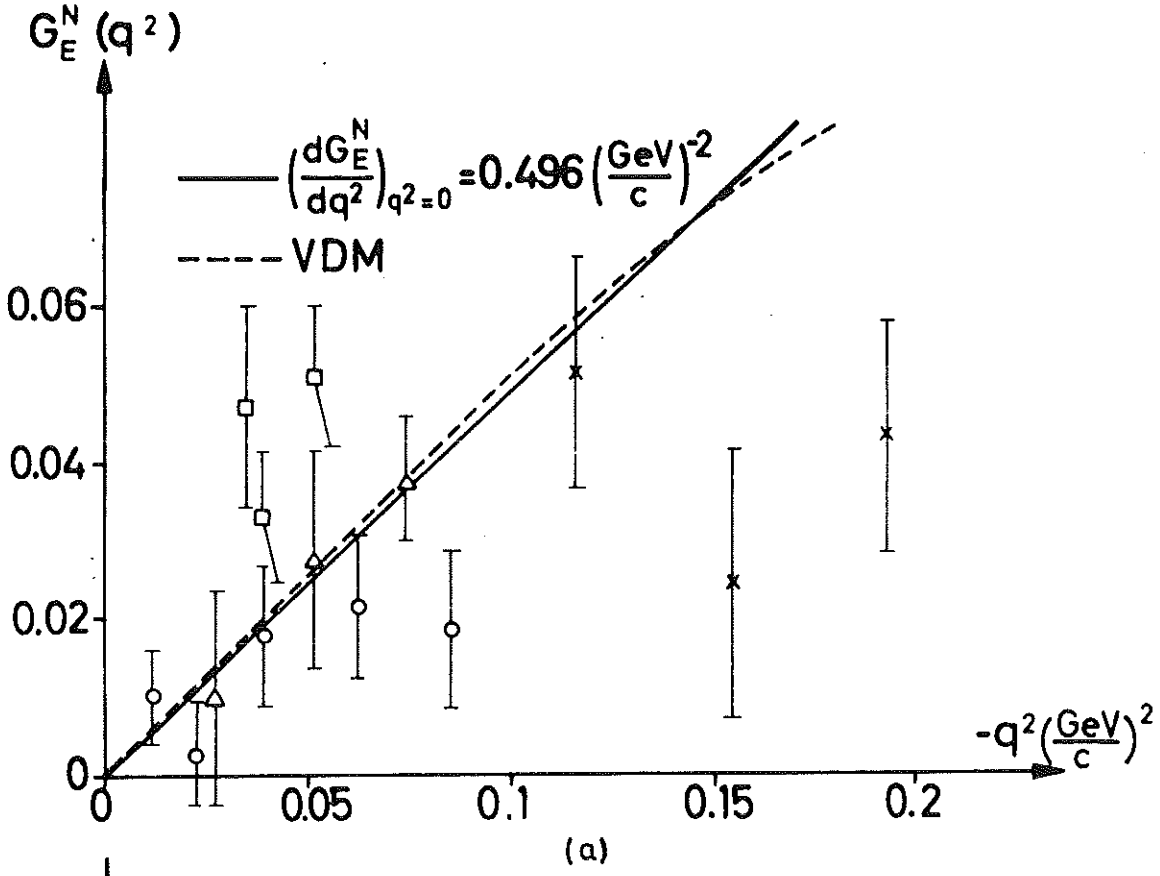
$G_E^N(q^2)$
$\left(\frac{dG_E^N}{dq^2}\right)_{q^2=0} = 0.496\left(\frac{GeV}{c}\right)^{-2}$
VDM
0.06
0.04
0.02
0
0
0.05
0.1
0.15
0.2
$-q^2\left(\frac{GeV}{c}\right)^2$

(a)

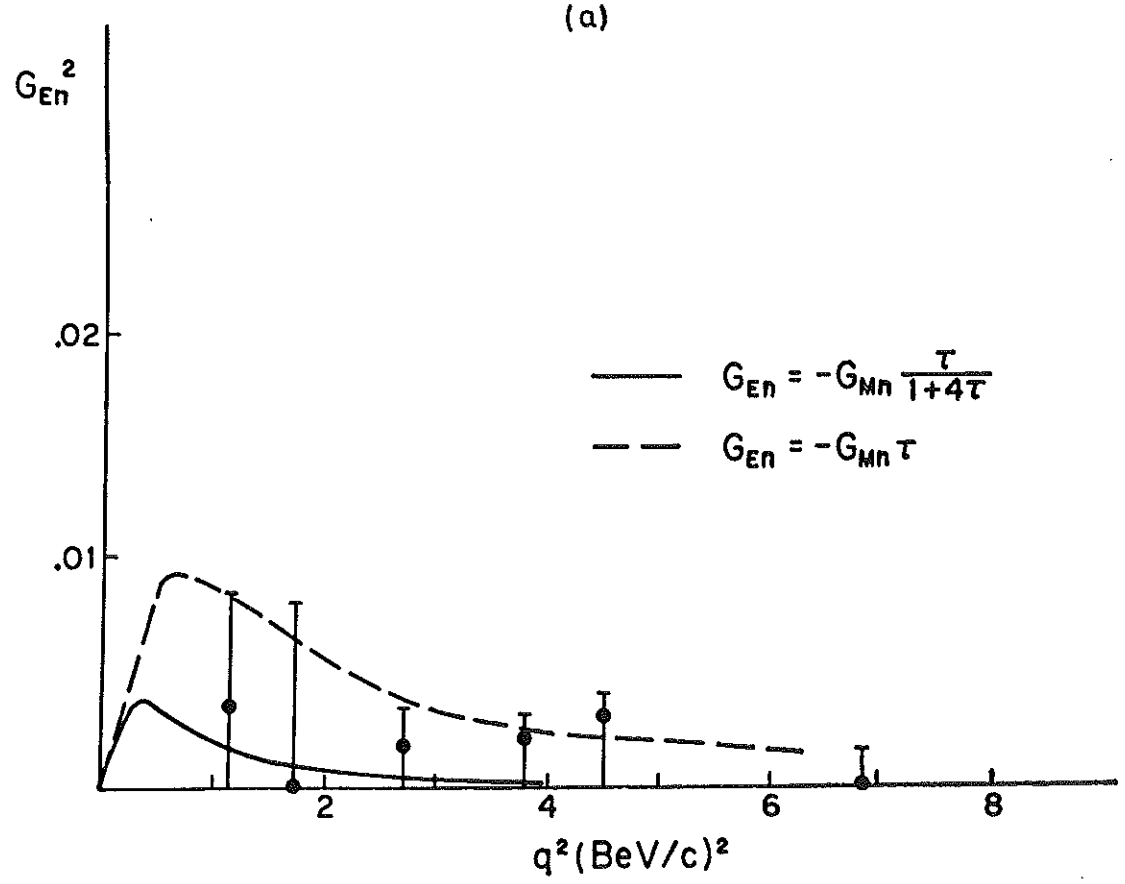
G_{En}^2
.02
.01
$G_{En} = -G_{Mn}\frac{\tau}{1+4\tau}$
$G_{En} = -G_{Mn}\tau$
2
4
6
8
q^2(BeV/c)²

(b)

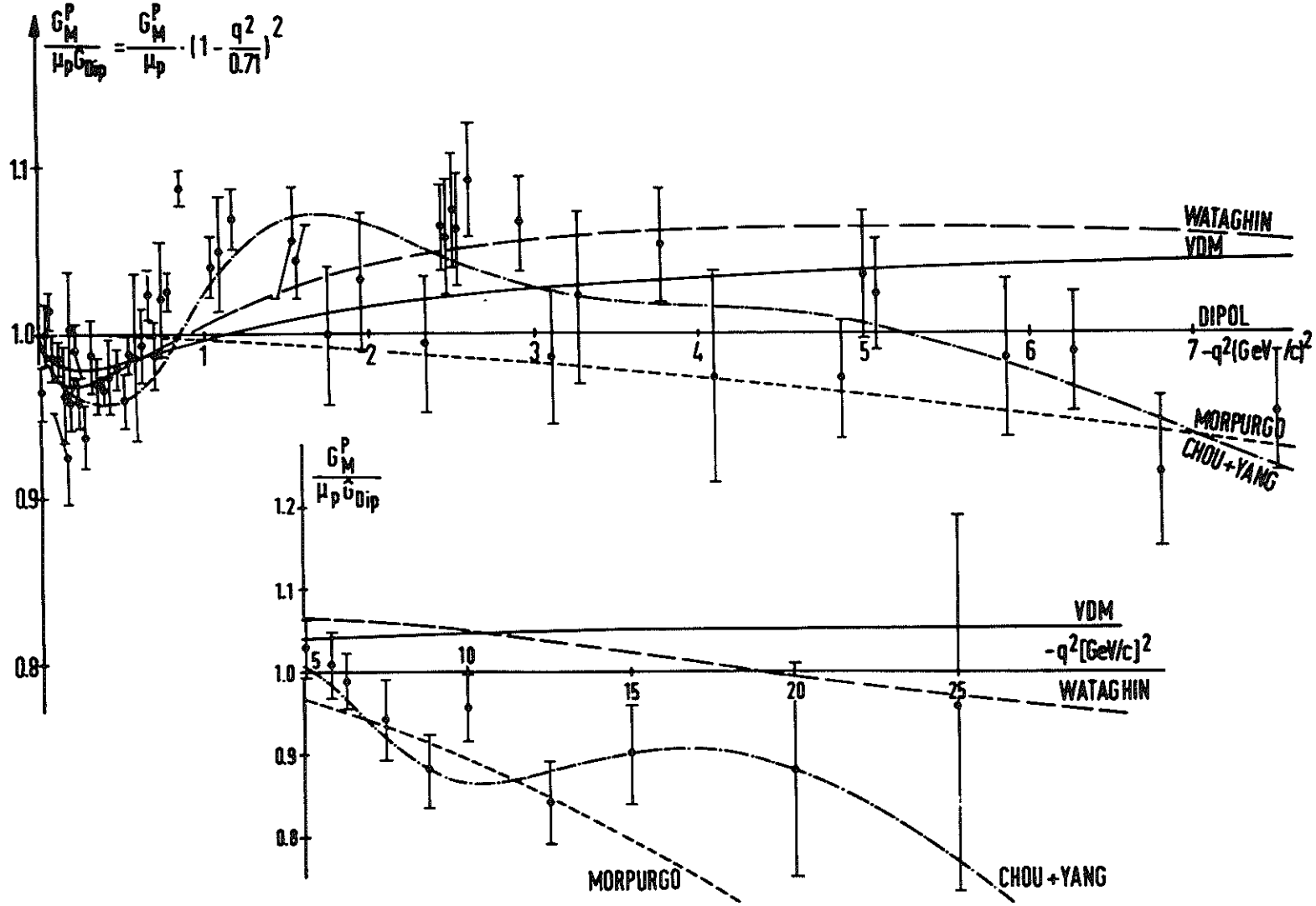
$\frac{G_M^p}{\mu_p G_{Dip}} = \frac{G_M^p}{\mu_p} \cdot (1 - \frac{q^2}{0.71})^2$
1.1
1.0
0.9
0.8
1
2
3
4
5
6
WATAGHIN
VDM
DIPOL
$7 - q^2 (GeV_T/c)^2$
MORPURGO
CHOU+YANG
$\frac{G_M^p}{\mu_p G_{Dip}}$
1.2
1.1
1.0
0.9
0.8
5
10
15
20
25
VDM
$-q^2 [GeV/c]^2$
WATAGHIN
MORPURGO
CHOU+YANG

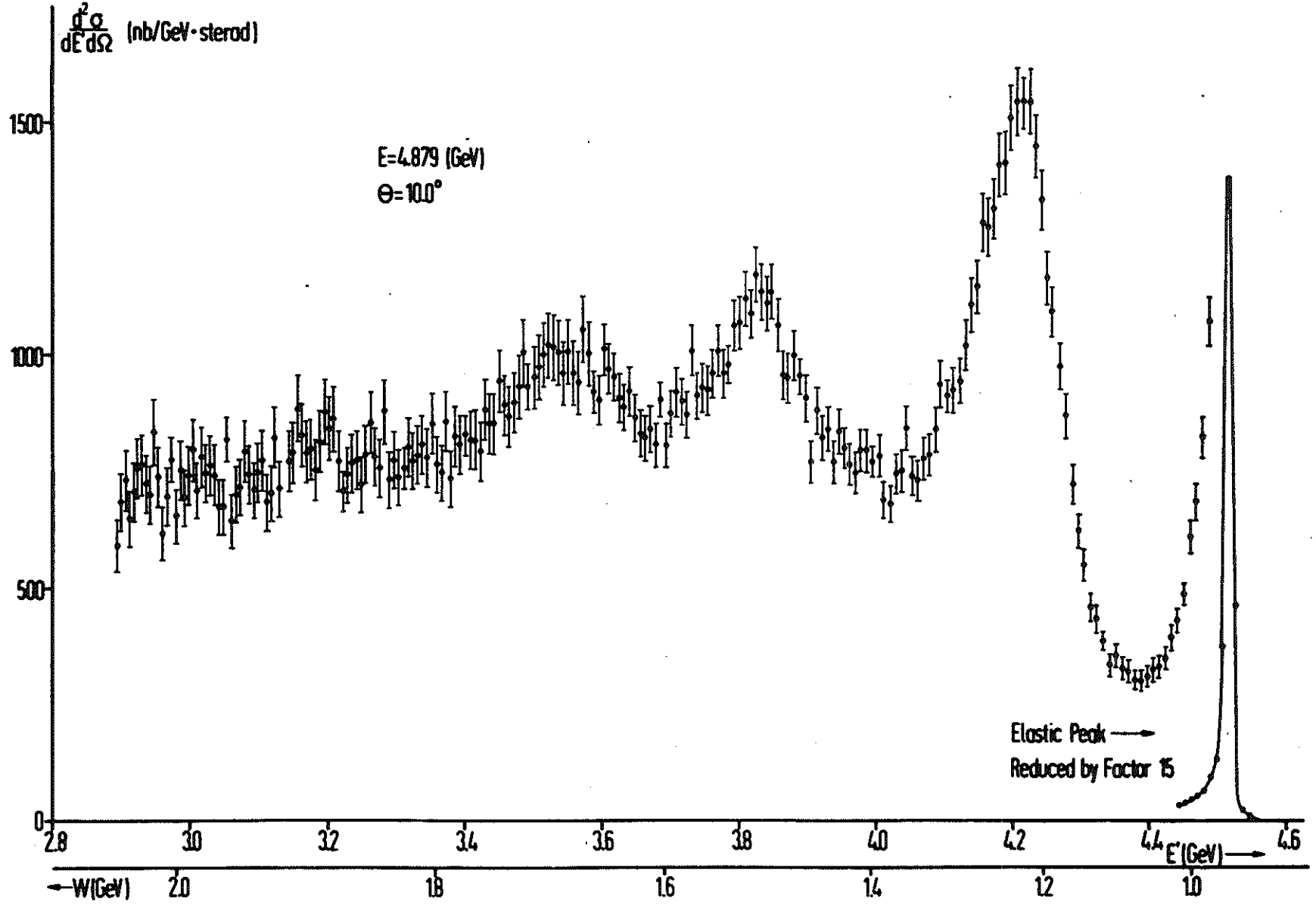
$\frac{d^2\sigma}{dE'd\Omega}$ (nb/GeV·sterad)
E=4.879 (GeV)
Θ=10.0°
Elastic Peak
Reduced by Factor 15
1500
1000
500
0
2.8
3.0
3.2
3.4
3.6
3.8
4.0
4.2
4.4
4.6
E'(GeV)
W(GeV)
2.0
1.8
1.6
1.4
1.2
1.0

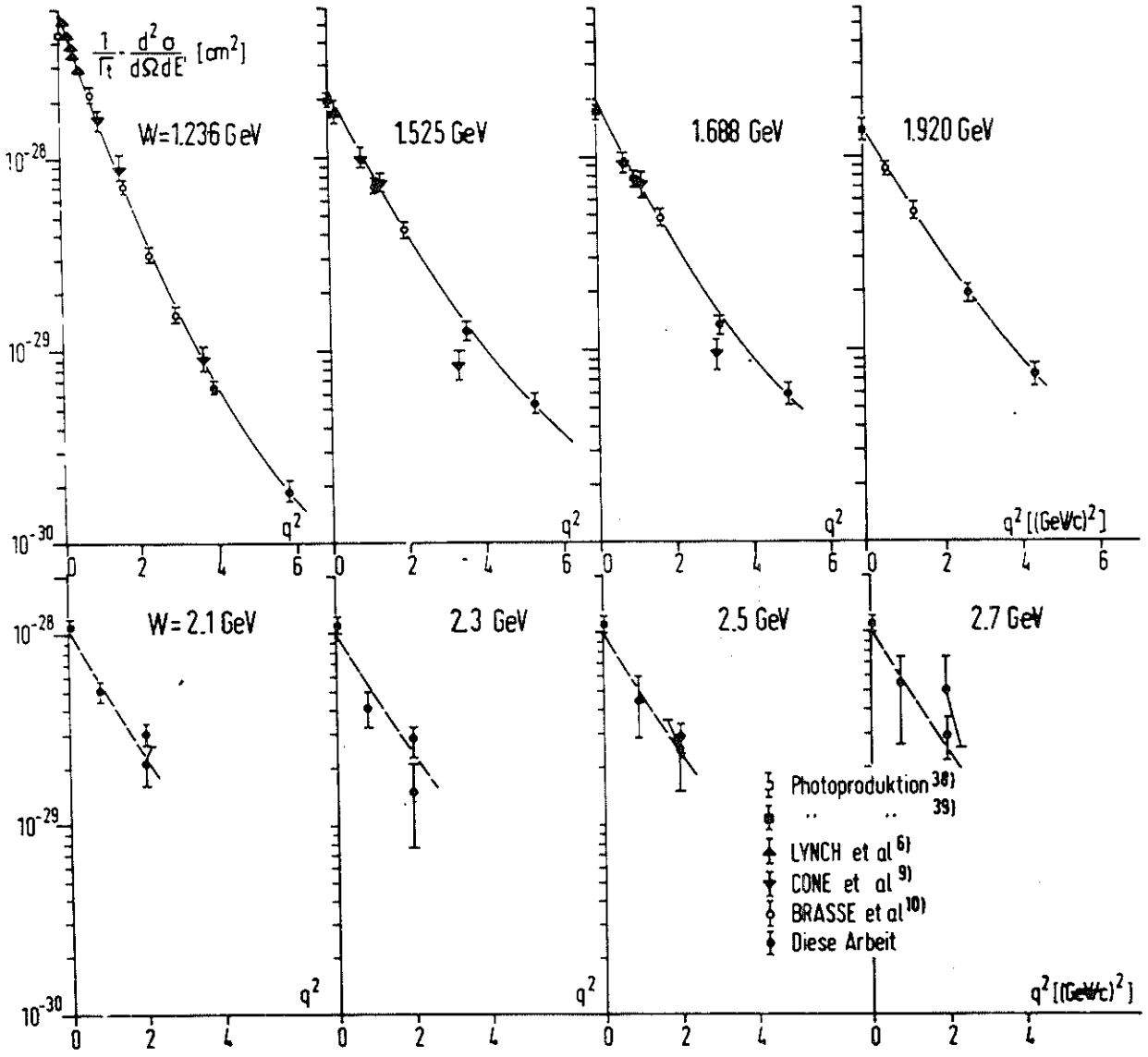
$\frac{1}{\Gamma_t}\cdot\frac{d^2\sigma}{d\Omega dE'}$ [cm²]
W=1.236 GeV
1.525 GeV
1.688 GeV
1.920 GeV
W=2.1 GeV
2.3 GeV
2.5 GeV
2.7 GeV
q^2
q^2 [(GeV/c)²]
Photoproduktion 38)
.. .. 39)
LYNCH et al 6)
CONE et al 9)
BRASSE et al 10)
Diese Arbeit

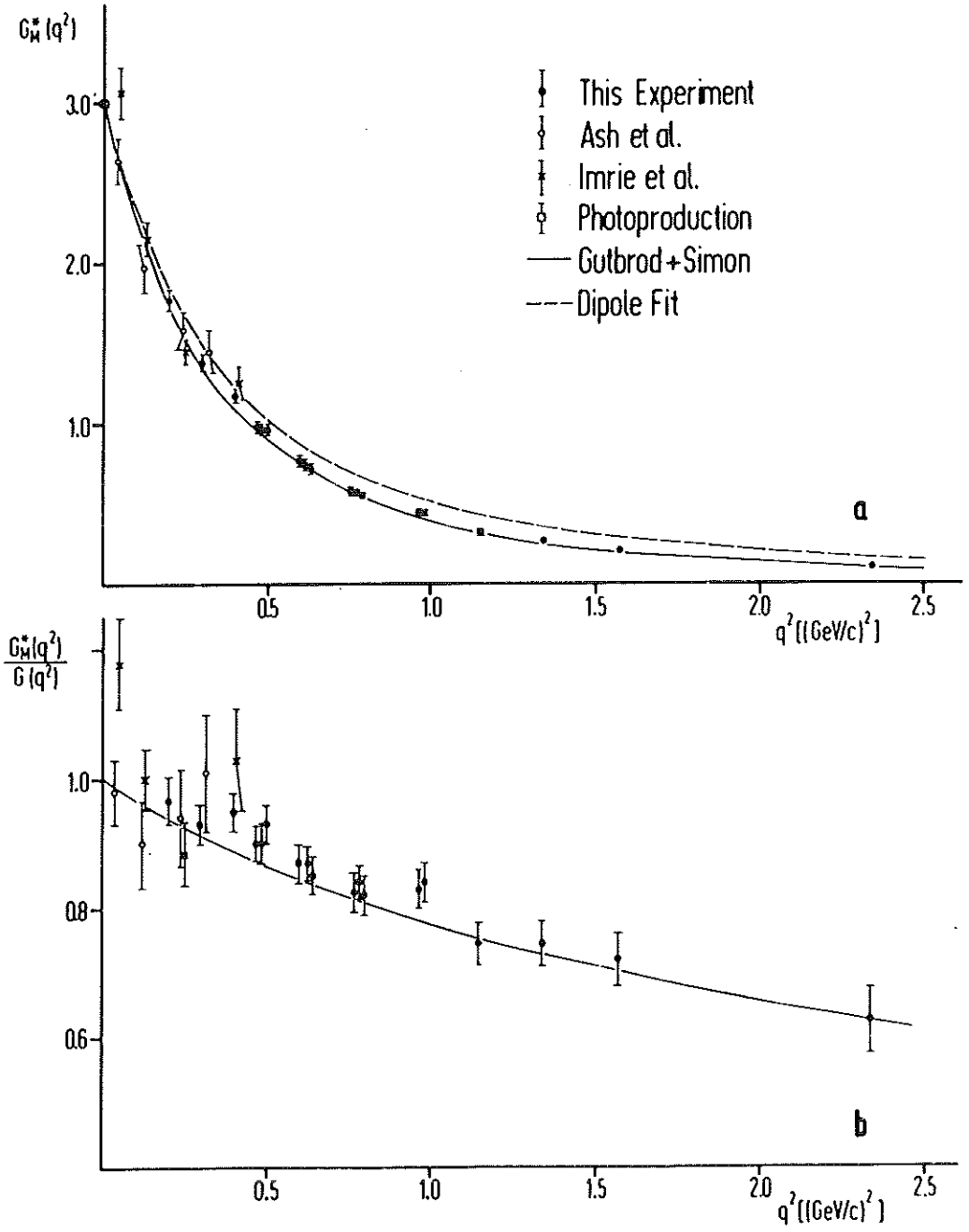
$G_M^*(q^2)$
3.0
2.0
1.0
This Experiment
Ash et al.
Imrie et al.
Photoproduction
Gutbrod+Simon
Dipole Fit
a
0.5
1.0
1.5
2.0
2.5
q^2[(GeV/c)^2]
$\frac{G_M^*(q^2)}{G(q^2)}$
1.0
0.8
0.6
b
0.5
1.0
1.5
2.0
2.5
q^2[(GeV/c)^2]

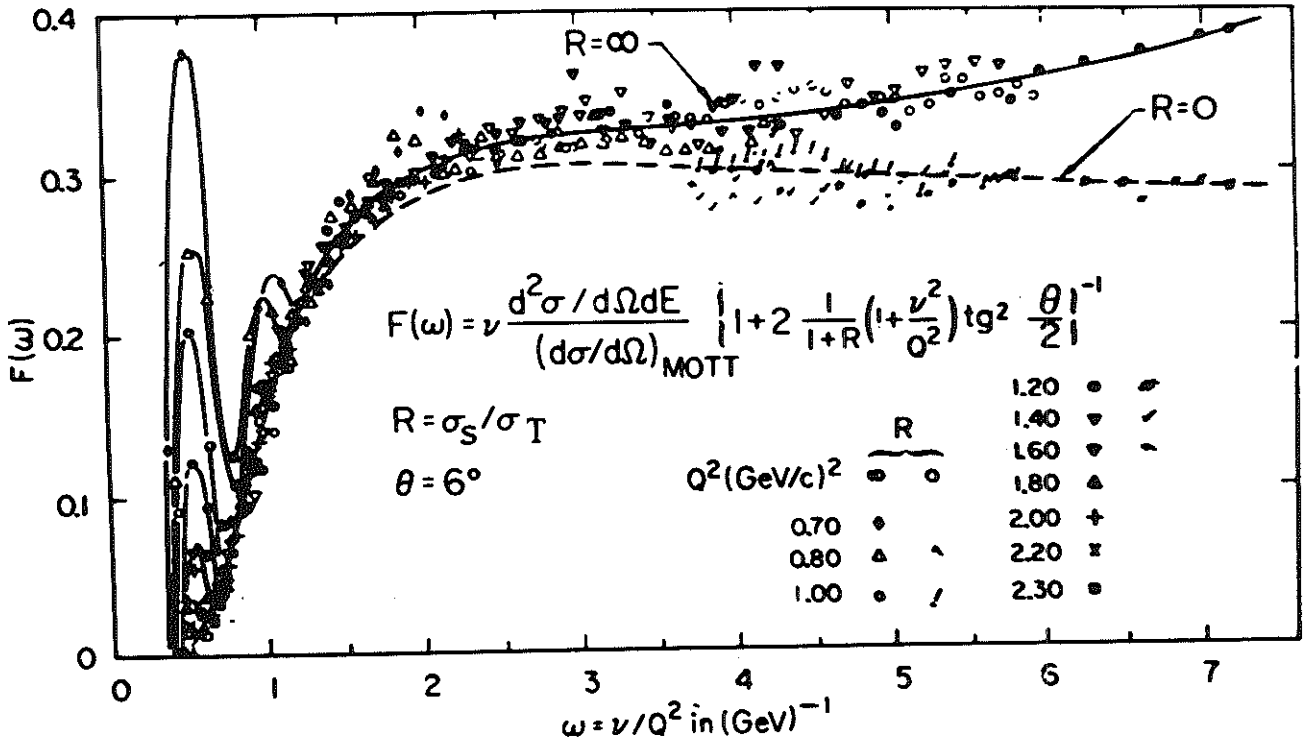

Fig. 30 Plot of $F(\omega) = \nu W_2(q^2,\nu)$, as a function of $\omega = \nu/q^2$.

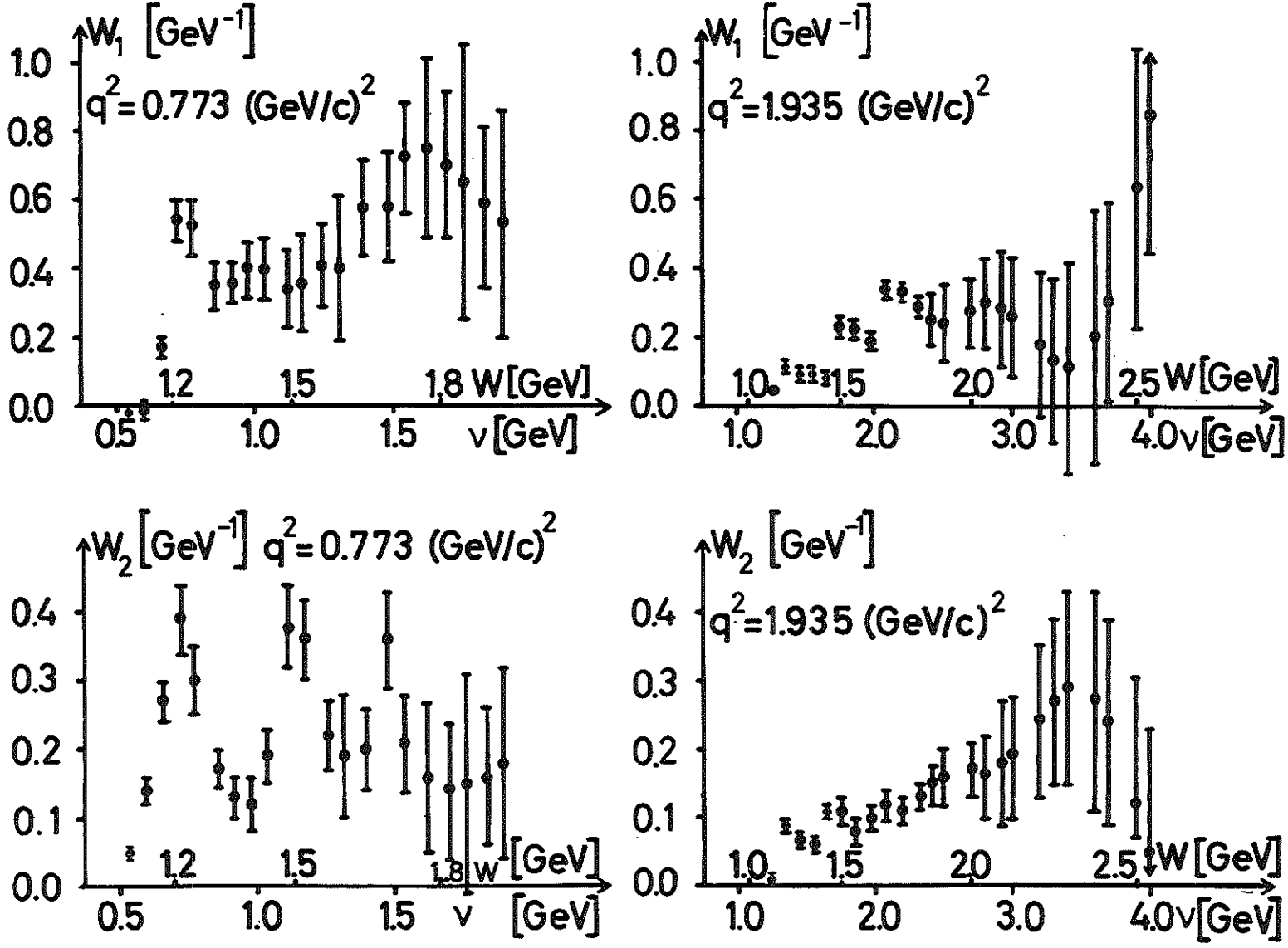
W1 [GeV-1]
q2=0.773 (GeV/c)2
1.0
0.8
0.6
0.4
0.2
0.0
1.2
1.5
1.8 W[GeV]
0.5
1.0
1.5
ν [GeV]
W1 [GeV-1]
q2=1.935 (GeV/c)2
1.0
1.5
2.0
2.5 W[GeV]
1.0
2.0
3.0
4.0 ν[GeV]
W2 [GeV-1] q2=0.773 (GeV/c)2
0.4
0.3
0.2
0.1
0.0
1.2
1.5
1.8 W [GeV]
0.5
1.0
1.5
ν [GeV]
W2 [GeV-1]
q2=1.935 (GeV/c)2
1.0
1.5
2.0
2.5 W [GeV]
1.0
2.0
3.0
4.0 ν[GeV]

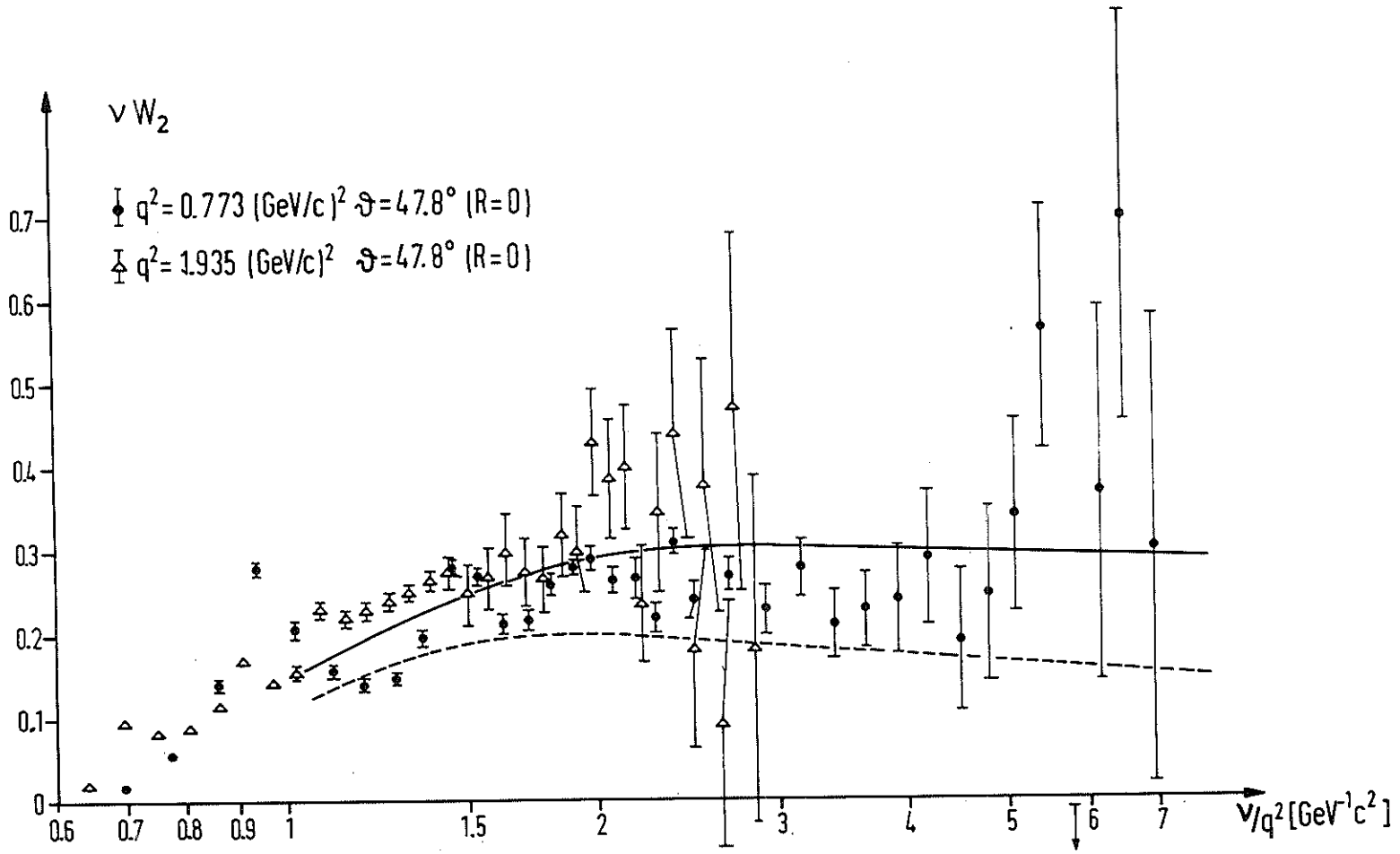
νW2
q2= 0.773 (GeV/c)2 ϑ=47.8° (R=0)
q2= 1.935 (GeV/c)2 ϑ=47.8° (R=0)
0
0.1
0.2
0.3
0.4
0.5
0.6
0.7
0.6
0.7
0.8
0.9
1
1.5
2
3
4
5
6
7
ν/q2 [GeV-1c2]

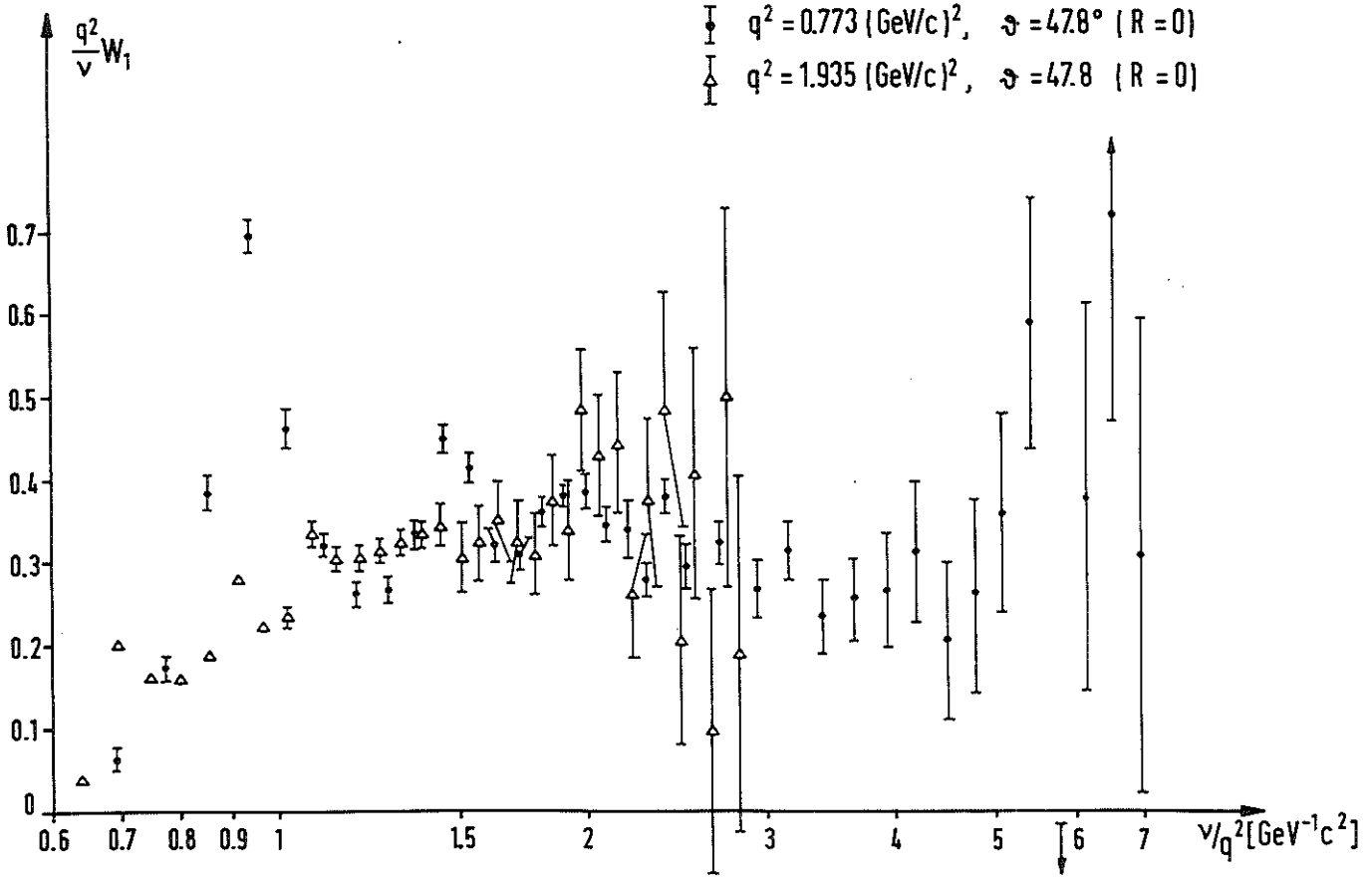
$\frac{q^2}{\nu} W_1$
$q^2 = 0.773\ (GeV/c)^2$, $\vartheta = 47.8°$ (R = 0)
$q^2 = 1.935\ (GeV/c)^2$, $\vartheta = 47.8$ (R = 0)
0
0.1
0.2
0.3
0.4
0.5
0.6
0.7
0.6
0.7
0.8
0.9
1
1.5
2
3
4
5
6
7
$\nu/q^2 [GeV^{-1}c^2]$

32b